An Analytical and Experimental Investigation of Nanoparticle Lubricants

By

Hamed Ghaednia

A dissertation submitted to the Graduate Faculty of
Auburn University
in partial fulfillment of the
requirements for the Degree of
Doctor of Philosophy

Auburn, Alabama
August 2nd, 2014

Keywords: Contact Mechanics, Friction, Lubrication, Nanoparticle, Oil Additive, Tribology, Wear

Approved by

Robert L. Jackson, Chair, Associate Professor of Mechanical Engineering
Jay M. Khodadadi, Alumni Professor of Mechanical Engineering
Hareesh Tippur, McWane Professor of Mechanical Engineering
W. Robert Ashurst, Associate Professor of Chemical Engineering

Abstract

This work investigated the tribological effects of nanoparticle additives on lubrication through experimental and analytical investigations on colloidal lubricants. The focus of this dissertation was to investigate and elucidate the enhancement mechanisms of nanoparticles.

Different types of particles including copper oxide, silver and diamond nanoparticles were used as lubricant additives. Various fluids were also used as the base lubricant in the experiments including mineral base oil, dodecane, polyethylene glycol 600, polyalphaolefin base oil and fully formulated SAE 5W20. The friction experiments were performed using a pin on disk and a disk on disk test setup. Studies were carried out using dry nanoparticles in powder form and lubricated experiments in the boundary, mixed and elasto-hydrodynamic lubrication regimes. Three dimensional surface metrology were performed using a stylus profilometer and an optical profilometer. Wear measurements were done through analysis of the wear grooves. Various surface analysis including scanning electron microscope (SEM), energy-dispersive x-ray spectroscopy (EDX) and auger electron spectroscopy (AES) was performed to assess the stoichiometry of the elements on the tested surfaces. X-ray photoelectron spectroscopy (XPS) surface analysis was also performed to detect the bonds between the elements on the surface and to confirm the stoichiometry. Analytical analysis was also adopted to study the system in depth. A contact model for nanoparticles in contact between rough surfaces was developed. This contact model was also adapted to the general case of particles that are of the same scale as the roughness. This model is useful for the contact of surfaces with contaminants such as sand or dust between them.

Based on the results, the mechanism of “the reduction in area of contact” for nanoparticles in boundary and mixed lubrication was proposed. The third body contact model was used to further verify this mechanism. The results showed that the nanoparticles reduce the friction force in the thin film elasto-hydrodynamic lubrication (EHL) regime. A mechanism was discovered and proposed to explain the effect of nanoparticles on friction in the EHL regime. That is the nanoparticles induce a plug flow and localize the shear to the layers adjacent to the walls which in turn reduce the friction force. Results also showed that the dry nanoparticles in powder form are effective in reducing friction and wear. Also, it was demonstrated that there is a critical concentration of nanoparticles below which they can’t sustain a reduced friction force. Based on all the results it was proposed that the nanoparticles have a dual effect on a contact’s tribology. A direct and an indirect effect which need to be added to find the overall effect of particles on the system. The results showed that diamond nanoparticles in fully formulated oil can effectively reduce friction and impose a positive polishing effect on the surfaces. Silver nanoparticles in fully formulated oil showed significant reduction in both the friction and wear.

Acknowledgments

I would like to acknowledge everyone who assisted me throughout my doctoral studies over the years. First and foremost I like to thank and dedicate all my success to my lovely wife. Her everyday love, support and encouragement was what made my doctoral studies and this dissertation possible.

I would like to acknowledge my advisor, Dr. Robert Jackson for his enthusiastic support and guidance which made my doctoral studies a very rewarding experience. Much thanks to Ms. Hannah Neuffer and Ms. Yang Zhao of Auburn University for helping with the experiments. I should express many thanks to my lab mates and friends, Hamid Ghaednia, Jimmy Gatherer, Hyeon Lee, Amir Rostami, Sara Pope, Yang Xu, Xianzhang Wang and Xiaohan Zhang, who provided me with support and good humor. My dissertation committee members for all of their guidance through the process.

Appreciation is expressed to Mr. Mohammad Sharif, Mr. Jason Darvin, Dr. Dan Clary and Dr. German Mills of Auburn University chemistry department for providing the colloids. Mr. Hasan Babaei and Dr. Jay Khodadadi of Auburn University mechanical department for doing the MD simulations. Many thanks to Dr. Michael Bozack and Dr. Mike Miller of Auburn University for providing support and assistance with the surface analysis. Dr. Andres Carrano and Mr. Kamran Kardel of Auburn University for assistance with the optical profilometer. Mr. Parker Sizemore of King Industries, Mr. Ralph Beard of Dorf Ketal Chemical and David Leith of Cool-X LLC for assisting in acquiring lubricants for testing.

I should also acknowledge the funding agencies. This material is based upon work partially supported by the US Department of Energy under Award Number DE-SC0002470.

This material is based upon work partially supported by the Taiho Kogyo Tribology Research Foundation (TTRF). I am also grateful to the Samuel Ginn College of Engineering and the Department of Mechanical Engineering at Auburn University for providing support for the College Fellowship (fall 2010-fall 2012) and also acknowledge financial support provided by the Alabama EPSCoR Program under the Graduate Research Scholars Program (round 7).

Last but not lease I like to thank my caring parents for their continuous support and inspiration. My brothers for their everyday encouragement and help. Many thanks to my parents-in-law, my sister-in-law and brother-in-law for their unhesitating support.

Table of Contents

Abstract ii

Acknowledgments iv

List of Figures ix

List of Symbols xiv

1. Introduction and literature review 16

2. Experimental investigations of stable CuO nanoparticle lubricants 21

   2.1. Nano-lubricant description 21

   2.2. Experimental setup and results 22

   2.3. Discussion 35

   2.4. Conclusion 38

3. Analytical multi-scale contact model for nano-lubricants 40

   3.1. Methodology and assumptions 41

   3.2. Modeling 44

      3.2.1. Rough surface sub-model 44

      3.2.2. Statistical nanoparticle contact sub-model 45

      3.2.3. Algorithm 48

      3.2.4. Friction and wear models 50

   3.3. Results 51

   3.4. Discussion 58

3.5. Conclusion 60

4. A third body contact model for a particle contaminated contact 62

4.1. The Contact Model 63

4.2. Electrical Contact Resistance 67

4.3. Results 69

4.4. Conclusion 74

5. The effect of nanoparticles on thin film elasto-hydrodynamic lubrication 75

5.1. Nano-lubricant and experiments 76

5.2. Surface analysis 80

5.3. Molecular dynamics simulations 82

5.4. Conclusion 88

6. Tribological performance of silver nanoparticle-enhanced polyethylene glycol lubricants in boundary and mixed lubrication regime 90

6.1. Viscosity measurements 91

6.2. Friction and wear tests 94

6.3. Surface analysis 98

6.4. Discussion and conclusion 99

7. The performance of nanoparticles in fully formulated oils 101

7.1. Experimental approach 102

7.2. Results 103

7.3. Discussion 122

7.4. Conclusion 126

8. Conclusion 128

9. References 132

Appendices..... 139

Appendix I. 139

Appendix II. 147

Appendix III. 149

List of Figures

Figure 1: (a) TEM image of CuO nanoparticles, (b) particle size distribution [58]. 22

Figure 2: (a) The disk on disk friction tester used in the experiments. (b) Schematic view of the disk on disk test setup. 23

Figure 3: Results showing the effect of nanoparticle concentration on friction and temperature. 24

Figure 4: (a) Viscosity versus temperature for different concentrations of nano-lubricants (b) viscosity versus volume fraction for T = 20^{o}C 26

Figure 5: Stribeck curve for different weight fractions of nano additives. 27

Figure 6: Wear analysis schematics. 28

Figure 7: Wear per sliding distance as a function of the nanoparticles concentration. .. 29

Figure 8: SEM image of the test surfaces as obtained and its material composition using EDS. 30

Figure 9: SEM image inside the wear groove for lubricant with no nanoparticles additive and its material composition using EDS. 31

Figure 10: SEM image for the surfaces tested with 0.5%wt CuO nano-lubricant and its material composition using EDS. 32

Figure 11: SEM image for the surfaces tested with 1.0%wt CuO nano-lubricant and its material composition using EDS. 34

Figure 12: SEM image for the surfaces tested with 2.0%wt CuO nano-lubricant and its material composition using EDS. 35

Figure 13: Illustration of the proposed mechanism, reduction of the real area of contact by the nanoparticles. 38

Figure 14: Illustration of stacked rough surface and statistical model. 42

Figure 15: Schematic of the spherical particle contact mechanics. 47

Figure 16: Schematic of the overall contact problem. 49

Figure 17: Schematic of the particle abrasive wear. 51

Figure 18: The effect of particle concentration (a) and particle average size (b) on the real contact area versus contact force. 52

Figure 19: The effect of particle distribution on the real area of contact. 54

Figure 20: Fractured particles as a function of surface separation. 54

Figure 21: The effect of surface roughness on (a) the real area of contact versus contact force, (b) change in the real area of contact as the result of nanoparticles. 55

Figure 22: Coefficient of friction and particle induced wear versus nanoparticle content. 56

Figure 23: Particle induced wear (a) and coefficient of friction (b) changing with particle average size and distribution. 57

Figure 24: Schematic of the rough surface and the dispersed sand particles. The graph on the right shows the corresponding height distribution and the definition of region I and II based on the surface separation. 64

Figure 25: Real area of contact (top) and electrical resistant (bottom) versus contact force for different values of sand content on the surface. Both A_r and R_e are very sensitive to the presence of sand in amounts over $m_p=0.1\times10^{-6}\ kg.m^{-2}$. 70

Figure 26: Real area of contact (top) and electrical resistant (bottom) versus contact force for various particle sizes. Particles larger than the average valleys on the surface have a higher possibility of engaging in contact and reducing the conductive area of contact hence increasing the contact resistance. 71

Figure 27: Real area of contact (top) and electrical resistant (bottom) versus contact force for various surface roughness values. Even though lower roughness values (smother surfaces) result in lower contact resistance, they are more susceptible to particle contamination. 73

Figure 28. Schematic of the contact pair. 76

Figure 29. Pin and disk profiles after the friction tests for one of the contact pairs. 77

Figure 30. Coefficient of friction versus contact pressure. 79

Figure 31. Picture of contact region obtained with scanning electron microscope, (a) AES spectra inside (b) and outside (c) the contact region. 80

Figure 32. AES analysis on the surfaces before (a) and after (b) drilling with Ar sputter cleaning. 82

Figure 33. Schematic of possible particle/surface interaction: (a) particles deposit on the surface and inside the valleys (b) scattered loosely adhered particles on the surface. .. 82

Figure 34. Schematic diagram of the simulation system and boundary conditions. 85

Figure 35. (a) Density curve for pure at *G*=54 Å, showing the formation of planar layers. (b) COF versus pressure at *G*=54 Å for pure system and two nanofluid systems containing nanoparticles with *D*=24 and 37 Å. 86

Figure 36. Examples of the velocity profiles for the pure and the nano-lubricant cases with *G*=54 Å and a pure case with *G*=18 Å. 88

Figure 37: Viscosity versus shear rate for (a) control lubricant, (b) 1.5 mM, (c) 30 mM, (d) 4.5 mM Ag nano-lubricant. 92

Figure 38: (a) Viscosity versus nanoparticle concentration at T = 30 ^{o}C, (b) Change in viscosity versus temperature. 93

Figure 39: Coefficient of friction versus sliding distance for various concentration of nanoparticles. 95

Figure 40: Three dimensional surface profile of a wear track obtained for wear measurements. 95

Figure 41: Effect of nanoparticle concentration on friction and wear. 96

Figure 42: The Stribeck curve obtained for the nano-lubricant and the control showing the performance of the lubricants in boundary and mixed lubrication regimes. 97

Figure 43: XPS analysis spectrum obtained inside the groove of a sample tested with the nano-lubricant. 98

Figure 44: XPS analysis spectrum obtained outside the groove of a sample tested with the nano-lubricant. 99

Figure 45: Pin on disk dry tests performed on CuO particles with the normal load of (a) F=20 N and (b) F=2.0 N 105

Figure 46: (a) The control disk without any nanoparticles, (b) The disk with the high concentration of dry nanoparticles, (c) The disk with the low concentration of nanoparticles stopped at 600 sec. (d) Disk on disk dry tests performed on CuO particles

with two different concentration of particles on the surface. (e) The low concentration curve was shifted to right to demonstrate the repeatability of the tests. 106

Figure 47: COF in a pin on disk dry test performed on CuO particles. The test was stopped when the nanoparticles stopped performing to add particles to the contact and resume the experiment. 108

Figure 48: XPS surface analysis inside the groove of a sample tested with the dry nanoparticles right before the particles stop performing to measure the critical nanoparticle concentration. 108

Figure 49: Wear measurement for a samples tested with the dry nanoparticles versus a dry control test. 109

Figure 50: COF versus test progress for CuO dodecane nano-lubricant and the control at normal load value of F=2.0 N. 110

Figure 51: Three dimensional profile of the wear track for a sample tested with the control dodecane solution at normal load of F=20 N. 111

Figure 52: Friction and Wear analysis for CuO nanoparticles suspended in dodacane at various normal loads. 111

Figure 53: COF versus test progress for CuO PAO nano-lubricant and the control at normal load value of F=20 N. 112

Figure 54: COF versus test progress for CuO PAO nano-lubricant and the control at normal load value of F=50 N. 112

Figure 55: Three dimensional profile of the wear track for a sample tested with the control PAO solution at normal load of F=50 N. 113

Figure 56: Friction and Wear analysis for CuO nanoparticles suspended in PAO at various normal loads. 113

Figure 57: Friction and Wear analysis for CuO nanoparticles suspended in the fully formulated SAE 5W20 engine oil at various normal loads. 115

Figure 58: XPS surface analysis performed on samples tested with (top) control and (b) the CuO nano-lubricant in the 5W20 oil at normal load of F=150 N. 116

Figure 59: Friction analysis for various concentrations of diamond nanoparticles suspended in the fully formulated SAE 5W20 engine oil. 117

Figure 60: Wear analysis for various concentrations of diamond nanoparticles suspended in the fully formulated SAE 5W20 engine oil. 118

Figure 61: Three dimensional surface profile of inside a wear track obtained using an optical profilometer. 119

Figure 62: A three dimensional profile of the wear track decomposed into a cylindrical fit (top) and the overlay roughness (bottom). 120

Figure 63: Overlay roughness for the control and the diamond nano-lubricant showing the effect of polishing of the diamond particles. 121

Figure 64: Friction and Wear analysis for Ag nanoparticles suspended in the fully formulated SAE 5W20 engine oil. 122

Figure 65: Schematic showing various roles of nanoparticles in a contacts' tribology.. 125

List of Symbols

A_r	*Total real area of contact*
A_s	*Contact area between surfaces*
A_{CS}	*Interference cross sectional area of particle/surface*
A_n	*Nominal (apparent) area of contact*
A_{NP}	*Single particle contact area*
A_p	*Contact area of particles*
A_v	*Void area induced by particles*
A_{void}	*Single particle void area*
B	*Ratio between amplitude and wave length of different scales of roughness*
D	*Nanoparticle or particle size*
E'	*Effective elastic modulus*
F_{ext}	*External force applied on the system*
F_{NP}	*Single particle force*
F_p	*Force carried by particles*
F_s	*Force between surfaces*
L	*Sliding distance*
N_{NP}	*Number of nanoparticles in contact*
N_p	*Number of particles*
P^*	*Average contact pressure*
R	*nanoparticle radius*
R_e	*Electrical contact resistance*
S_y	*Yield strength*
V_{NP}	*Particle induced wear volume*
a	*Single particle radius of contact*
a_{asp}	*Single asperity radius of contact*
a_{rs}	*Average rough surface contact radius*
a_v	*Radius of void area for single particle*
d	*Surface separation*
m_p	*Mass of the particles*
v_{NP}	*Volume of the nanoparticles*
v_p	*Volume of the particles*
vol%	*Volume percent of nanoparticle*
wt%	*Weight percent of nanoparticle*
δ	*Amplitude of different scales of roughness*
ϕ	*Size distribution of nanoparticles*
ϕ_p	*Size distribution of particles*
ϕ_s	*Height distribution of the surface*
η	*Nanoparticle density per nominal area*
η_p	*Particle density per nominal area*
η_s	*Surface asperity density per nominal area*

λ	*Wave length of different scales of roughness*
ν	*Poisson ratio*
ρ	*Density of the nanoparticles*
ρ_p	*Density of the particles*
ρ_e	*Electrical resistivity*
σ_q	*RMS roughness*
τ	*shear stress between surfaces in contact*
ω	*Particle indentation*

Superscripts

I	*Region 1 of contact problem*
II	*Region 2 of contact problem*
c	*Conductive*

Subscripts

asp	*Asperity*
avg	*Average*
NP	*Nanoparticle*
p	*Particle*
s	*Surface*

1. Introduction and literature review

The unique behavior of materials at the nano scale has drawn great attention as a possible solution to conventional engineering challenges. The first step toward this goal is through the fabrication and close observation of nano structures. Nano structures such as nano-whiskers, nanowires, pillars and nanoparticles have been the topic of intense research in recent years [1-11]. Historically, nano- and micron-sized additives for lubricants have been used without being explicitly explored as "nano-additives", sometimes referred to as "solid lubricant additives". Chemists have long been very active in investigating nanoparticle suspensions known as "colloidal fluids" but recently these colloidal fluids using a lubricant as the main solvent have been labeled nano-lubricants. A nano-lubricant usually consists of three components; the main solvent which is a conventional lubricant, the nanoparticles that are often made of metallic or anti-friction materials and the surfactant that occupies the interface area between the fluid and the particles [12]. Previous literature suggests that the nanoparticles as additives can induce marked effects on the lubricant properties [13-26].

There are several reasons why nanoparticles are interesting as a potential lubricant additive. First and foremost is their small size. Nanoparticles are small enough to penetrate the gaps between the surfaces and alter the tribology of the contact pair. Also they are small enough to pass through oil filters. Nanoparticles usually possess scale dependent properties such as elevated hardness. Different nanoparticles have versatile characteristics. Therefore the combinations of different nanoparticles and lubricants can result in numerous nano-lubricants. The nano-lubricant can be tailored to a specific application.

However there are challenges associated with the nanoparticles as well. Nano-lubricants as well as any other colloidal solution exhibit problem of suspension's stability (i.e. the

particles can precipitate out of suspension due to agglomeration). Some of the nanoparticles pose environmental issues and therefore need to be reclaimed after use as oil additives. Some types of the particles are often expensive. Perhaps the most crucial challenge of the nanoparticle additives is that the mechanisms by which the nanoparticles enhance the tribology of contacts are unknown or unestablished.

A main focus of this dissertation is on the tribological properties of colloidal nano-lubricants of copper oxide (CuO) in organic solvents such as mineral oils. A few researchers have investigated the effect of CuO on common lubricating oils and have shown promising results. Sajith et al. [16] found that although the CuO and Al_2O_3 particles had only a slight effect on the fluid viscosity, the flash temperature of the fluid decreased significantly, thus improving the fluid stability without affecting its lubricating capabilities. Wu et al. [25] found that the addition of CuO nanoparticles reduced friction and improved the wear resistance. Hernandez Battez et al. [22, 24] tested different concentrations of CuO nanoparticles suspended inside PAO6 using a block on a ring tribometer. They found that 2 %wt CuO nano-lubricant lowers the wear rate significantly but the modification of the friction coefficient was minor. They suggest that tribo-sintering of nanoparticles results in the formation of a tribofilm and consequently enhanced tribological properties. Lee et al. [23] evaluated fullerene and CuO nano-lubricants to enhance the overall performance of refrigerator compressors.

However, in some works, the nanoparticles were mixed into the oil along with a dispersing fluid such as glycol. The dispersing fluid was not added to the base oil used as the control and so could also be causing the change in the lubricant performance. In addition, usually commercial oils are used as base solvents for particles. High concentrations of different additives in commercial oils may result in secondary and uncontrolled chemical reactions with the particles. The reaction between boundary lubricant additives and metallic nanoparticles could be a possible secondary reaction. Therefore, there is an uncertainty about the original cause of the changes in the oil properties.

In addition, some of the papers lack proper wear or viscosity measurements and therefore it is hard to draw a meaningful conclusion out of the data. For instance, a nano-lubricant is useless if the particles reduce friction and increase wear that in turn reduces the life of the surface. Lack of information on the stability of the nano-lubricants is another issue with some of the previous works in the literature. It is common practice to disperse dry particles in the lubricants using a sonicator and perform experiments quickly. Some of these friction experiments take hours to finish but there is uncertainty if the suspension is stable through the experiments. Also, unstable nano-lubricants would result in aggregations and clustering. Large clusters of nanoparticles may not enter through the gaps to the contact zone and be effective. In addition, instability would cause the properties and concentration of the nano-lubricant to change and decay with time. Therefore one the goals of this work is to study the isolated effect of the nanoparticles on lubrication. This would be accomplished through investigation of the stable suspension of nanoparticles in base oils (in the absence of other additives) and in fully formulated oils.

Although it has been well known for many years that the mechanics at the atomic scale or just above are very important for a complete understanding of friction and wear, in the past several decades advances in technology have allowed the actual control and fabrication of nano-scale tribological features. The incorporation of small size manipulation and measurement equipment such as the atomic force microscope (AFM) and electron microscopy yielded a great deal of data on various fundamental tribological phenomena [27]. Also, numerical chemistry methods such as molecular dynamics has shed light on many unobservable tribological aspects by providing in depth mechanical and chemical analysis tools for researchers as shown by the pioneering work of the late eighties and nineties [28-32]. The system of interest in this work, nanoparticles, have been the topic of many careful studies [2-4, 7, 8, 10, 11, 33-35] using methods such as single nanoparticle indentation and molecular dynamics modeling. Other researched topics include single nanoparticle fracture, scale dependent strength of free standing

nano structures, surfactant coated nanoparticles and the interfacial chemistry of nanoparticles. As a result, the literature on the nanoparticle tribology is rich and ever growing. Nonetheless, a review of nanoparticle lubrication literature [13-17, 19, 20, 22, 24, 36-42] shows many contradicting results and conclusions. It is claimed that the nanoparticles may exhibit mechanisms in the mixed and boundary lubrication regimes to affect performance, such as: (1) the particles affect oil viscosity [25], (2) the particles affect the thermal properties and thermal stability [26, 43], (3) the particles could roll between the surfaces and act as "nano ball bearings" [11], (4) the particles could mend worn surfaces by adhering to them and also forming a protective tribo-film [25, 44], (5) the particles can also induce abrasive wear which will result in a higher wear rate [22]. However, defining the active and dominant mechanisms causing friction reduction and improved wear of nano-lubricated surfaces are also the subjects of debates.

There are two aspects of nano-lubricant systems which makes it difficult to produce conclusive investigations. First is the multiscale nature of the system, meaning that nanoparticles, micron size roughness features and macro size effects coexist and play roles simultaneously. Secondly, due to their nature, nanoparticles in lubricants are governed by a wide variety of physical mechanisms, such as adhesion, Brownian motion, scale dependent strength, interfacial and chemical interactions, cluster formation, hydrodynamics, abrasive wear and erosion. Therefore, the second goal of this work is to study the enhancement mechanism of nanoparticles through analytical and experimental analyses. Analytical investigation of nanoparticles includes developing a third body contact model for nano-lubricants between rough surfaces. Although a great deal of work exists on modeling rough surface contact, including very small scales [45-52] and individual nanoscale asperity contact, very little work has attempted to explicitly include nanoparticles in a rough surface contact model. Actually, the most relevant advances have been made in the area of modeling third bodies in contact such as powder and particulate lubrication [53-55] and third body abrasive wear analysis [56, 57]. The contact model would include different scales of contact in the system and helps to solve the multi-

scale complexity of the nano-lubricants. The experimental methods consist of the preparation and characterization of nano-lubricants, performing various friction and wear tests in different lubrication regimes, viscometry and rheometry on the lubricants, and post-test evaluation using profilometry, SEM, EDX, AES and XPS.

The next six sections elaborate on the results and progress of the project. These sections discuss the approaches, methodologies and techniques employed to effectively investigate the problems as well as the results and discussions on the topics. Section 2 presents the experimental investigation of stable CuO particles in a mineral base oil. The goal of this study was to demonstrate the effectiveness of nanoparticle additives in the absence of any other conventional additives. Based on the observations of this study a mechanism was proposed for nanoparticle additives in the boundary lubrication regime. Sections 3 and 4 present the contact models developed for nano-lubricants and nanoparticles in contact between rough surfaces. The contact model presented in section 3 considers nano-lubricants in the boundary lubrication regime. This study was intended to verify the contact area mechanism proposed in section 2. The contact model presented in section 4 is applicable to a general system of particles in contact between rough surfaces (not necessarily nano sized particles). Section 5 explores the effect of nanoparticles on thin film elasto-hydrodynamic lubrication. The goal of this study was to elucidate the enhancing mechanism of nanoparticle additives in the elasto-hydrodynamic lubrication regime. Section 6 presents a novel nano-lubricant consisting of metallic silver particles suspended in polyethylene glycol. The goal of this study was to evaluate the effect of nanoparticle additives in different lubrication regimes. Section 7 investigates the effect of nanoparticle additives on fully formulated oils. The studies presented in this chapter used strategically designed experiments to investigate the role of nanoparticles in lubrication. The final section is a conclusion of all the discussions of the dissertation.

2. Experimental investigations of stable CuO nanoparticle lubricants

In this work, base lubricants with no additives have been used as the base solvents to isolate the results and investigate the effect of particles explicitly. Also the effect of different concentrations of nano-lubricants on the friction and wear properties of lubricants is investigated. The nanoparticles used are unique CuO nano-particles developed recently by Clary and Mills [58]. The nano-lubricant used in this work is exceptionally stable which makes it a viable candidate for analysis and possibly for industrial applications. To perform the experiments, a disk-on-disk test setup is used that measures the friction coefficient using torque and load sensors, in addition to the temperature of the lubricant. The surface samples are submerged in a small reservoir of the nano-lubricant. The experiments will be discussed in more detail later. The wear and surface analysis are evaluated by surface profilometery, electron microscopy and electron dispersive X-ray spectroscopy.

2.1. Nano-lubricant description

CuO nanoparticles used in this paper are developed by Clary and Mills [58] which are especially designed for dispersion in hydrocarbons. In their method, sodium oleate (SOA) is used as a surfactant to help the dispersion of particles in non-polar solutions. They monitored the CuO concentration in non-polar solvents spectroscopically at room temperature and proved stability over a period of at least eight months. They also conducted stability studies for repeated phased change cycles and reported no significant precipitation. Particles were observed to be quasi-spherical in shape with an average diameter of 9 nm and 90% of the population existing within the range of 5-15 nm (Figure 1). It is also proven that the addition of these particles to alkanes modifies the thermal properties of the solution in terms of the specific heat and thermal conductivity [43]. The base oil used in this paper is a 50% volumetric blend of “mineral 600HC heavy base oil”

and “mineral 100HC light base oil” (10 %wt dodecane is also added to the final solution). The base oils used are group II base oils with more than 99% of saturates.

In order to make the nano-lubricant, first CuO particles are dispersed in dodecane ($C_{12}H_{26}$) at a 10% weight fraction (dodecane acts as a dispersing agent that helps create a more stable and higher concentration of nano-lubricants). The solution is first stirred and heated for 4 hours and then diluted to the desired weight fraction by blending with the base oil. A solution of the same concentration of dodecane in the blended base oil without nanoparticles is prepared as a control sample.

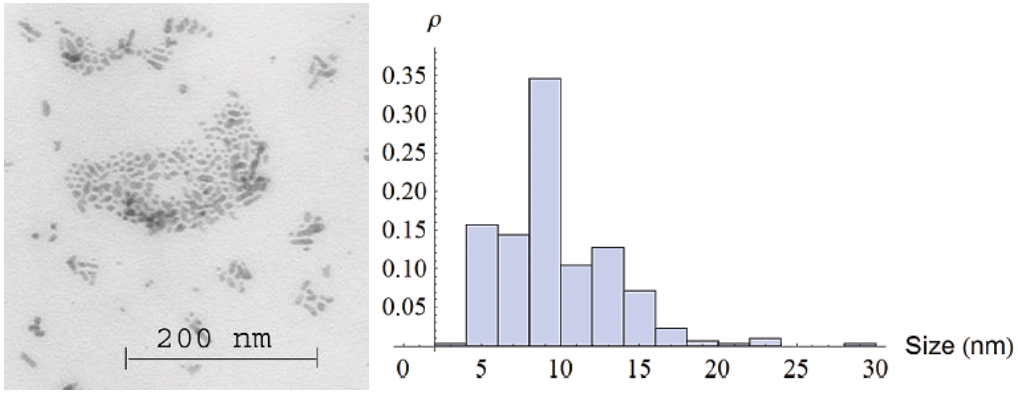

(a) (b)

Figure 1: (a) TEM image of CuO nanoparticles, (b) particle size distribution [58].

2.2. Experimental setup and results

Figure 2 shows the schematic of the disk on disk test setup used in this work (also known as a thrust washer test). The drive shaft rotates the disks on one another and induces the desired sliding motion. Surface samples are submerged in the nano-lubricant inside a reservoir, see Figure 2. The frictional torque between the surfaces is measured using a torque sensor. The normal load is monitored using a load cell supporting the reservoir. The friction coefficient is calculated from the torque using the method introduced by Jackson and Green [59]. A thermocouple is also deployed to determine the temperature of the lubricant. A data acquisition system and user interface software records and

controls the experiments. This test setup is designed for conducting boundary lubrication experiments with a small volume of lubricant. Surface samples are zinc plated steel disks with an inner and outer diameter of 9.5 mm and 22.2 mm, respectively. The average root mean square (RMS) roughness of the samples is 4 μm.

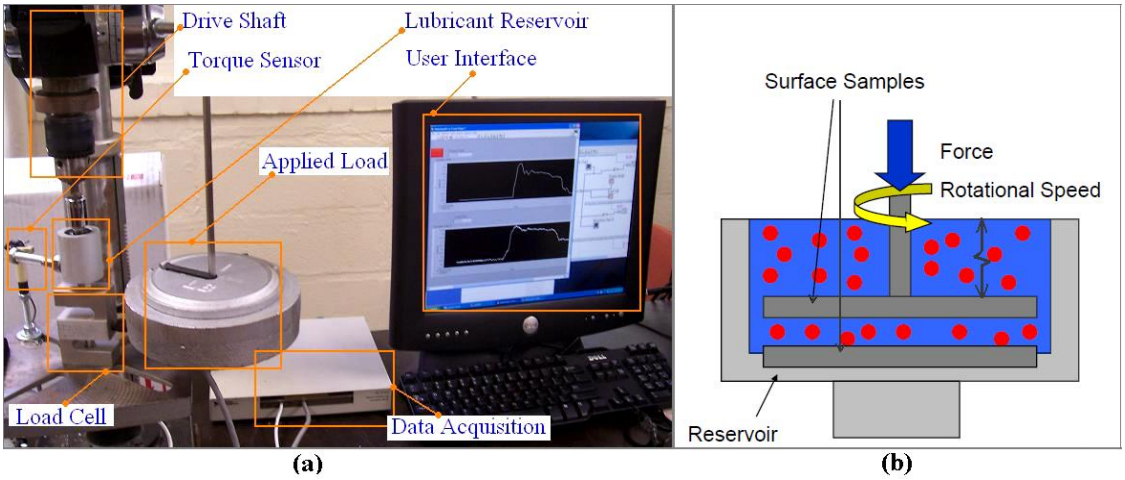

Figure 2: (a) The disk on disk friction tester used in the experiments. (b) Schematic view of the disk on disk test setup.

Friction enhancement of the nano-lubricants is investigated through direct friction coefficient analysis and viscosity measurements. Figure 3(a) presents the results of the tests for the control sample which is a 10 %wt solution of dodecane in the blended base oil and also for several other concentrations of nano-lubricants. Each test was repeated three times. Surfaces went through a run-in process and then data was recorded for a duration of three minutes at the rotational speed of 570 rpm. Results indicate that the nanoparticles decrease the coefficient of friction. The effect of nanoparticles is more influential at higher loads and nanoparticle concentrations. The system works in the boundary lubrication regime which is the case where the lubricant film thickness between surfaces approaches the surface RMS roughness. In this lubrication regime, there is substantial contact between surfaces but also some parts of the surfaces are separated by the lubricant film. Therefore, an increase in the normal load would squeeze more lubricant out of the contact region which reduces the lubricant film thickness between

surfaces. This would escalate the probability of contact between surfaces and hence, increases the probability of particle engagement in the contact (i.e. the particles are more influential further in the boundary lubrication regime).

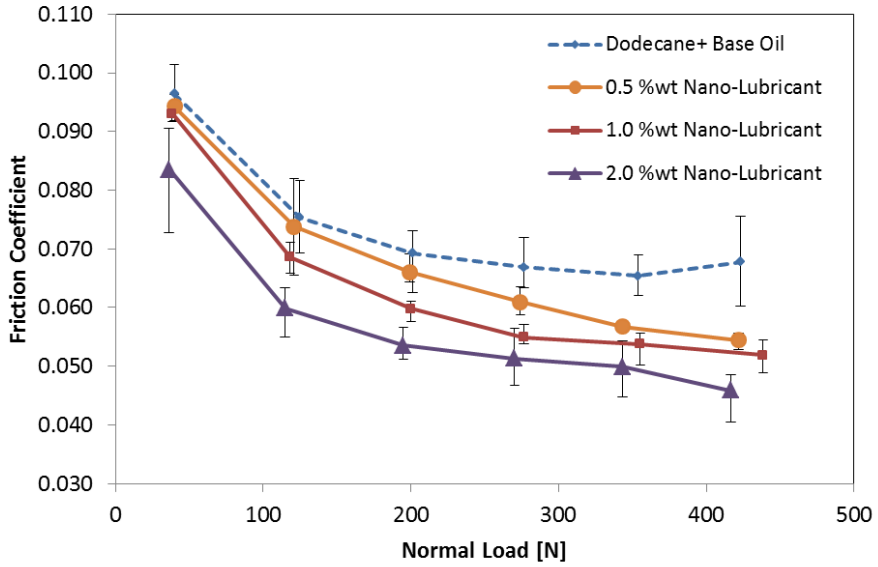

(a)

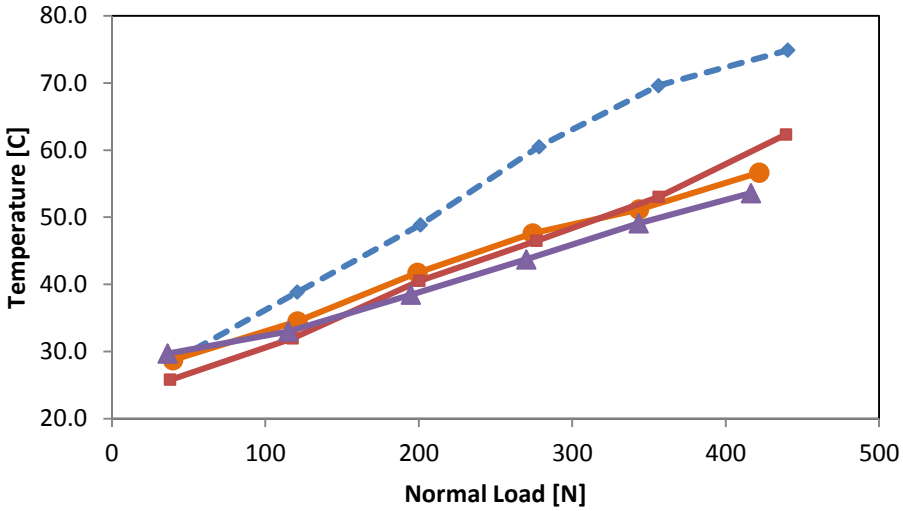

(b)

Figure 3: Results showing the effect of nanoparticle concentration on friction and temperature.

Figure 3(b) shows the steady state temperature of the lubricant at the end of the experiment. In the case of nano-lubricants, a lower friction coefficient results in less heat production and consequently the final temperature is lower. As mentioned, the CuO nanoparticles also have proven to affect the thermal properties of the solution (such as conduction) which could result in better heat dissipation. Therefore the combination of these effects appears to result in a significant reduction in the temperature in comparison to the lubricant without nano particles. One of the known effects nanoparticles have on fluids is to change the viscosity. The fluid flow pattern is affected in the presence of the solid nanoparticles suspended in the liquid that results in an increase in dissipated energy and an increase in the viscosity of the nano fluids. Figure 4 shows the results of viscometry for different concentrations of CuO nano-lubricants versus temperature using a Brookfield® DV-II +Pro rotational viscometer capable of measuring small volumes at controlled temperatures. The temperature range was selected to match the steady state temperatures reported in Fig. 3(b). The average of five readings were taken for each temperature. The average error for the results shown in Fig. 4 is 2.30%. At a given temperature, an increase in the viscosity in response to raising the particle concentration is observed. The relative change in viscosity is fairly constant at different temperatures. For example, for all temperatures between 20 ^{o}C and 70^{o}C, the average viscosity increase for a 2.0 %wt increase of nanoparticles is 20.4% with a standard deviation of 0.02%. The present viscosity results (see Fig 4(b)) confirm some of the experimental data from the literature [60] which report viscosities for nano-fluids that are greater than that predicted by the Einstein model [61].

The data from the friction and viscosity measurements is collapsed into the widely used Stribeck curve [62] in an attempt to develop generalized observations (see Fig. 5). In Fig 5, P, μ, η and ω are the average contact pressure, friction coefficient, viscosity and rotating speed respectively. The Stribeck curve is able to account for the effect of changes in viscosity due to temperature rise and particle concentration, along with pressure in one combined plot. The change of viscosity versus the steady state temperature is considered

in Fig. 5 using the data shown in Figs. 3(b) and 4(a). In the experiments of this paper, the surfaces in the contact undergo severe wear at the higher loads so clearly the system is operating in the boundary lubrication regime (more data is available in the surface analysis section).

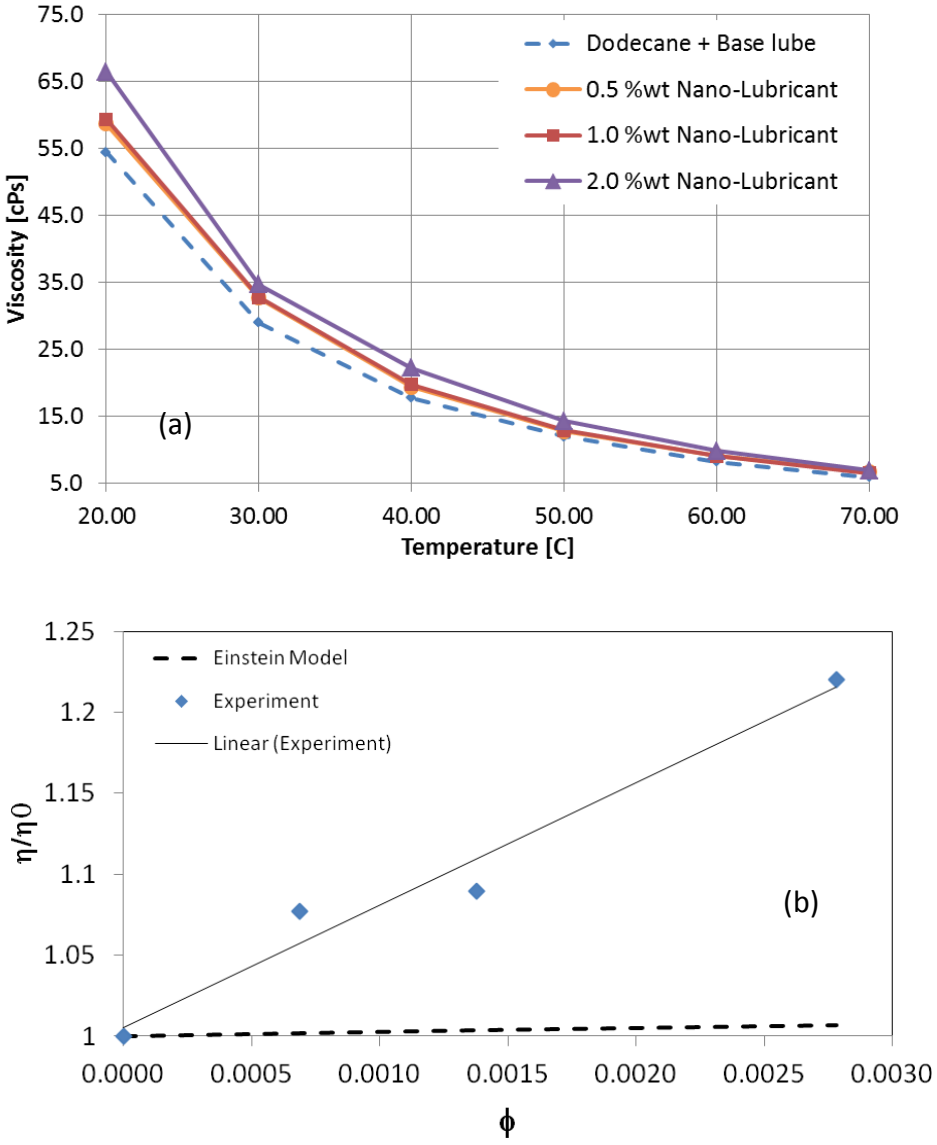

Figure 4: (a) Viscosity versus temperature for different concentrations of nano-lubricants (b) viscosity versus volume fraction for T = 20°C.

In Fig. 5, the friction coefficient decreases as more nanoparticles are introduced in the lubricant and as contact pressure increases. As contact pressure increases, more asperities in the contact region yield and undergo plastic deformation. Lower resistance to the applied tangential load is exhibited, causing the overall friction coefficient to drop in accordance with existing friction theories [63-71]. Figure 5 shows that CuO nanoparticles additives decrease friction coefficient deep into the boundary lubrication regime (on the far left of the curve).

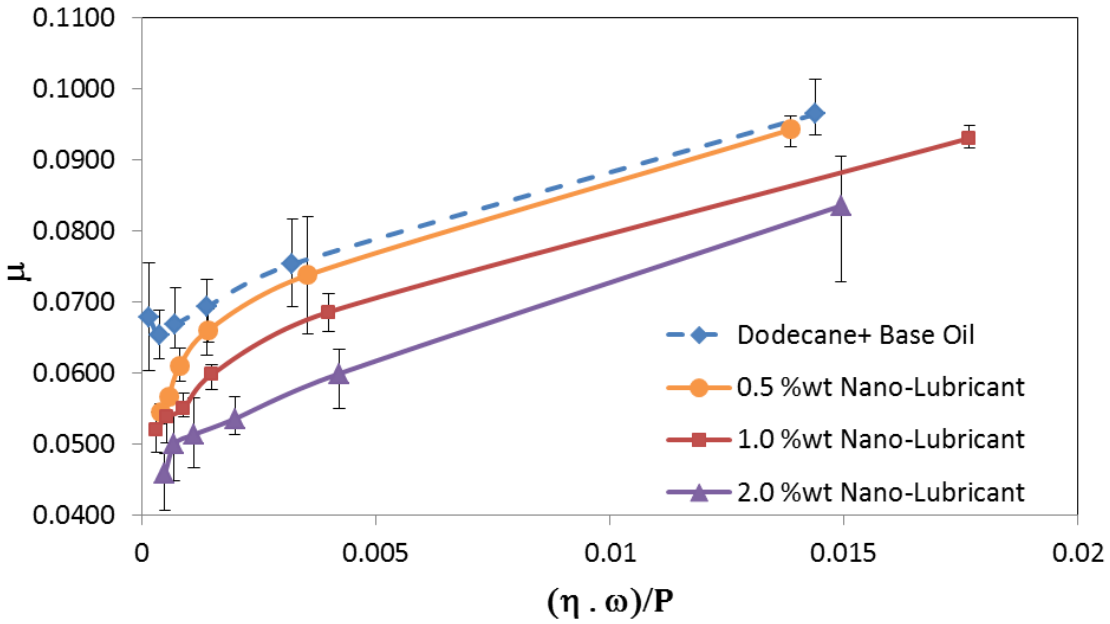

Figure 5: Stribeck curve for different weight fractions of nano additives.

After testing, the surfaces are analyzed using a Veeco Dektak 150 stylus profilometer and three dimensional profiles of the surfaces are obtained (see Figs. 8-10(a)). The 3D surface profiles show clear evidence of surface contact and wear grooves which prove that the system is working in the boundary lubrication regime.

One of the disks used in the friction tests is smaller, resulting in a smaller worn region than the larger washer surface area. Consequently, the unworn surfaces provide a reference plane (baseline) with which to use in a volumetric wear analysis. Figure 6 shows

a sample cross section profile of a surface after the test. Based on the original surface baseline and the grooves geometry one can integrate the area below the baseline and find the wear volume. Figure 7 presents the predicted volumetric wear rates based on the surface profilometery results discussed. *V* and *s* in this figure represent the wear volume and the sliding distance. Results show an increase in wear up to the 1.0 %wt concentration of nanoparticles and a decrease as particle concentration increased up to 2.0 %wt (although the inflection point is not defined due to the limited data points). Since wear is larger at the 1.0% weight fraction of nanoparticles and minimum at 2.0%, the results suggest that the addition of nano-lubricants can in some cases increase wear, while in other cases reduce it. Due to the scaling effect on material strength, nanoparticles exhibit higher hardness than bulk materials [1-5, 7, 10] which potentially makes them a source of abrasive wear. The same trend for wear of different nanoparticles has been reported by Hernandez Battez et al. [22]

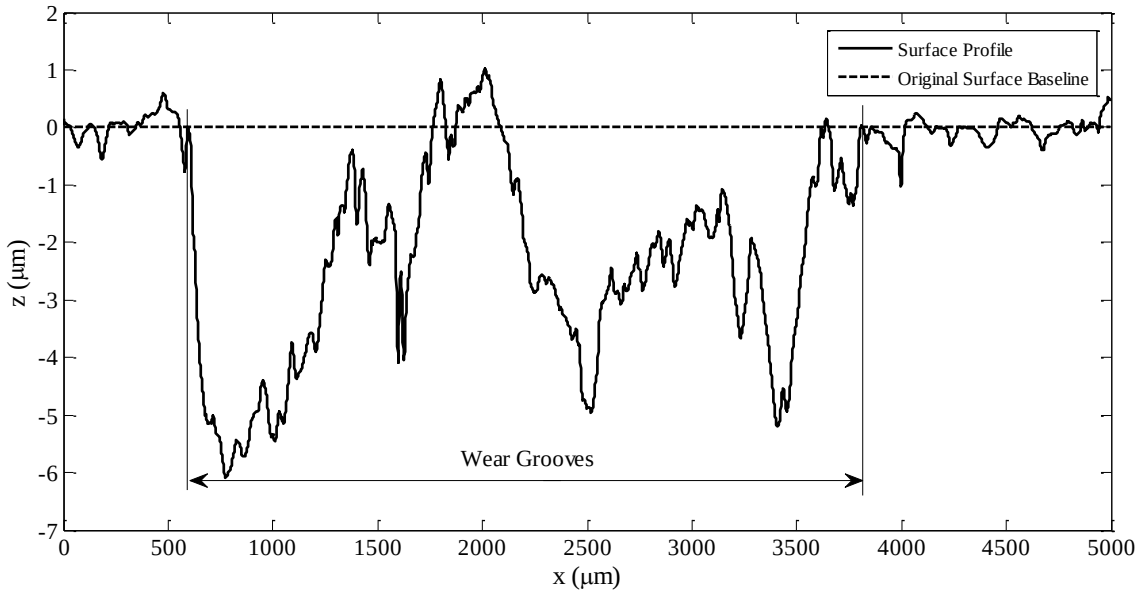

Figure 6: Wear analysis schematics.

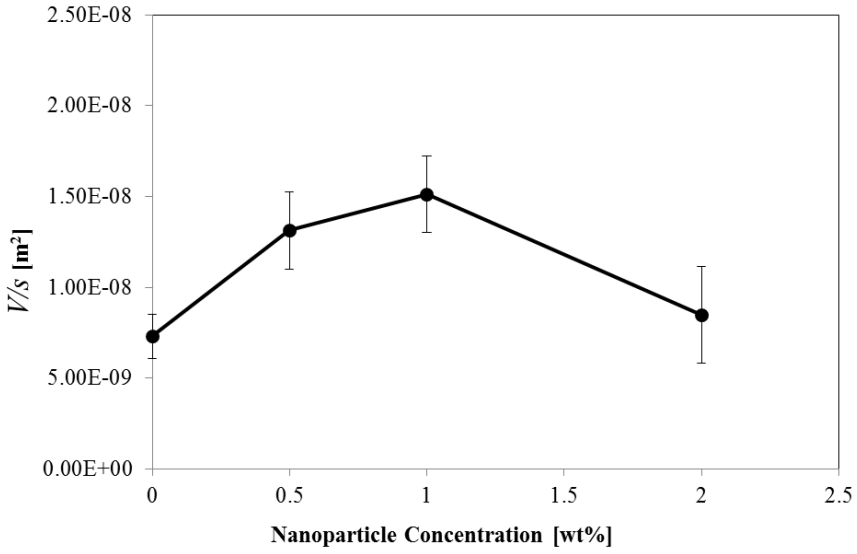

Figure 7: Wear per sliding distance as a function of the nanoparticles concentration.

Scanning electron microscopy (SEM) and electron dispersive X-ray spectroscopy (EDS) were also used to investigate the material composition of the surfaces before and after tests. All surfaces were cleaned with acetone before SEM/EDS tests.

Figures 8-12 present the SEM/EDS microscopy results. SEM/EDS results for surfaces before testing (Fig. 8) and for surfaces tested with a base oil only, i.e. no particles, (Fig. 9) are reported as control samples. Note that in the second case the wear is severe and results in the coating being worn through. Cases where the coating is not worn away can be compared to the new surfaces, while cases of the severe wear through the coating should be more compatible to the second case. Figure 8, presents the SEM image of test surfaces before performing any test and its material composition. As one expects, the majority of the unworn test surfaces are composed of zinc. Whereas, SEM/EDS results show that the majority of the samples worn under a pure base oil are composed of iron inside the wear grooves (Fig. 9). It is also evident in Figs. 8 and 9 that there is no trace of the element copper on the surface samples used in this work, prior to surfaces being exposed to CuO particles. Figure 10 shows the SEM/EDS analysis for a sample surface tested with a 0.5%wt CuO nano-lubricant. The x-ray analysis indicates that traces of the element copper exists on the surfaces after being exposed to the nano-lubricant during

the test. The high concentration of zinc on the surface suggests that the coating at the SEM/EDS analysis is still largely intact on the surface. This is also made more apparent by comparing to the x-ray analysis of the control sample (Fig. 8).

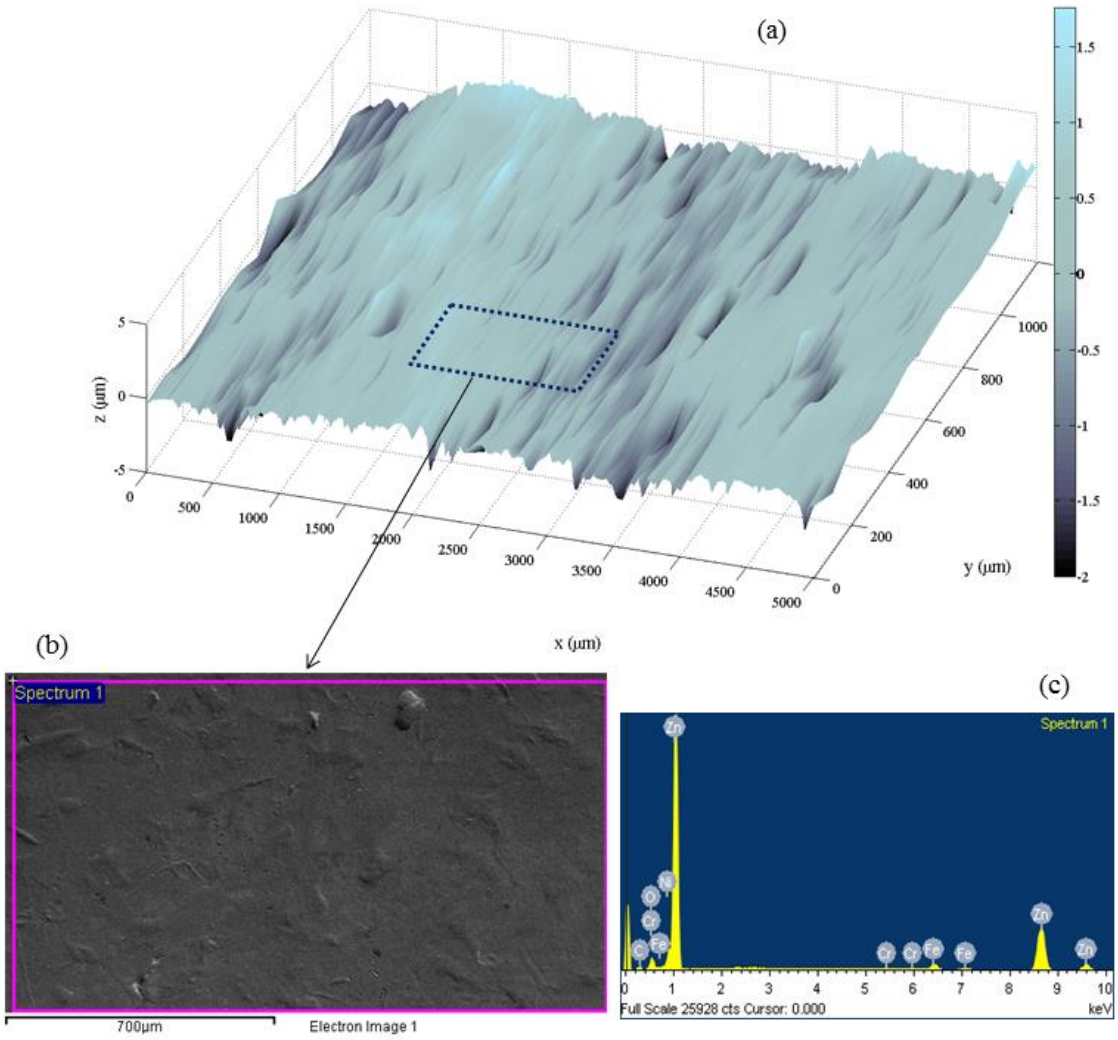

Figure 8: SEM image of the test surfaces as obtained and its material composition using EDS.

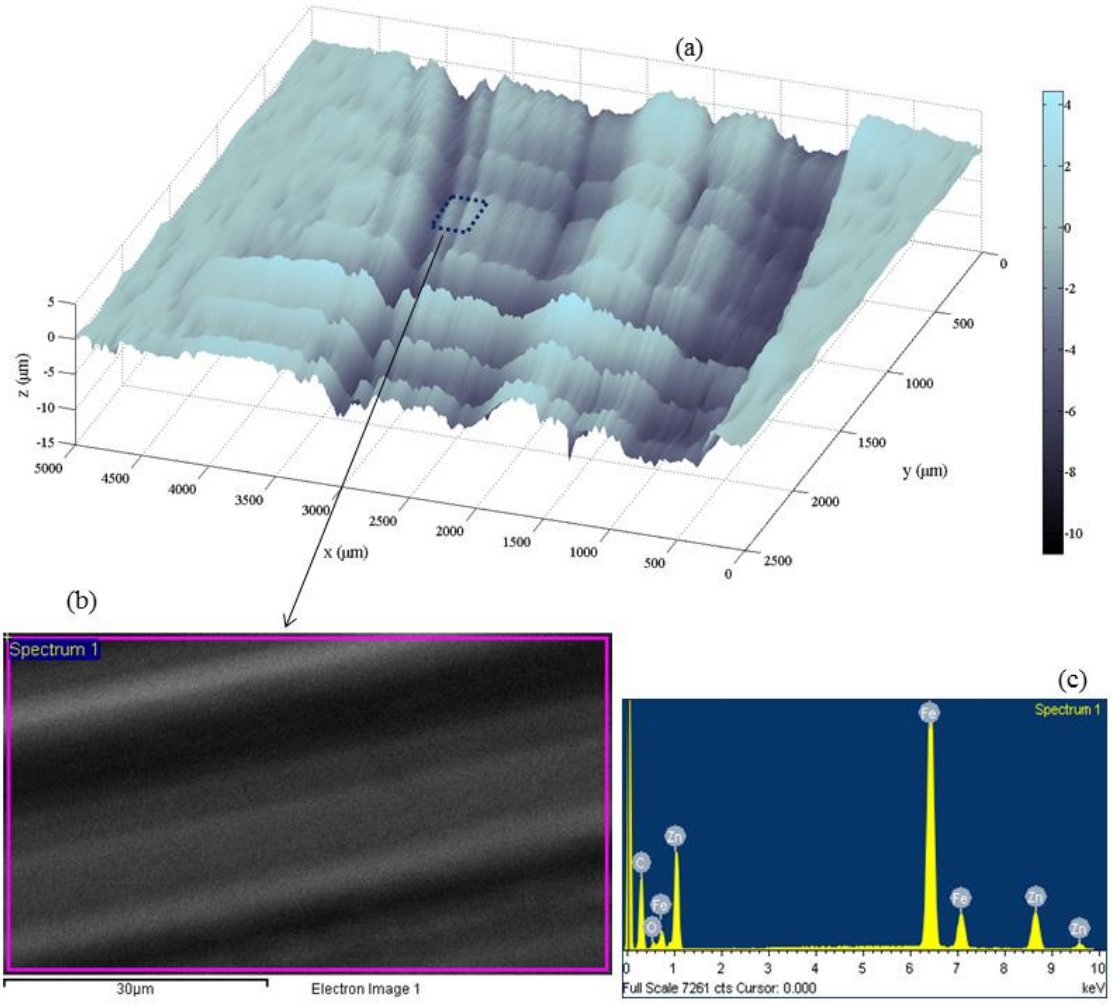

Figure 9: SEM image inside the wear groove for lubricant with no nanoparticles additive and its material composition using EDS.

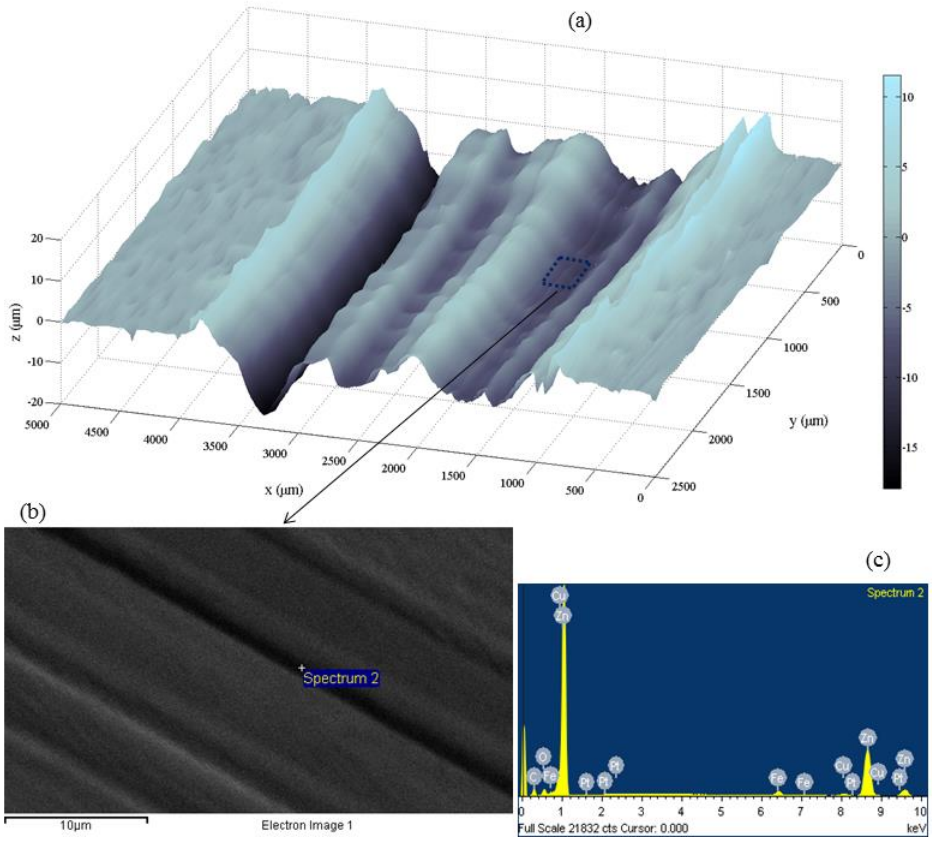

Figure 10: SEM image for the surfaces tested with 0.5%wt CuO nano-lubricant and its material composition using EDS.

Figures 11 and 12 present the SEM/EDS result for surfaces tested with 1.0% and 2.0%wt nano-lubricant, respectively. In Fig. 11(c), the high traces of iron suggests that the zinc plating has worn through, but the concentrations of copper suggest that the CuO particles could also be deposited on the inside of the wear grooves. This is in contrast to the surfaces worn while submerged in a base lubricant with no CuO particles because they have no signs of copper (see Fig. 9). Figure 11(d) shows the copper element mapping of the same surface and indicates a well dispersed distribution of nanoparticles adhering to the surface in and outside of the wear grooves. The same arguments stand for Fig. 12 and the copper element trace appears to also be randomly distributed. Using EDX the average weight fraction of copper detected on the surfaces exposed to the nano-lubricant was measured to be 1.51 %at.

The sample surfaces studied in this work are zinc-coated steel disks and therefore, a comparative study of the surface composition yields more insight on the particle-surface interaction. That is why the analysis of the original surface (Fig.8 (c)) shows that the majority of the surface is made out of zinc with some minor trace of the steel beneath the coating is detected (Fe, C, Cr). Fig. 9(c) shows the composition of a surface tested with the base oil. Here higher traces of steel and less traces of zinc are detected which indicates that the coating is partially worn. Fig. 10(c) shows the composition of a surface tested with the 0.5 %wt CuO nano-lubricant. High traces of zinc and low traces of steel (Fe, C, Pt) beneath the coating suggest that this is a relatively shallow groove. Fig. 11(c) shows the composition of a surface tested with the 1.0 %wt CuO nano-lubricant. High traces of steel (Fe, C) and low traces of zinc suggest that this is a relatively deep groove where the coating is almost worn away. Fig. 12(c) shows the composition of a surface tested with the 2.0 %wt CuO nano-lubricant. Mild traces of zinc and steel (Fe, C) suggest that this is a medium groove. Therefore the overall conclusion of Figs 10, 11, 12 is that particles are adhered to the surfaces in all cases regardless of the depth of the grooves. This suggests that the adherence of the particles does not depend on the high pressures within the asperity contacts as is theorized to be the case with many lubricant additives. The minute trace of platinum (Pt) in Fig. 10(c) and chromium (Cr) in Fig. 8(c) is coming from the additives in the alloy steel and concentrations are marginally detectable in the accuracy of the EDX machine and that is why these elements are not detected in the rest of the results.

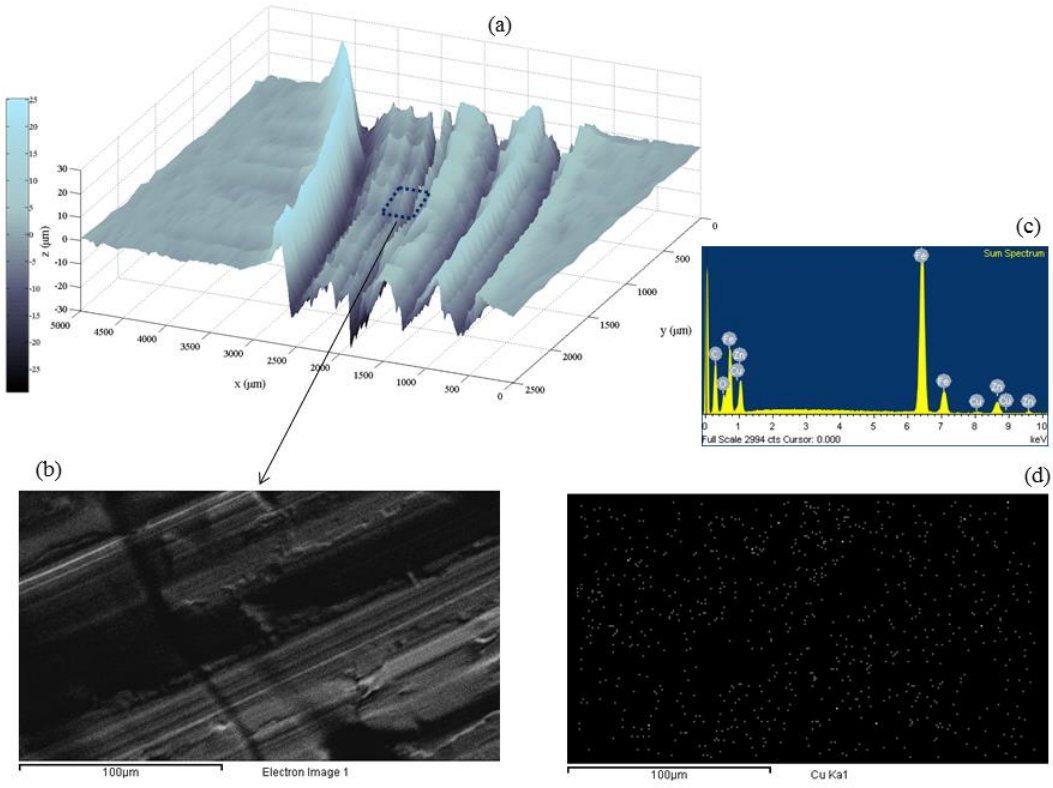

Figure 11: SEM image for the surfaces tested with 1.0%wt CuO nano-lubricant and its material composition using EDS.

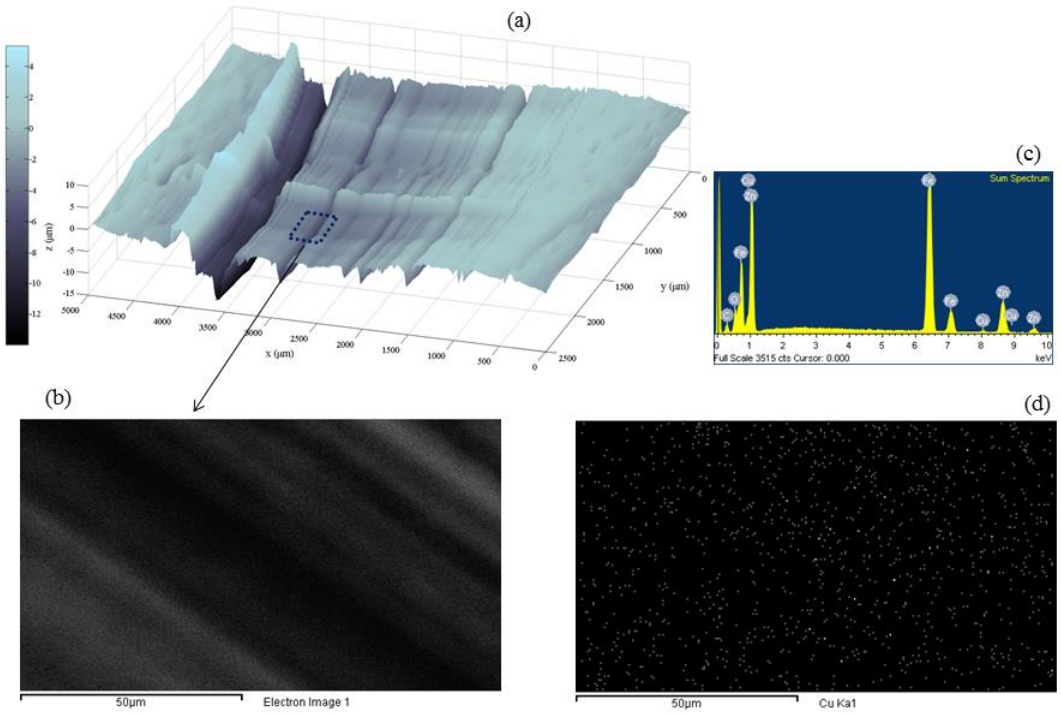

Figure 12: SEM image for the surfaces tested with 2.0%wt CuO nano-lubricant and its material composition using EDS.

2.3. Discussion

Several enhancing and modification mechanisms have been proposed for nanoparticle lubricants in the boundary lubrication regime in the literature, such as: viscosity alteration, thermal stability enhancement, mending worn surfaces and the rolling effect of nanoparticles. Based on the results and discussions presented in this paper, viscosity and thermal properties are affected by the CuO nanoparticles. However, the effect of these two mechanisms is minimal in the boundary lubrication regime where tribology is dominated by the contact of asperities. Particle deposition is evident and the element of copper is present at all the sample surfaces tested with the nano-lubricant. However, the dispersion of particles on the surface is random and is not sufficient to replace a significant portion of the worn material. Therefore, the mending mechanism is not evident in our tests. In contrast, the deposition of nanoparticles happens randomly in the contact zone and the average concentration of CuO deposited on the surface is on the

same order as the nanoparticle concentration in the lubricant. The other mechanism, nanoparticles rolling and acting as nano ball bearings implies that the use of a nano-lubricant should result in minimal wear which is not the case in our studies. It is proven that nanoparticles can roll in between surfaces in contact [11], however, based on the extensive wear in our samples it is probably not a dominant mechanism for the current type of particles. Particles of the stable nano-lubricants (such as the one studied in this paper) are able to exist as individual particles and don't form clusters in the suspension. In this paper particles are well coated with the surfactant and several filtration techniques [58] were used to ensure the quality of surfactant in the nano-lubricant. One can use the Kinetic energy theory and Brownian motion to characterize the motion of suspended particles. Calculations show that nanoparticles studied in this paper have an average Brownian velocity of 0.4 m/s which is significant and suggests that particles are dispersed throughout the contact region and are not likely to sediment physically in the local valleys. Moreover, Figs 11(d) and 12(d) show a random distribution of particles throughout the contact zone on peaks and in the valleys. Therefore, it is evident that particles are dispersed randomly throughout the contact zone and are able to infiltrate the contact regions. This would disregard the hypothesis that the majority of particles fill up valleys and are not engaged in contact.

Alternatively, the reduction of friction monotonically continues as more nanoparticles are dispersed in the lubricant. Also, wear seems to be a function of nanoparticle concentration. Based on the all the discussions and results, we would like to suggest the nanoparticles actually reduce the real area of contact and therefore reduce friction in the boundary lubrication. This theory implies that, particles engaged in contact would keep surfaces apart around the particles which results in the reduction of real area of contact, see Fig. 13. A decrease in the real area of contact translates to a reduction of the friction coefficient. As more concentrated nano-lubricants are used, more particles would be engaged in the contact which explains the monotonic reduction in the friction coefficient versus particle concentration in the tests. In addition, these particles would bear high

pressures and induce abrasive wear by plowing on the surface. The number of particles in the contact would increase as the nanoparticle concentration increases which is going to decrease both the average particle/surface contact pressure and the plowing abrasive wear. It should be noted that the stability of the nano-lubricants is crucial to avoid any aggregation, precipitation and clustering effects. In order to avoid these effects, the concentration of nano-lubricants is limited to 2.0 %wt in this study. However, it is reported in the literature [38-40] that the nanoparticle effect on wear and friction would saturate at a certain concentration. The saturation concentration depends on the type and size of the particle, as well as the properties of the base oil.

The mechanism of reduction in the real area of contact needs further investigation and study to be fully proven. One helpful study could be the characterization of the size of nanoparticles prior to and after the tests which can prove the abrasive nature of particle-surface contact. It should be added that various nanoparticles behave differently based on their mechanical behavior as governed by chemical and physical properties (As an example, the enhancing mechanism of fullerene-like WS2 (MoS2) nanoparticles is known to be exfoliation and coating the surface) and arguments raised in this chapter are currently limited to the CuO/SOA nanoparticles studied.

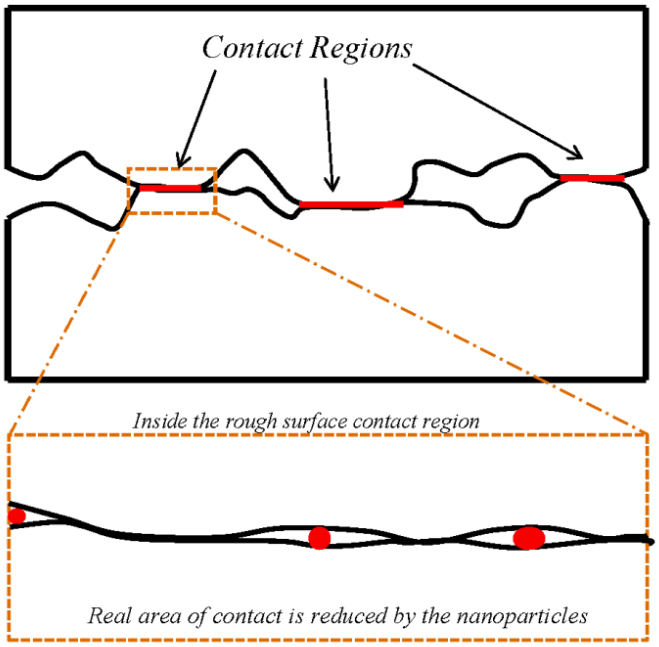

Figure 13: Illustration of the proposed mechanism, reduction of the real area of contact by the nanoparticles.

2.4. Conclusion

CuO/SOA nanoparticles are added to mineral base oil in the absence of any other lubricant additives using dodecane as a dispersing agent. The results for the nano-lubricant are then compared to the results of a base oil with the same concentration of dodecane. A disk-on-disk friction tribometer is used to test lubricants in the boundary lubrication region. The values of the friction coefficient and steady state temperature are then recorded for different values of applied normal load. Results show that, the friction coefficient decreases by 14 and 23% for the CuO nanoparticle concentrations of 1.0 and 2.0%wt, respectively. The steady state temperature is also 10^{o}C lower on average for nano-lubricants which could be the result of the higher thermal performance of nanofluids and/or the lower friction of the nano-lubricants. The viscosities of the nano-lubricants increase by an average value of 10% and 20% for the nanoparticle concentrations of 1.0% and 2.0%wt, respectively. The Stribeck curve was introduced

which consolidates the friction and the viscosity results into one curve. Wear volume shows a peak at the 1.0%wt and is less for a 2.0%wt concentration of nanoparticle in the lubricant. The SEM/EDS analysis measured the stoichiometry of copper element to be 1.51 %at on the surface samples tested with the nano-lubricants. Based on the results different possible enhancing mechanisms were discussed and the reduction of real area of contact was proposed as the dominant mechanism for the CuO particles in this work. The proposed mechanism is compatible with the friction and wear experimental results. Nonetheless, more investigations are needed to fully prove the proposed mechanism.

3. Analytical multi-scale contact model for nano-lubricants

Prior to this work, there was no contact model for nanoparticle lubricants in contact between rough surfaces. The effect of nanoparticles on the real area of contact and contact force can be investigated using an analytical model. The goal of this part of the current work is to develop such a contact model and relate the contact parameters to measurable parameters such as friction and wear. This model can also be used to further investigate the proposed reduction in the real area of contact mechanism. That is believed to reduce the friction in the nanoparticle lubricated surfaces.

The focus of this study is to investigate the mechanisms governing the wear and friction in the lubrication system of silicon nanoparticles suspended in a lubricant. Silicon nanoparticles are chosen because of the relative wealth of available knowledge compared to other particles. The methodology used in this work uses two sub-models to handle the different scales of contact (i.e. a rough surface contact model and a statistical particle contact model). The rough surface contact model considers the contact of roughness features and provides predictions of the average contact pressure and rough surface contact area. The statistical particle model is used to model particles inside the contact regions of the rough surfaces. This sub-model reports the area of contact of the actual nanoparticles, the void area around the particles, the forces acting on the particles, and the distribution of the deformation mechanisms of the particles [72]. The results from the model are presented and discussed throughout the section.

The approach taken in this section tries to identify, quantify and evaluate the most influential contact parameters affecting the system into a model that can illuminate the mechanisms behind the friction and wear behavior of nano-lubricants. This model is based on the extensive available data on the nanoparticles and nanotribology mentioned earlier. However, it is still early to claim that such a model would be quantitatively

accurate and includes all the critical details. Rather, its objective is to understand the 'big picture' and relationships between the mechanics of particles and surfaces with friction and wear.

3.1. Methodology and assumptions

The system of interest in this paper is composed of rough surfaces separated by a stable nano-lubricant, such as those in [58], working in the boundary lubrication regime with no significant hydrodynamic lift (nominally flat surfaces). If surfaces were pushed into contact, the lubricant would squeeze out until asperities initiate contact resulting in contact regions between peaks or asperities. Once the surface separation is lower than the particle diameter, particles are entrapped into contact within these contact spots. Particles in contact would separate surfaces locally, resulting in the formation of void areas in the vicinity of particles (see Fig.14). The change in the real area of contact induced by the voids as well as the particles reaction force would alter the contact mechanics.

Therefore, the system of interest in this paper includes two distinct ranges of scale which dominate the mechanics. Contact between rough surfaces which depend on the roughness features that are known to be in the scale of microns (for most engineering surfaces), and at smaller scales there are the nano-sized particles. The methodology in this work utilizes two well-known contact sub-models to handle these different scales. A multi-scale rough surface contact model solves the contact between surface asperities. The model reports the real area of contact between surfaces (A_s) and average contact pressure (P^*). A statistical (Greenwood Williamson type[73]) contact sub-model considers the effect of particles inside A_s and also includes the scale dependent properties of particles. This sub-model reports force (F_p), contact area (A_p) and the void area (A_{void}) created by particles. Before discussing more details on the afore-mentioned sub-models, certain assumptions need to be discussed.

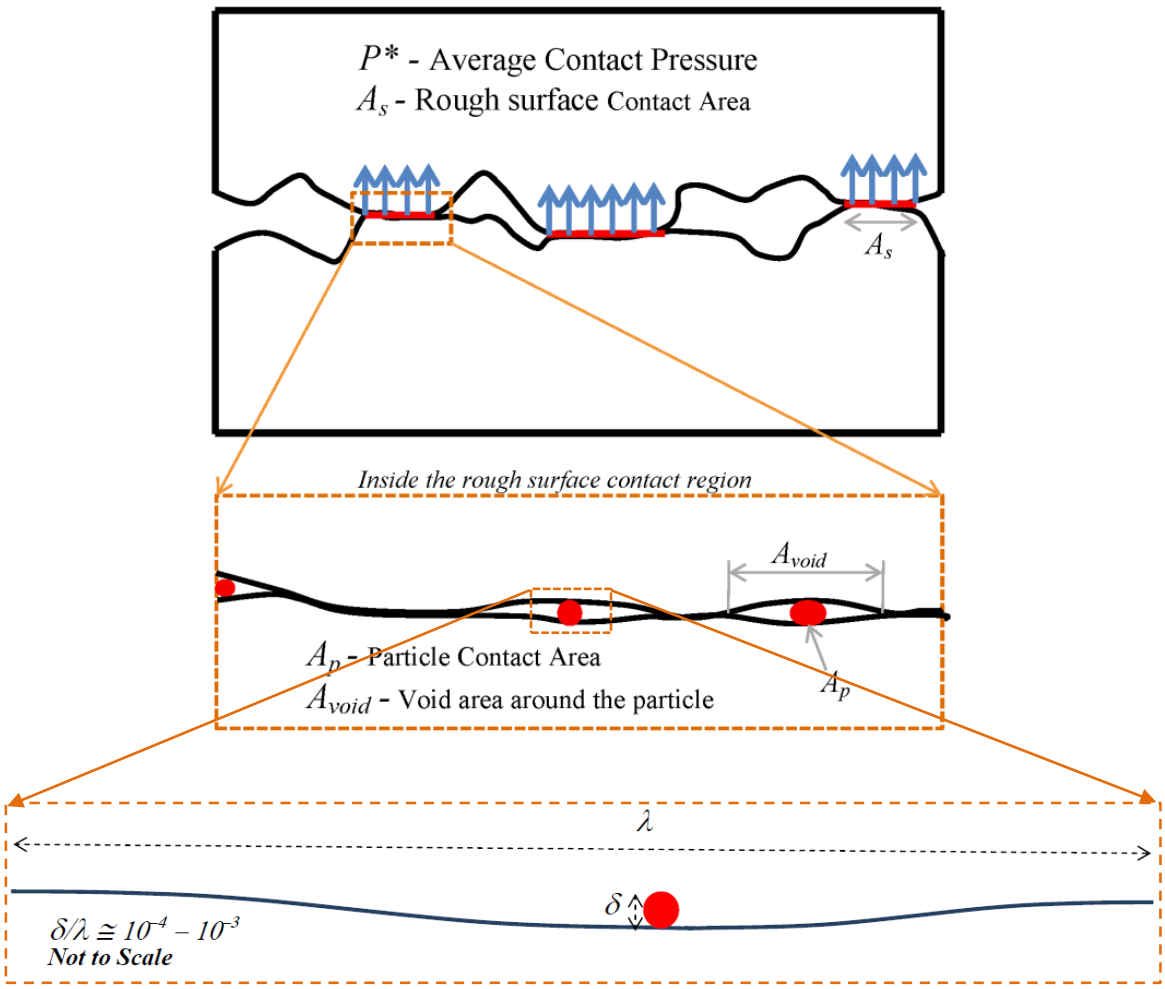

Figure 14: Illustration of stacked rough surface and statistical model.

One assumption associated with the statistical particle sub-model is that the surfaces inside the contact region are effectively flat compared to the dimensions of the particles. The goal is to show that the surface dimples at the nano-scale can't accommodate a nanoparticle and are in fact much wider as compared to the geometry of the spherical nanoparticles. In order to show this, a fast Fourier transform is used to decompose the surface into different scales. Each scale is defined by a sine wave which is also defined by an amplitude (δ) and wavelength (λ). Measurement on different engineering surfaces shows that the ratio of amplitude to wavelength ($B = \delta/\lambda$) is usually in the range of 10^{-4} to 10^{-3} regardless of the scale [74]. The dimples on the surface at the nano-scale can be

regarded as the valleys of the sine waves at that scale which has a *B* value of about 10^{-4} to 10^{-3}. The aspect ratio of spherical particles is *one* which means that if a particle of size δ is placed into the valley of a sine wave with an amplitude that is equal to the particle diameter (δ), the wave length of that sine wave is 10^{4} to 10^{3} times the value of δ (see Fig. 14). The difference in the aspect ratio of the decomposed surface sine waves and nanoparticles at the same δ value suggests that surfaces around the particles are effectively flat in comparison to the geometry of the particles.

The effect of fluid pressure also needs to be examined. The fluid pressure around a particle could alter the deformation and fracture characteristics of the nanoparticle. In order to evaluate the importance of this effect one can compare the fluid pressure to the failure strength of silicon nanoparticles considered in this section. The maximum fluid pressure should be less than the surface contact pressure. Therefore, for the sake of evaluating the assumption and considering the worst case scenario, the maximum fluid pressure is deliberately overestimated using a dry contact model. In addition, the lubricant pressure would result in a rise in the hydrostatic stress of the particle which would not cause yielding, but may cause brittle failure. Calculation for three different actual surfaces assumed in this work has been done according to the multi-scale contact model [74]. Results show that the maximum fluid pressure corresponds to the roughest surface ($\sigma_q = 0.18\ \mu m$) and is *0.41 GPa* whereas the minimum failure strength of the nanoparticles considered in this study is measured to be *10 GPa* [3, 33]. So the overall effect of pressure on the failure of particles is less than 5.0% and for the sake of simplicity in the current work the effect of fluid pressure on the particle deformation and failure is ignored. Nevertheless, the fluid pressure would resist the compression of the particles and delay the fracture of the particle. Therefore it would promote the effectiveness of the particles inside the contact region. However due to the presence of non-continuum and size effects in the particle/surface/lubricant system (especially under tangential motion) further investigation of the system is necessary.

3.2. Modeling

This section discusses and describes the details of the full model. Firstly the contact sub-models, namely the multi-scale rough surface contact model and statistical nanoparticle model, are discussed. Secondly, the algorithm used to find the overall solution is presented. Lastly, the fundamental models for friction and wear are presented.

3.2.1. Rough surface sub-model

A multi-scale rough surface model [74, 75] was chosen to describe the contact between rough surfaces. The model uses fast Fourier transforms to decompose the rough surface into stacked sine waves. Using superposition the model finds the average contact pressure required to overcome all the scales of roughness and predicts the real area of contact. Equations (1-4) present the model, where B is the ratio of δ/λ for different scales of roughness, E' is the effective elastic modulus (contact modulus), S_y is the yield strength, ν is the Poisson ratio, P^* is the average contact pressure, and F_s and A_s are the contact force and real area of contact between surfaces. The model predicts a contact pressure based on the maximum value of B represented by B_{max} and distinguishes between the elastic and elastic-plastic regimes by the critical value of B_c (see Eq.(3)).

$$P^* = \sqrt{2}\pi E' B_{\max} \qquad \text{for } B_{max}<B_c \tag{1}$$

$$P^* = \sqrt{2}\pi E' B_{\max}\left[\left(\frac{12\pi E' B_{\max}}{\sqrt{2}S_y e^{2\nu/3}} + 7\right)\Big/ 11\right]^{-3/5} \qquad \text{for } B_{max}>B_c \tag{2}$$

$$B_c = \frac{\sqrt{2}}{3\pi}\frac{S_y}{E'}e^{2\nu/3} \tag{3}$$

$$A_s = \frac{F_s}{P^*} \tag{4}$$

The average rough surface contact radius (a_{rs}) can also be found using this model. According to Jackson et al [76] a_{rs} is found to be given by Eq. (5) where λ_{max} is the asperity wavelength corresponding to B_{max}.

$$a_{rs} = \frac{\lambda_{\max}}{\sqrt{2\pi}} \tag{5}$$

3.2.2. Statistical nanoparticle contact sub-model

Greenwood and Williamson (GW) [73] originally developed their model to consider rough surfaces in contact. However, a similar statistical approach can be re-engineered to model nanoparticles in contact between two flat surfaces. The height distribution and the asperity density considered in the original GW model can be reinterpreted as the particle size distribution and nanoparticle density between surfaces, respectively. The nanoparticle density (η) and density of the nano-lubricant (ρ_{sol}) need to be modeled based on practical and measurable parameters. The density of the nano-lubricant can be found from Eq. (6)

$$\begin{aligned} \rho_{sol} &= 100\left(\frac{wt\%}{\rho_{NP}} + \frac{100 - wt\%}{\rho_{\text{lub}}}\right)^{-1} \\ vol\% &= \left[0.01 - \frac{\rho_{NP}}{\rho_{\text{lub}}}\left(0.01 - wt\%^{-1}\right)\right]^{-1} \end{aligned} \tag{6}$$

where ρ and *wt%* are the density and weight percent of nanoparticles in the final solutions. Subscripts "*NP*", "lub" and "sol" refer to nanoparticle, lubricant and solution respectively. The relation between vol% and wt% is also given in Eq. (6) based on simplistic proportionalities.

Nanoparticle density (η) is considered to be the number of nanoparticles (N_{NP}) in contact per nominal area (A_n). Considering d as the separation of two surfaces, the total volume of nano-lubricant in between the surfaces is $v_{sol} = A_n d$. The total nanoparticle volume is presented in Eq. (7) where v_{NP} is the total volume of nanoparticles in the lubricant.

$$v_{NP} = \frac{\rho_{sol}\ wt\%\ A_n d}{\rho_{NP}} \tag{7}$$

Assuming spherically shaped nanoparticles with the distribution of $\phi(D)$, which is a function of nanoparticle size (D), one can formulate v_{NP} as a function of the distribution.

$$v_{NP} = \frac{\pi}{6} N_{NP} \int_0^\infty \phi(D)\ D^3 dD \tag{8}$$

Using Eqs. (7) and (8) the number of nanoparticles per nominal area of contact could be found from,

$$\eta(d) = \frac{N_{NP}}{A_n} = \frac{\rho_{sol}\ wt\%\ d}{100\rho_{NP}\left(\frac{\pi}{6}\int_0^\infty \phi(D)\ D^3 dD\right)} \tag{9}$$

Note that η is a function of surface separation (d) and as surfaces get closer this formulation automatically accounts for the change in the nano-lubricant volume and number of nanoparticles between the surfaces. In this work, the nanoparticle distribution (ϕ) is assumed to be a normal Gaussian function which is characterized by the average particle size and standard deviation (σ_g).

The statistical model also requires a single nanoparticle indentation model that accounts for nanoparticle deformation and failure. Close observation and in-situ experiments on single spherical silicon nanoparticles have been reported in the literature [2, 3, 33, 35]. Spherical silicon nanoparticles of size 30 to 150 nm were observed to act as brittle materials. The particles do not exhibit much hardening beyond failure and smaller particles show higher failure strength. Failure strain and failure strength of different size particles is reported. Based on the availability of data on the silicon nanoparticles, this type of nanoparticle was chosen for this work. A single nanoparticle indentation model is also needed to be employed in the statistical model. As reported [3], on average particles deform 45% prior to fracture. Therefore an already developed model [77] for heavily deformed spheres was modified to fit nanoparticle deformation data, see Appendix II for

more details. The model solves for the single particle area of contact and particle force, Eq. (A1-4).

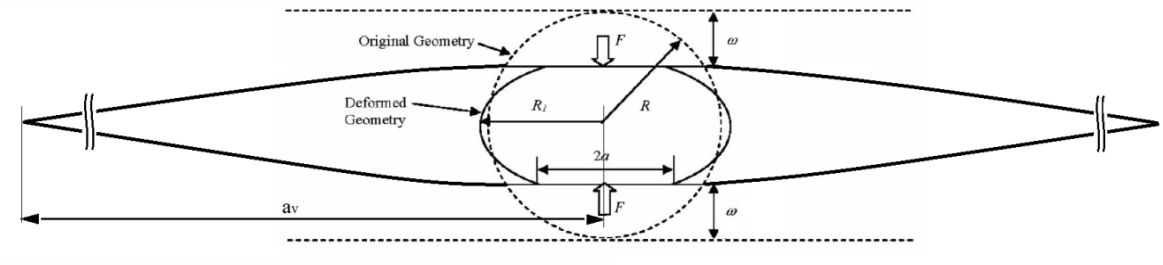

Figure 15: Schematic of the spherical particle contact mechanics.

As mentioned in the methodology section, particles separate surfaces resulting in void areas in the vicinity of particles (see Fig.15). Each nanoparticle in contact acts as a nano-indenter deforming the surfaces. However, the surfaces possess scale dependent properties as well (e.g. an experiment [78] on steel reports the nano-hardness to be around 10 GPa). Therefore for an accurate modeling of particle/surface interaction further investigation is required. In order to approximate the radius of the void area in this paper a half space elastic model [79] was used. Half the deformed particle diameter R-ω was assumed as the indentation on the surface and the surface profile equations were solved to find where the surfaces meet again and find the void radius per particle (a_v) and void area ($A_{void}=\pi a_v^2$), as shown in Fig. 15. R is the particle original radius and ω is the particle indentation depth as shown on the Fig. 15. The void radius is limited to the average rough surface contact radius (a_{rs}) (Eq.(5)). When the load on the particle exceeds the failure strength, the particle fails and the void is assumed to close. Note that in reality, particles are trapped and the voids could not completely close even if the particles fracture. This assumption would underestimate the void area and hence underrates the effectiveness for fractured particles. Therefore it is a conservative assumption which can be further improved once a better understanding of the surface/nanoparticle interaction in the lubricant medium has been achieved. So far three single nanoparticle parameters have been discussed; particle area of contact (A_{NP}), particle force (F_{NP}) and the void area

(A_{void}). Also, nanoparticle density (η) and size distribution (ϕ) was introduced and formulated. Rearranging and substituting all these parameters in a GW type model [73] yields the final form of the statistical nanoparticle model, given by

$$\begin{aligned}
\frac{A_p(d)}{A_n} &= \int_d^\infty \eta(y)\ \phi(y)\ A_{NP}(\omega, D)\ dy \\
\frac{F_p(d)}{E' A_n} &= \int_d^\infty \eta(y)\ \phi(y)\ \frac{F_{NP}(\omega, D)}{E'}\ dy \\
\frac{A_v(d)}{A_n} &= \int_d^\infty \eta(y)\ \phi(y)\ A_{void}(\omega, D, a, F)\ dy
\end{aligned} \tag{10}$$

A_p, F_p and A_v are the total contact area, force and void area of particles. In Eq. (10) particle interference ω is defined as $\omega=(y-d)/2$. Also note that in this set of equations η is a function of y and particles come into contact once the surface separation is smaller than the particle diameter. Also, ϕ is a function of y to account for particles of different sizes. The composite Simpson's method is used to solve the integrals of Eq. (10) in this work.

3.2.3. Algorithm

As discussed, the rough surface model uses the surface profile to find the average contact pressure (P^*) and the rough surface real area of contact (A_s). The statistical model solves for contact between two surfaces with the particles in-between and finds the real area of contact for particles (A_p), force carried by particles (F_p) and the void area induced by particles (A_v), see Fig.16 (Note that A_v also includes A_p).

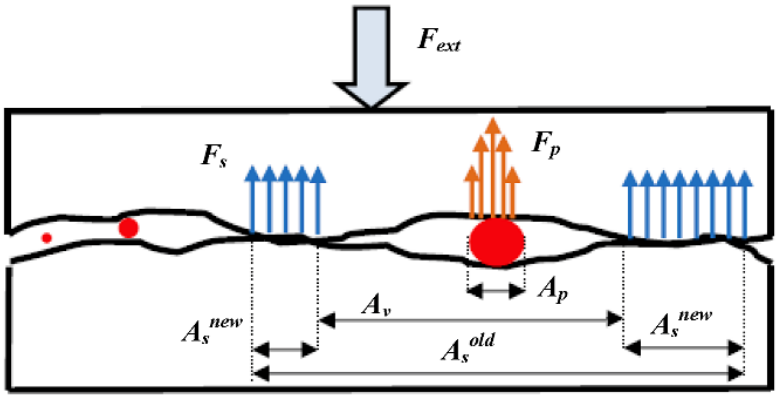

Figure 16: Schematic of the overall contact problem.

An algorithm was developed to solve the overall contact problem by balancing the forces between the two sub-models. The goal is to determine how much of the external load (F_{ext}) is carried by the surface (F_s) and how much is carried by the particles (F_p) and to check the force balance equation $F_{ext}=F_s+F_p$. Firstly, an external force of F_{ext} is assumed to be acting on the system and assuming all the load is being carried by the surface, the multi-scale model is used to find the P^* and A_s. Then initially assuming that the same average pressure, P^* is exerted on the particles, F_p is found to be

$$F_p = A_s P^* \tag{11}$$

Note that particles are assumed to be in contact where surfaces are in contact and this means that A_s should be regarded as the nominal area of contact for the statistical model. Based on the value of F_p the corresponding surface separation is found and A_p and A_v are found (using Eqs. (11)). Then the surface area of contact is updated as follows

$$A_s^{new} = A_s^{old} - A_v \tag{12}$$

The new surface force is then found based on the updated surface area $F_s=A_s P^*$. The force carried by particles is then updated based on $F_p=F_{ext}-F_s$ and the statistical model is used to find the new values of A_p and A_v. The next solution is found by going back to Eq. (12), updating the surface area and iterating through the steps again. The convergence is

checked in each iteration according to $\left|\left(F_s^{new}-F_s^{old}\right)/F_s^{old}\right|<10^{-3}$. The final solution is found by iterating through the loop and checking for the convergence criterion. In order to get a faster convergence the statistical model was solved first for various values of *d* and the solution was determined from a table and using interpolation through the overall algorithm.

3.2.4. Friction and wear models

The final solution of the contact problem reports A_s, F_s, A_p, F_p and A_v along with the statistical information on the nanoparticles in contact. Validating the direct result from the model is practically impossible. However, fundamental and simplistic friction and wear models can be utilized to translate the change in the contact force, real contact area and the statistical data on nanoparticles into measurable parameters. The accuracy of the friction and wear models will influence the quantitative accuracy of the final results but validation over general trends of the enhancement is made possible using fundamental models. The friction of the surfaces in contact is governed by the real area of contact and forces acting in the normal and tangential directions. Equation (13) can be used to find the coefficient of friction.

$$\mu=\frac{A_s\tau_s+A_p\tau_p}{F_{ext}} \tag{13}$$

τ_s and τ_p are shear stresses working on the surface/surface and particle/surface interfaces during sliding, respectively. There have been experimental and theoretical efforts to shed light on the behavior of nanoparticles in dynamic contact [11, 80, 81]. However, in this paper τ_s and τ_p are evaluated as the shear strength between lubricated surfaces in contact.

Combining the effect of particles and surfaces to find an overall model for wear in the system is a challenging task. However, based on the statistical data on particles one can find the particle induced wear using plowing abrasive wear models [79] (see Fig. 17).

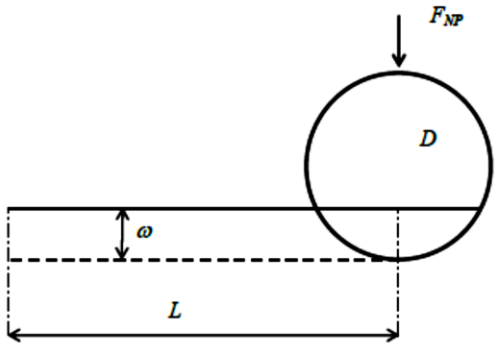

Figure 17: Schematic of the particle abrasive wear.

Spherical particles plowing on the surface can induce abrasive wear that is proportional to the cross section of particle to surface interference, see Eq. (14) and Fig. 17.

$$\frac{V_{NP}}{L} = \int_d^{\infty} \eta(y)\ \phi(y)\ A_{CS}(\omega, D)\ dy$$
$$A_{CS} = \frac{D^2}{8}\left\{ Sin^{-1}\left[\frac{8\omega(D-\omega)(D-2\omega)}{D^3}\right] - \frac{8\omega(D-\omega)(D-2\omega)}{D^3}\right\} \quad (14)$$

Where V_{NP}, L and A_{CS} are wear volume (induced by particles), sliding distance and interference cross sectional area between the particle and surface.

3.3. Results

This section presents the results of the discussed model for various case studies. The effects of particle concentration, distribution, size and surface roughness on the real area of contact and contact pressure have been studied. Consequently, the change in the real area of contact and pressure at the particle-surface interface is translated to an alteration in friction force and particle induced wear. See Appendix III for the numerical values used in the model and other complimentary data about the simulations.

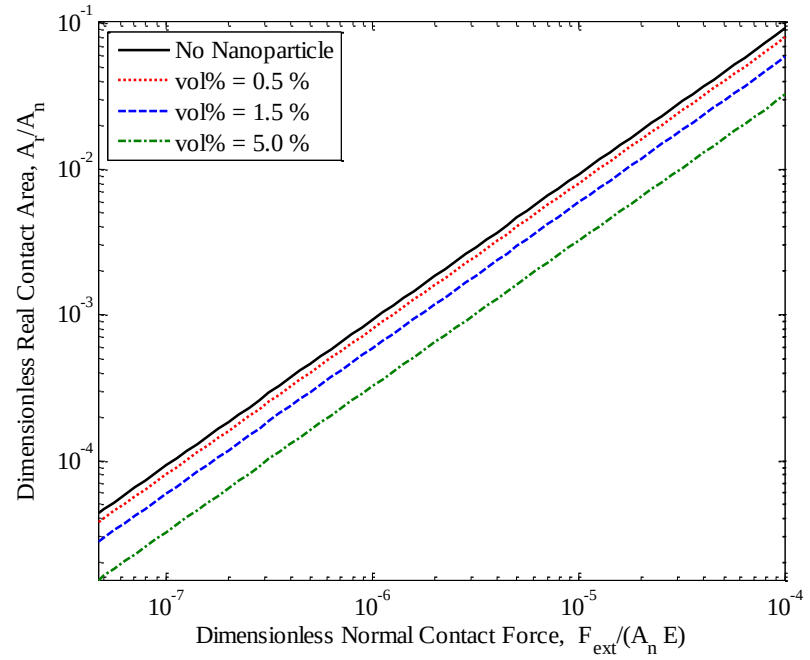

(a)

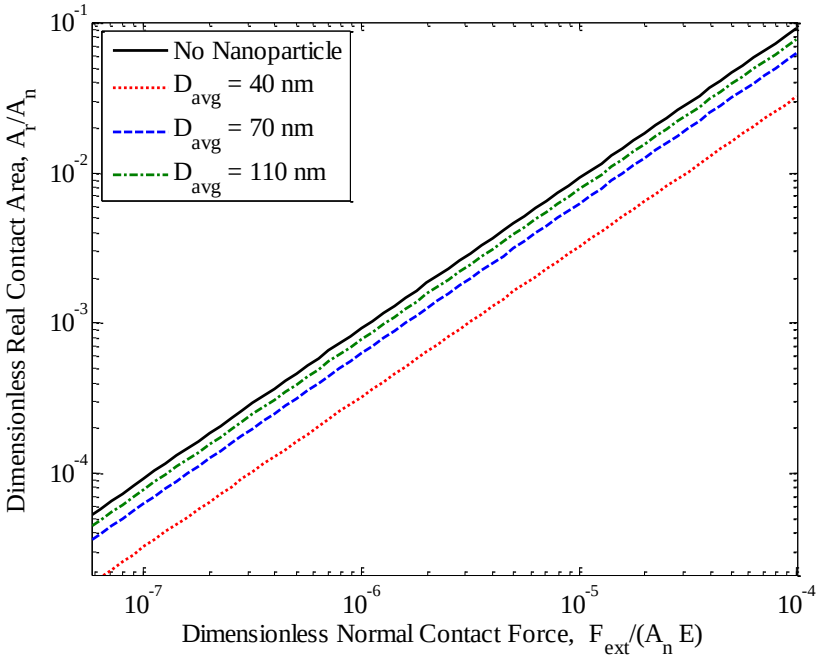

(b)

Figure 18: The effect of particle concentration (a) and particle average size (b) on the real contact area versus contact force.

The effect of nanoparticle concentration and average particle size is shown in Figure 18. In this study the surface roughness is 0.05μm and the standard deviation of the particle distribution is σ_g = 1.5 nm. A_r in this figure is the total real area of contact which is the combined particle and surface contact area, $A_r=A_s+A_p$. Figure 18(a) represents the effect of particle concentration for an average particle diameter of 40 nm. As the volume percent increases, the number of particles engaged in the contact escalates. This increases the void area induced in the vicinity of particles and reduces the real area of contact. The effect of various particle sizes for a volume concentration of 5.0% is presented in the Fig. 18(b). A decrease in the particle size results in a raise in the number of particles (given that volume concentration is held constant), which would consequently reduce the real area of contact. In this case, smaller particles also exhibit higher strength which amplifies the accumulative effect. In either case shown in Fig 18, the particles bear high pressures at the particle-surface interface and keep the surfaces apart in the vicinity of particles. This decreases the real area of contact and causes high pressure spikes in the particle-surface interface.

The effect of particle distribution on the real contact area is shown in Fig. 19. Figure 19(a) shows the dimensionless real area of contact versus dimensionless normal contact force for different distributions of particles all having the same average size (vol% = 5 and Rq=0.05 μm). The distribution of particles versus size is displayed in the Fig 19(b). Results suggest that, a sharper distribution of particles results in more reduction in the real area of contact between surfaces. Particles with a wider distribution engage in contact gradually which results in an enormous force on each particle and consequently particles tend to fracture in a cascading fashion. Whereas particles with a narrower distribution engage in contact simultaneously which results in a stiffer contact (in other words, particles withstand the contact force in large numbers). Figure 20, presents the number of fractured particles as a function of the surface separation that shows the cascading fracture of particles with a wider distribution.

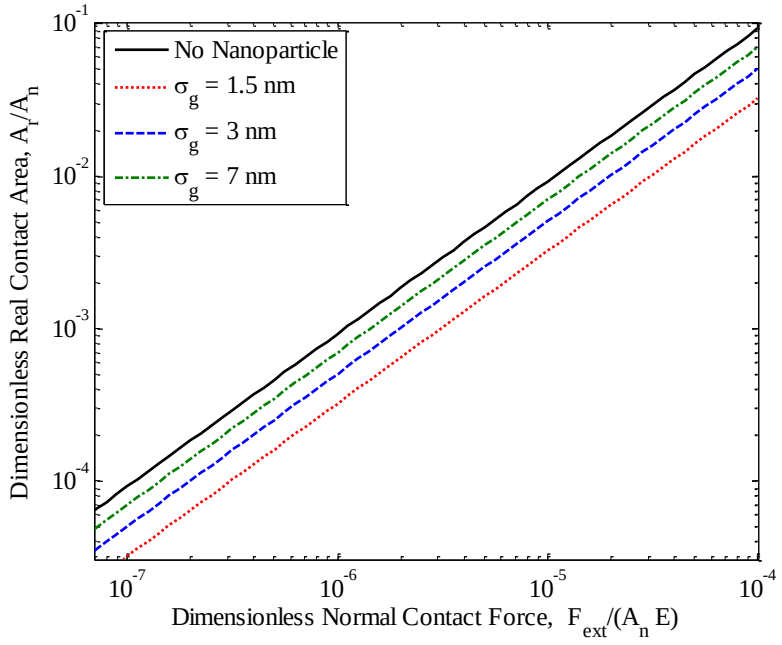

(a)

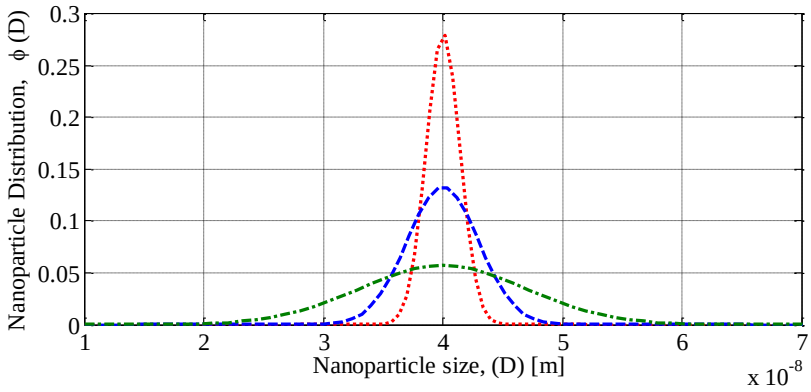

(b)

Figure 19: The effect of particle distribution on the real area of contact.

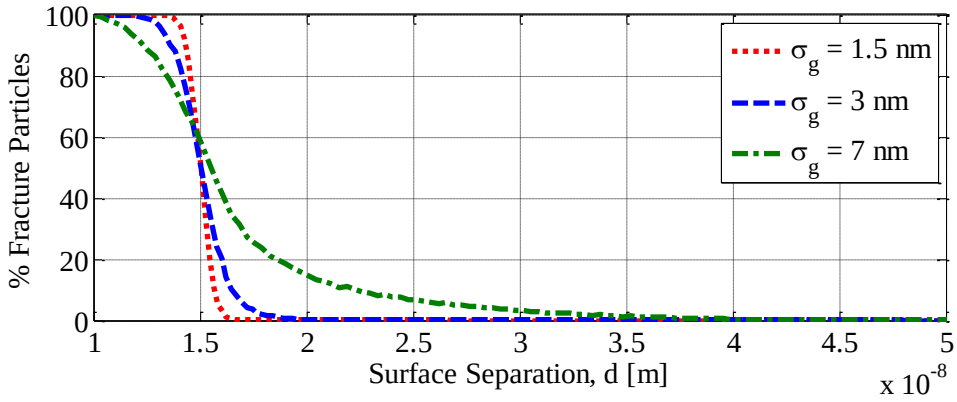

Figure 20: Fractured particles as a function of surface separation.

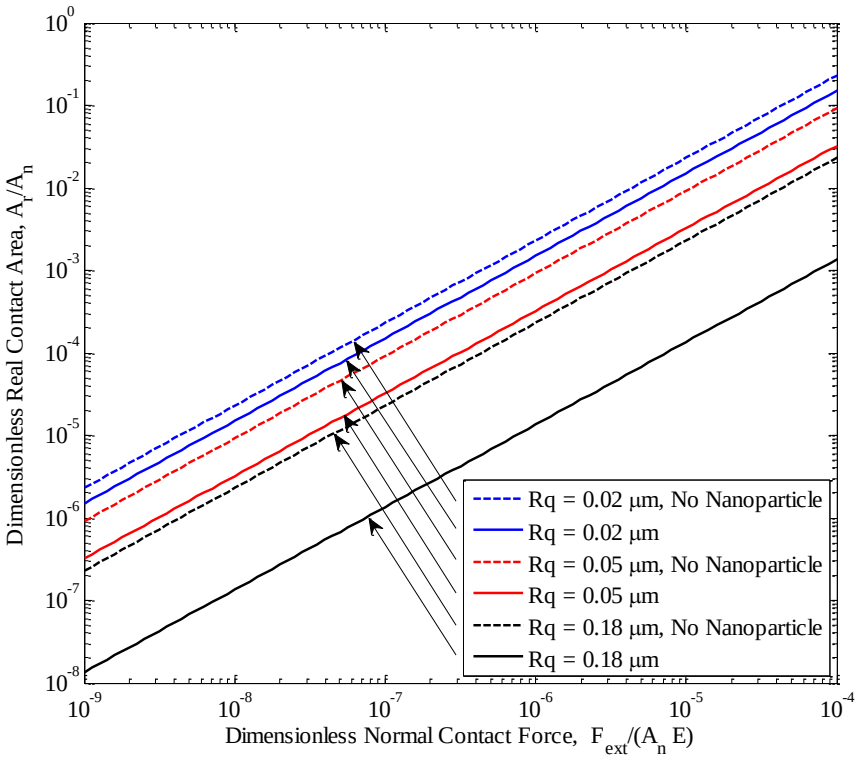

(a)

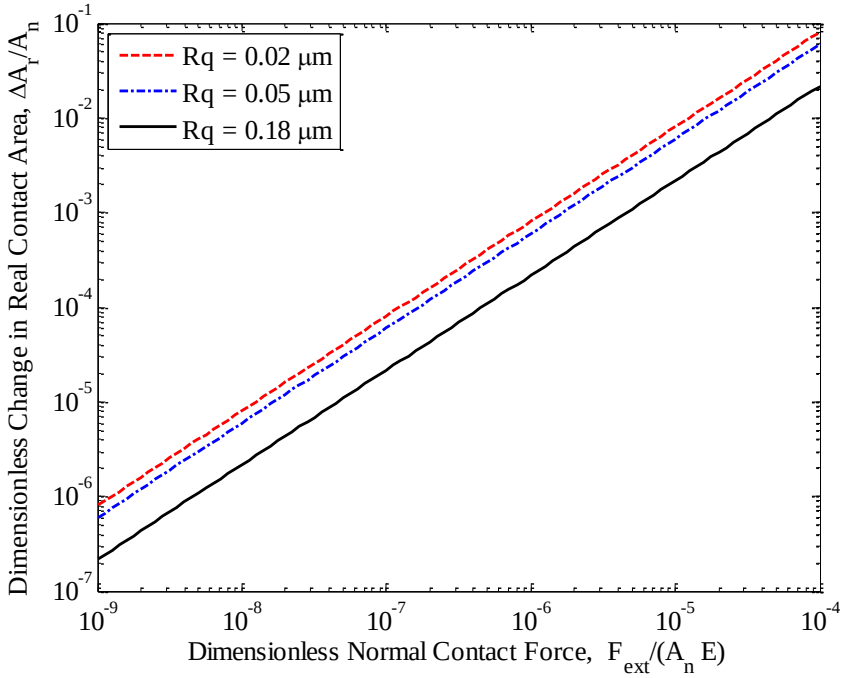

(b)

Figure 21: The effect of surface roughness on (a) the real area of contact versus contact force, (b) change in the real area of contact as the result of nanoparticles.

The effect of roughness on the contact's characteristics is presented in Fig. 21(a). In this study the particle content is 5.0 %vol and the average size of the particles is 40 nm with the distribution of σ_g = 1.5 nm. Particles stiffen the contact for different values of roughness. As would be expected the reduction in the real area of contact (Fig. 21(b)) is more as the surface roughness decreases which suggests that particles are more influential in the contact of smoother surfaces.

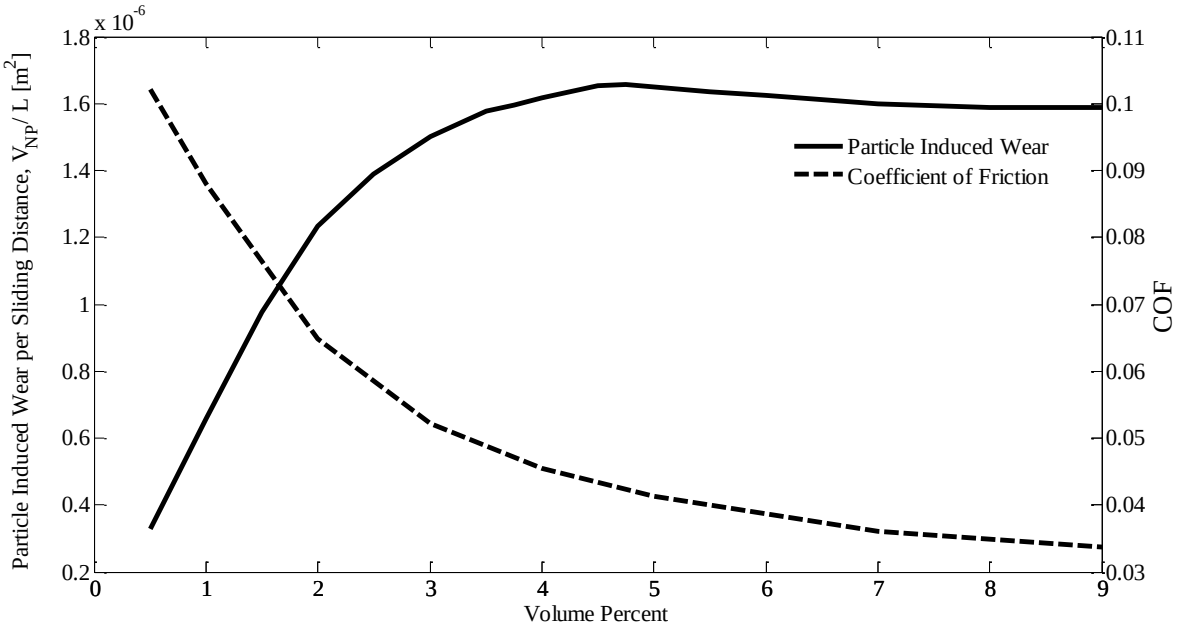

Figure 22: Coefficient of friction and particle induced wear versus nanoparticle content.

Figure 22 shows the variation of coefficient of friction (COF) and particle induced volumetric wear per sliding distance versus nanoparticle volume percent for Rq=0.05 μm, σ_g=1.5 nm and average particle size of 40 nm. An increase in the content of nanoparticles reduces the friction and lowers the COF and increases wear induced by particles. The decrease in friction is caused by the reduction in the real area of contact. As the particle concentration increases and more particles engage in contact, the average particle force decreases which will cease the increase in wear at a certain particle concentration. Note that the particle induced wear shown on Fig. 22 drops to zero as nanoparticle

concentration approaches zero which is due to the fact that conventional surface wear has not been included here.

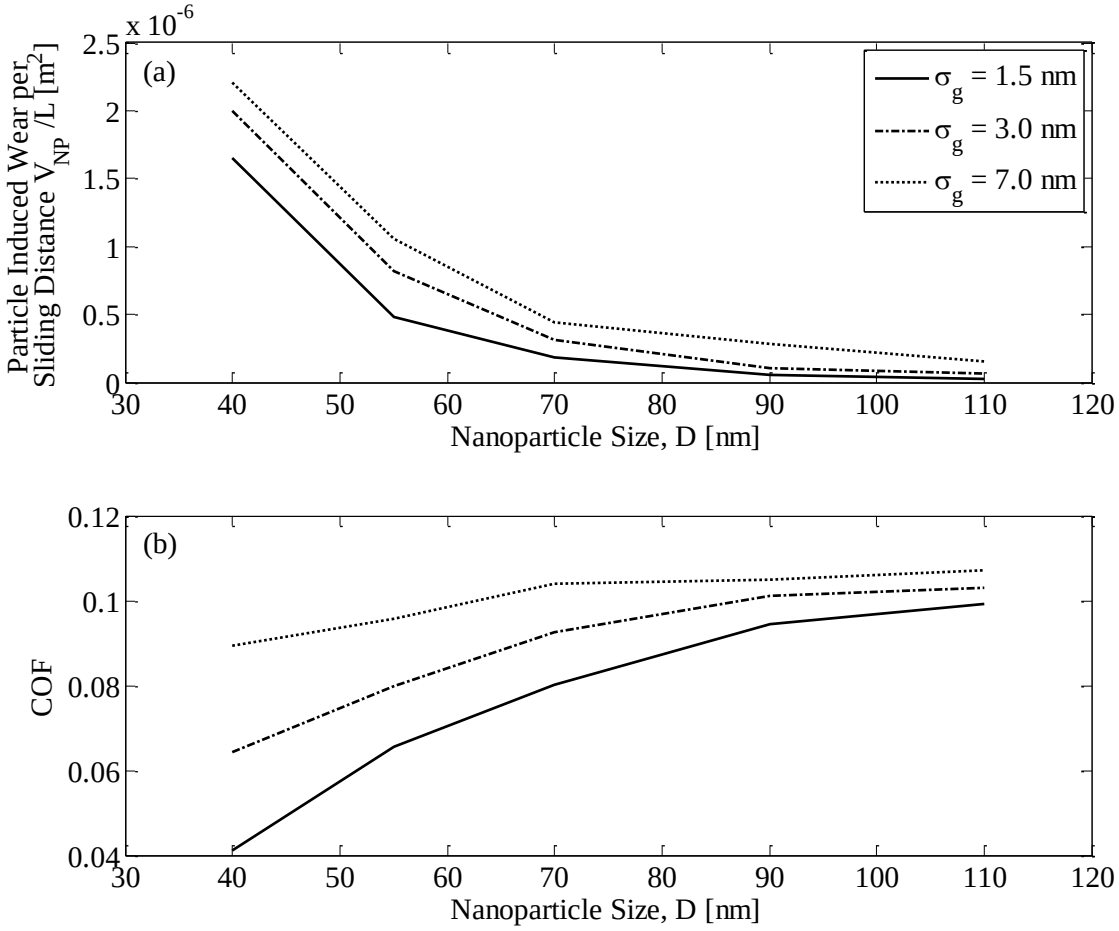

Figure 23: Particle induced wear (a) and coefficient of friction (b) changing with particle average size and distribution.

The effect of nanoparticle size and distribution on the particle induced wear and COF is presented in Fig. 23 for Rq=0.05 and 5.0 %vol of particles. Figure 23(a) suggests that smaller particles and particles with wider distributions of size, induce more wear. Here is a simple sequence to show this: 1. Wear is related to the number of particles multiplied by the cross section or $wear \propto N_{NP} \times A_{CS}$. 2. According to Eq.(9), $N_{NP} \propto vol\% / v_{avg,NP} \propto 1/D^3$ where $v_{avg,NP}$ is the average particle volume and vol% is constant. 3. $A_{CS} \propto D^2$ according

to Eq. (15). Thus combining the equations yields $wear \propto 1/D$ which suggests that wear is higher for smaller particles. Figure 23(b) shows that smaller particles and the particles with sharper distributions are more effective in reducing friction. This behavior is partially because of the size dependent properties of particles and partially controlled by the number of particles in contact. For instance, when the concentration of particles in a solution is held fixed the total number of the particles is also dependent on the average particle size.

3.4. Discussion

The third body nanoparticle multi-scale contact model presented in this study models the nanoparticles in contact and reports the change in the real area of contact and contact force. Even though silicon nanoparticles were studied, for the sake of available data, the general observations may stand for other kinds of particles as well. This is because nano-structures, including nanoparticles in general, exhibit an elevated strength [1-5, 33-35, 82] which is the source of the mechanisms modeled in this paper. Therefore, unless for particles with special physical or chemical characters e.g. particles capable of bonding with the surface, the general mechanism of reducing the real area of contact is in action. This makes the model applicable for qualitative comparison as long as the size of particles is substantially smaller than the average rough surface radius of contact, $D<<a_{rs}$.

The developed model suggests that particles reduce the friction in the system by keeping surfaces out of contact locally, resulting in a reduction in the real area of contact. Even though the force carried by the particles is small comparing to the force carried by the surfaces (for example on average $F_p/F_{ext} = 0.083$ for a lubricant with 3.0 %wt particles), the overall effect of particles on the contact area is found to be consequential. Figure 22 shows that friction further reduces if more particles are introduced in the lubricant yet eventually this effect saturates. This behavior has been observed experimentally and reported throughout the literature, repeatedly [37, 39, 41, 42] but never theoretically confirmed.

One of the key observations of the nanoparticle contact model is the effect of particle size distribution (σ_g) on the nano-lubricant effectiveness. σ_g controls the number of nanoparticles in contact (η, Eq. (9)) and also a wider distribution of particles could result in the gradual engagement of nanoparticles in contact and reduce effectiveness (Figs. 19-20). Particle induced wear and the friction coefficient also changes with σ_g, (see Fig 23), which makes σ_g an important parameter in nano-lubricant optimization and design. Despite this, the particles size distribution is not always a control parameter in the studies which could be one of the reasons that comparison between different nano-lubricants investigations is sometimes inconclusive.

In this work only the particle induced abrasive wear was modeled and the effect of different parameters was studied. The accumulative effect of surfaces and particles on the overall wear of the system is very complicated and needs further investigation. However, based on the developed model, very helpful observations and predictions can be made that helps better selection of nano-lubricants for further studies. In this work it is assumed that the particles are harder than the surface and abrade the surface. Therefore, soft particles and fullerene like particles[11, 80] (that can deposit layers on the surface) would not induce abrasive wear. Furthermore, these particles reduce the real area of contact which would diminish surface to surface wear and the overall effect of particles is a decrease in the system's wear. Harder particles, such as the silicon nanoparticles studied in this work, would induce wear. One can compare the particle induced wear (approximated by the model) to the lubricated surface wear (without particles) and decide if particles can practically promote wear. For instance, if particle induced wear is greater than the lubricated surface wear then the nanoparticles would increase wear. If the particle induced wear is predominantly lower than the lubricated surfaces wear then the addition of particles would not change the wear practically. However, if particle induced wear is on the same order as the lubricated surface wear, the competing effects of particle induced wear and reduction in the real area of contact would determine the overall effect of particles on the system. Therefore, particle induced

wear, as modeled in this study, can provide some guidelines for the better selection of particles for a lubricating system. Moreover, this argument suggests that particles could increase or decrease wear based on the lubricant and the surfaces in contact. Thus, particles should be carefully selected for different lubricating systems. Wear of different combinations of surfaces and particles have been studied and the results seem to agree with the general observations from the model and the arguments raised in this investigation [22, 38, 40].

3.5. Conclusion

A model for the third body contact of nanoparticles between rough surfaces has been developed. The model uses two sub-models to handle different scales of contact. Silicon nanoparticles of 40 nm to 110 nm with normal Gaussian size distributions are considered. The model suggests that particles separate surfaces locally resulting in a reduction in the real area of contact and a decrease in the friction of the system. Results also suggest that high concentrations of particles, smaller particles, narrower distributions of particles and smoother surfaces can boost the friction enhancement.

Wear induced by the particles is also reported that suggests hard particles would promote abrasive wear on the surfaces. However, results also suggest some methodologies to control the wear rate; (1) narrower distributions of particles help distribute the load on more particles and hence decrease the average pressure on the nanoparticles. (2) Particles reduce the real area of contact so if surface abrasive wear is higher than particle induced wear, particles could help separate surfaces locally and decrease wear. (3) Bigger particles produce less abrasive wear but are less effective in reducing the friction, therefore particle size is a tradeoff parameter one can use to tune wear and COF in the acceptable range.

The fact that there is not a single universal friction and wear model available (even for dry surfaces in contact) shows the challenges incorporated with modeling the friction and wear. Granted that the model can be further improved, the third body multi-scale contact

model presented in this work is a plausible and reasonably successful effort in connecting the properties of nano-lubricants to the measurable data. One of the products of the developed nanoparticle contact model is to provide guidelines for future experimental investigations and lubrication design engineers. Carefully designed experiments can focus on the mechanism proposed by the model and further verify the exact mechanisms. The results and discussions presented in this paper are only valid for the assumptions stated and similar approaches can be utilized to explore the nature of other nanoparticle lubrication systems.

4. A third body contact model for a particle contaminated contact

In the previous section [83] a system of nano sized particles (nanoparticles) was modeled between two rough surfaces in contact. The goal of that previous work was to recognize the relationships between the mechanics of nanoparticles and surfaces, with the change in the real area of contact, friction and wear. The model takes advantage of certain assumptions due to the specific scale of nanoparticles such as; 1. Particles are in contact where surfaces are in contact, 2. The surfaces around the particles are effectively flat as compared to the geometry of the nanoparticles. However, these assumptions are not valid for larger particles such as sand. The current work presents a statistical contact model for third body contact between rough surfaces. The model extends the Greenwood and Williamson (GW) [73] statistical method to a general third body contact model.

In order to apply the model to a practical situation and be able to evaluate the model by comparing to the experiments the sand contaminated electrical contact application was chosen. An electrical connectors' reliability is affected by several factors including corrosion [84], mechanical vibration [85], thermal effects [86] and contamination [87]. Dust particle contamination at the contact interfaces can cause electrical contact failures [87-90]. There are several early works published by Williamson et al [88], Mano [89] and Reagor et al [90]. A review in 2007 given by Ji Gao Zhang [87] reported the effect of dust contamination on electrical contact failure and showed that dust particle contamination was a main problem that could cause contact failures. The composition of dust is complicated. It was found that about 80% by weight of the materials were inorganic compounds, including quartz, various feldspars (albite, anorthoclase), micas (muscovite, biotite), gypsum, calcite, etc [91], roughly 20% of the dust contained approximately 20 kinds of organic materials, mainly alkanes and two ortho-benzendicarboxylic acid esters

[92]. Analysis of failed connector contacts showed that not only hard materials, such as silicon compounds, but also soft materials such as gypsum, mica and organic materials, may cause contact problems[87]. Thus, it is importance to study the contact model of particle contaminated electrical contacts and the effect of particle contamination on contact failure for device reliability. Sand (quartz) was chosen for this simulation since it is usually a main component of ordinary dust.

4.1. The Contact Model

First we need to choose appropriate parameters to characterize a system of particles on a surface. Let's assume that a group of particles with a total mass of M_p are uniformly dispersed on a surface having a total area of A_n, therefore the areal mass density of particles is, $m_p = M_p / A_n$. Also, let's assume that the particles possess a size distribution over a rage, characterized by $\phi_p(D)$, where D is the size of the particles. One can show that the areal volume density ($v_p = V_p / A_n$) of the particles [83] is

$$v_p = \frac{\pi N_p}{6A_n} \int_0^\infty \phi_p(D) D^3 dD \qquad (15)$$

where N_p is the total number of particles on the surface. Using the particles' density one can find v_p to be, $v_p = m_p / \rho_p$. Equating this equation with Eq. (15) one can find the number of particles per area to be as shown in Eq. (16). Equation (16) connects the number of particles per area to the measurable parameters m_p, ρ_p and ϕ_p.

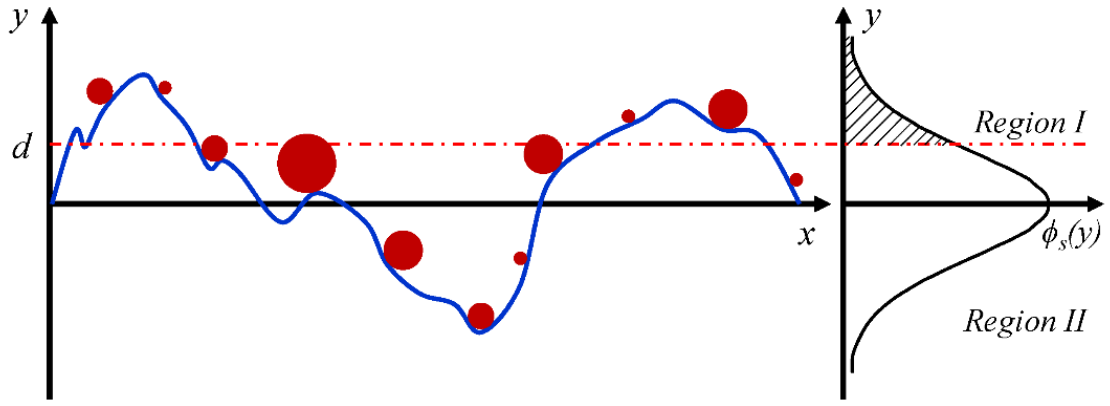

Figure 24: Schematic of the rough surface and the dispersed sand particles. The graph on the right shows the corresponding height distribution and the definition of region I and II based on the surface separation.

$$\eta_p = \frac{N_p}{A_n} = \frac{6m_p}{\pi\rho_p}\left(\int_0^\infty \phi_p(D)D^3 dD\right)^{-1} \tag{16}$$

It is common practice to develop contact models in terms of the surface separation (d). In order to define surface separation we need to assume that a rigid flat surface is in contact with a rough surface. The distance between the rigid surface to the average height of the rough surface at any given moment is the surface separation. Let's assume that the rough surface is isotropic with a height distribution of $\phi_s(y)$ and its profile is defined by, $y = y(x)$. In order to effectively develop the contact model, two regions have been defined based on the surface separation: Region 1, which refers to the portion of the surface with, $y \geq d$ and region 2 where, $y < d$. Fig. 24, shows the surface profile with the scattered particles on top and the corresponding surface height distribution. The surface separation of d is drawn with a red dashed line. Therefore the surface portion above the line is region 1 and the rest is defined as region 2. It is obvious that all the particles that happen to be sitting in region 1 are in contact for a surface separation of d. However, particles in region 2 may or may not be in contact depending on their location and size. As shown in Fig. 24, some of them can be in contact while others are out of contact.

In region 1 both particles and surface asperities (peaks) are in contact, therefore one can combine the effect of both to find the overall contact force and area of contact, as shown by Eq. (17).

$$\begin{aligned}
\frac{F^I(d)}{E' A_n} &= \int_d^\infty \eta_s \ \phi_s(y) \ \frac{F_{asp}(\omega)}{E'} dy + \int_0^\infty \eta_p^I(d) \ \phi_p(y') \frac{F_p(\omega', y')}{E'} dy' \\
\frac{A_r^I(d)}{A_n} &= \int_d^\infty \eta_s \ \phi_s(y) \ A_{asp}(\omega) \ dy \\
\frac{A_p^I(d)}{A_n} &= \int_0^\infty \eta_p^I(d) \ \phi_p(y') \ A_p(\omega', y') \ dy'
\end{aligned} \tag{17}$$

In Eq. (17), η_s is the areal asperity density for the surface, *E'* is the reduced elasticity, F_{asp} and A_{asp} are the single asperity force and area, F_p and A_p are the single particle force and area and ω, ω' are the asperity and particle indentations, respectively. η_p^I is the areal density for the particles in region 1 which is defined as follows.

$$\eta_p^I(d) = \eta_p \int_d^\infty \phi_s(y) dy \tag{18}$$

Note that in Eq. (17), the first integral calculates the overall effect of the surface asperities by integrating over asperity height and the second integral calculates the effect of the particles in region 1 by integrating over the particle size. Also, note that A_p^I is not added to A_r^I because it overlaps the area of the asperities.

Region 2 is more complex because only a portion of the particles in this region are in contact. Equation (19) presents $\eta_p^{II}(d,y'')$ which is the areal density of the particles sitting on the surface at $y = y''$ and in contact when surface separation is *d*. Here is an explanation for (5), N_p is the total number of the particles, so therefore $N_p \times \phi_s(y'')$ is the number of the particles sitting at height $y = y''$. Among these particles only the ones larger than the

gap (*d-y″*) are in contact, therefore the number of particles in contact would be $N_p\ \phi_s(y'')\int_{d-y''}^{\infty}\phi_p(q)dq$, which is Eq. (19) if divided by A_n.

$$\eta_p^{II}(d,y'') = \eta_p\ \phi_s(y'')\int_{d-y''}^{\infty}\phi_p(q)dq \tag{19}$$

The next step is to find the average force and area of contact for particles in region 2 sitting on the surface at *y=y″* and when the surface separation is *d*. Particles in contact in this region are of different sizes. The average force and area of contact for these particles can be formulated as given by Eq. (20).

$$\begin{aligned}\frac{F_{avg}^{II}(d,y'')}{E'} &= \left(\int_{d-y''}^{\infty}\phi_p(q)\ \ \frac{F_p(\omega'',q)}{E'}dq\right)\left(\int_{d-y''}^{\infty}\phi_p(q)dq\right)^{-1}\\ A_{avg}^{II}(d,y'') &= \left(\int_{d-y''}^{\infty}\phi_p(q)\ \ A_p(\omega'',q)dq\right)\left(\int_{d-y''}^{\infty}\phi_p(q)dq\right)^{-1}\end{aligned} \tag{20}$$

Equation (20) represents the average force (F_{avg}^{II}) and area of contact (A_{avg}^{II}) as the summation of force and area for different sizes of particles divided by the total number of particles in contact. ω'' in Eq. (20) is the particle indentation and is equal to $\omega''=[q-(d-y'')]/2$. The force and real area of contact for all the particles engaged in contact in region 2 can then be calculated by integrating over *y″* as shown in Eq. (21).

$$\begin{aligned}\frac{F^{II}(d)}{E'A_n} &= \int_{-\infty}^{d}\eta_p^{II}\frac{F_{avg}^{II}}{E'}dy'' = \int_{-\infty}^{d}\left[\eta_p\ \phi_s(y'')\left(\int_{d-y''}^{\infty}\phi_p(q)\ \ \frac{F_p(\omega'',q)}{E'}dq\right)\right]dy''\\ \frac{A_r^{II}(d)}{A_n} &= \int_{-\infty}^{d}\eta_p^{II}A_{avg}^{II}dy'' = \int_{-\infty}^{d}\left[\eta_p\ \phi_s(y'')\left(\int_{d-y''}^{\infty}\phi_p(q)\ \ A_p(\omega'',q)\ \ dq\right)\right]dy''\end{aligned} \tag{21}$$

Equations (17) and (21) present the contact force and area for all the asperities and particles in contact. The effect of particles and surfaces for the contact problem are accumulated as shown in Eq. (22).

$$F = F^{I} + F^{II}, \;\; A_r = A_r^{I} + A_r^{II} \tag{22}$$

Note that the area of contact for particles in region 1 (A_p^{I}) is left out of Eq. (22) because it overlaps with A_r^{I}. However, it should be accounted for if the conductive area of contact is of interest, which is the case in this work. For the case where only the surfaces are conductive, the overall conductive area is as follows:

$$A_r{}^{c} = A_r^{I} - A_p^{I} \tag{23}$$

In this work it is assumed that the sand particles' contribution to contact conduction is negligible, therefore Eq. (23) is used to find the conductive area of contact.

The contact model presented in this section is a general 3rd body contact model which can be applied to various practical applications. However, the appropriate material properties, single asperity and single particle models need to be used to capture the interaction of the surfaces and the particles. For example, if the model is to be used for submicron particles, the use of scale dependent material properties should be considered.

4.2. Electrical Contact Resistance

Electrical contact resistance (R_e) for a rough surface contact which has multiple asperity contact of a_i radius can be formulated as Eq. (24) [93].

$$R_e = \frac{\rho_e}{2\sum a_i} \tag{24}$$

Equation (24) is the rough surface contact resistance which can be rewritten as Eq. (25).

$$\frac{1}{R_e} = \frac{2}{\rho_e} A_n \int_d^\infty \eta_s \phi_s(y) a_{asp}(\omega) dy \qquad (25)$$

ρ_e is the resistivity and a_{asp} is the asperity contact radius in Eq. (25). Equation (25) can be added to the contact model to provide a prediction of the electrical contact resistance.

The current paper aims to model micron size sand particles in contact between rough golden surfaces. This system is particularly of interest because sand contamination is a major cause of fault in electrical connectors. The presence of sand in the electrical connectors would hamper the direct contact between surfaces, hence increasing the electrical contact resistance. Using nanoindentation experiments on micron size sand grains, Daphalapurkar et al. [94] measured the material properties of sand grains (mostly made of SiO_2) to be; $S_{y,p} = 6.1\ GPa$, $E_p = 90.1\ GPa$. The yield stress of gold is $S_{y,s} = 120\ MPa$, therefore the gold substrate is much softer than the sand particles. In order to properly model the interaction between a softer substrate and harder particles (F_p) an elastic-plastic indentation contact model by Komvopoulos and Ye[95] was used. This model is capable of modeling the indentation interaction between the particles and surfaces. To model the asperity versus asperity interaction (F_{asp}) it is better to use a flattening type of contact model. This paper used the elastic-plastic flattening contact model by Jackson and Green [96] for this purpose.

The surface parameters were estimated based on the surface profilometry measurements of actual connectors [97, 98]. It was observed that there are 29 peaks in a 149μm profile, which translates to $\eta_s = 3.788\times10^{10}\ m^{-2}$ for an isotropic surface. The average distance between the peaks is found to be 5.15 μm and the peak-to-valley distance was measured to be 1.47 μm. Assuming the asperities follow a sine wave profile, one can estimate the radius of curvature at the tip of the sine wave as follows; $R_{asp} = \lambda^2/(4\pi^2\Delta) = 0.9\ \mu m$. The surface roughness of the connectors was also measured to be

0.3 μm. The contact force in an actual cell phone connector is about *0.5 N* to *1.5 N* and the nominal contact area was measured to be $A_n = 2.22\ mm^2$.

4.3. Results

Assuming that the particles' sizes and the asperities' heights have a normal distribution, the contact model (Equations (17), (21), (22), (25) and (25)) has been solved for various sets of parameters. Figs. 25, 26 and 27 present the predictions of the model. This study focuses on the effect of sand content, surface roughness and sand particles' average size.

Fig. 25 presents the solution for the sand particle content (m_p) in term of the real area of contact and the electrical resistance versus the contact force. In this study, surface roughness is 0.3 μm and the average particle size is 1.0 μm. Based on the typical contact force and area presented in the previous section, one can calculate the typical contact pressure for a connector to be $F/(E.A_n) = 5\times10^{-6} \sim 1.5\times10^{-5}$. The resistance of a clear cellphone contact point is about *5* $m\Omega$ in this pressure range. Experiments also suggest that the presence of sand particles increase the contact resistance by many orders of magnitude to about 25 Ω. Comparing this to the predictions made by the model one can see that the model may under predict the contact resistance. This is probably due to the fact that the measurements include bulk resistance or the connectors may have degraded farther due to the sand. However, the model is successful in capturing the effect of sand contamination on electrical contact resistance. The model is also capable of measuring the critical particle content, which can substantially alter the contact resistance. The critical particle content for the study presented in Fig. 25 seems to be approximately 0.1 $\times 10^{-6}\ kg.m^{-2}$.

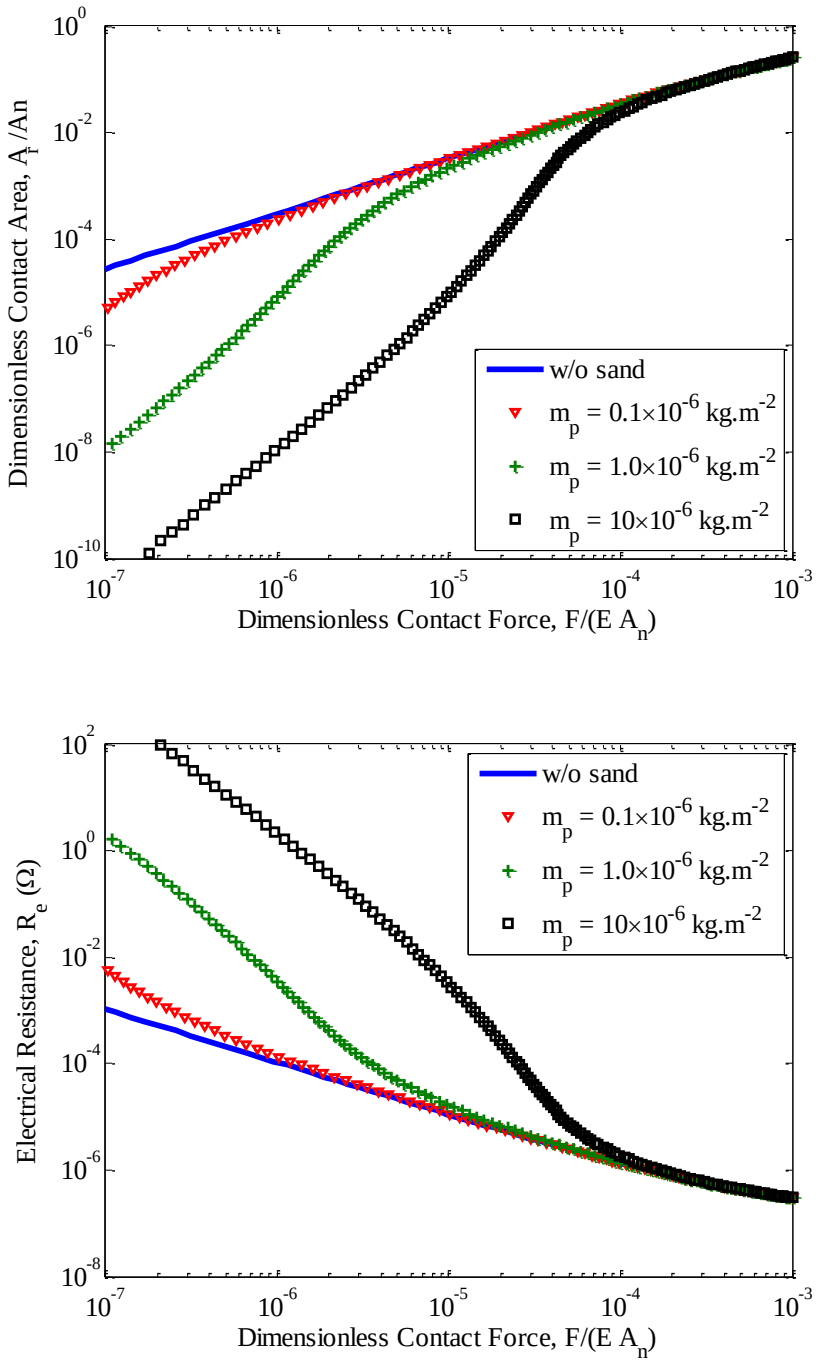

Figure 25: Real area of contact (top) and electrical resistant (bottom) versus contact force for different values of sand content on the surface. Both A_r and R_e are very sensitive to the presence of sand in amounts over $m_p=0.1\times10^{-6}$ kg.m^{-2}.

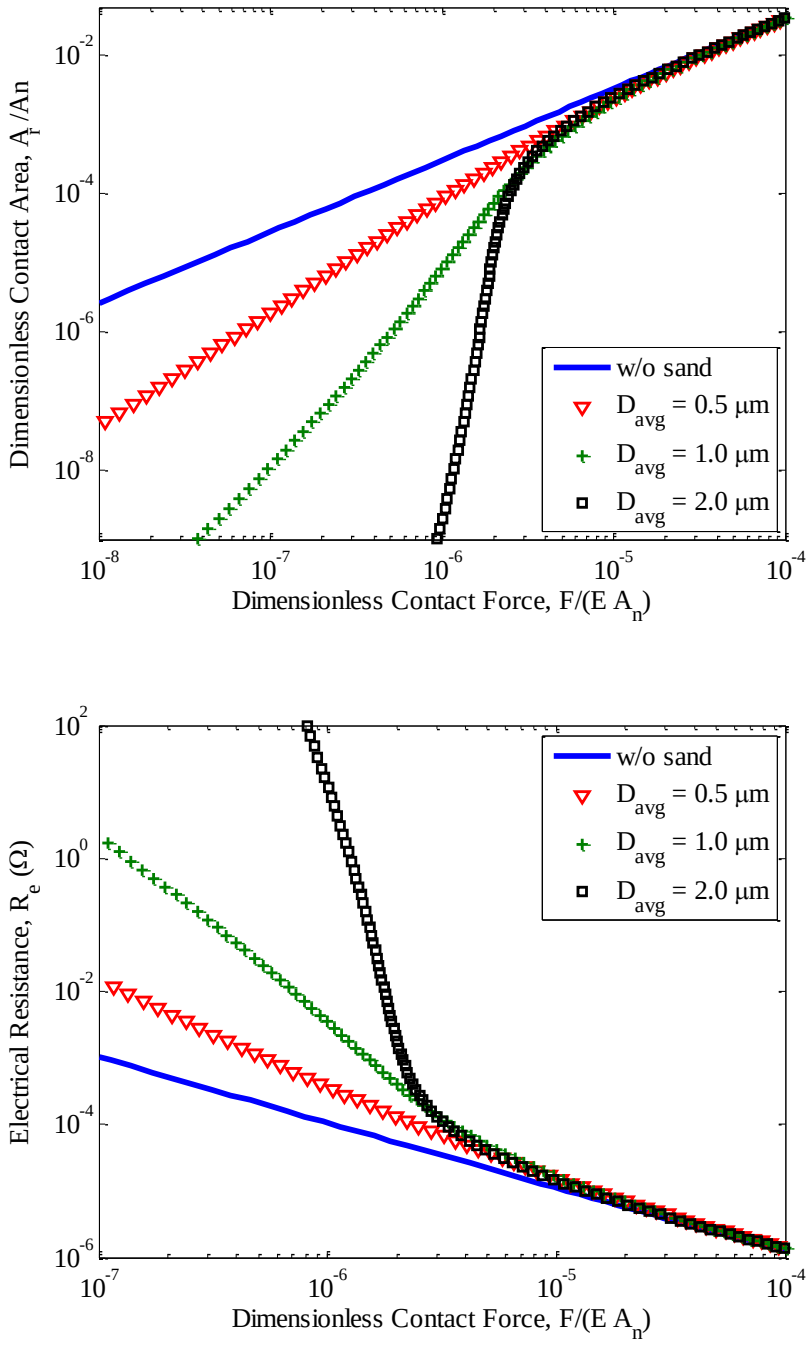

Figure 26: Real area of contact (top) and electrical resistant (bottom) versus contact force for various particle sizes. Particles larger than the average valleys on the surface have a higher possibility of engaging in contact and reducing the conductive area of contact hence increasing the contact resistance.

Fig. 26 represents similar plots for particles of different sizes. In this study the surface roughness is 0.3 μm and the particle content is m_p=1.0×10^{-6} $kg.m^{-2}$. The larger the particles are, the higher is the possibility for them to engage in contact. Especially when the contact pressure is low and the majority of contact is mainly made through the larger particles.

Fig. 27 shows the effect of surface roughness on electrical resistance and particle contamination. Obviously a smoother surface (lower roughness value) produces more contact area and hence lower contact resistance. However, on a smooth surface there is very little room for third body contamination, such as sand particles, which makes them susceptible and less robust. This is because the average roughness valley on a smooth surface is small and particles can't simply fit in these gaps and therefore engage in contact more often. The results in Fig. 27 show that when the surface roughness is equal to the particle average size, the sand contamination has a minor effect on electrical resistance (however, this also depends on particle content, m_p). This means that when surface valleys can accommodate the majority of the particles, the particles have a small effect on the electrical contact.

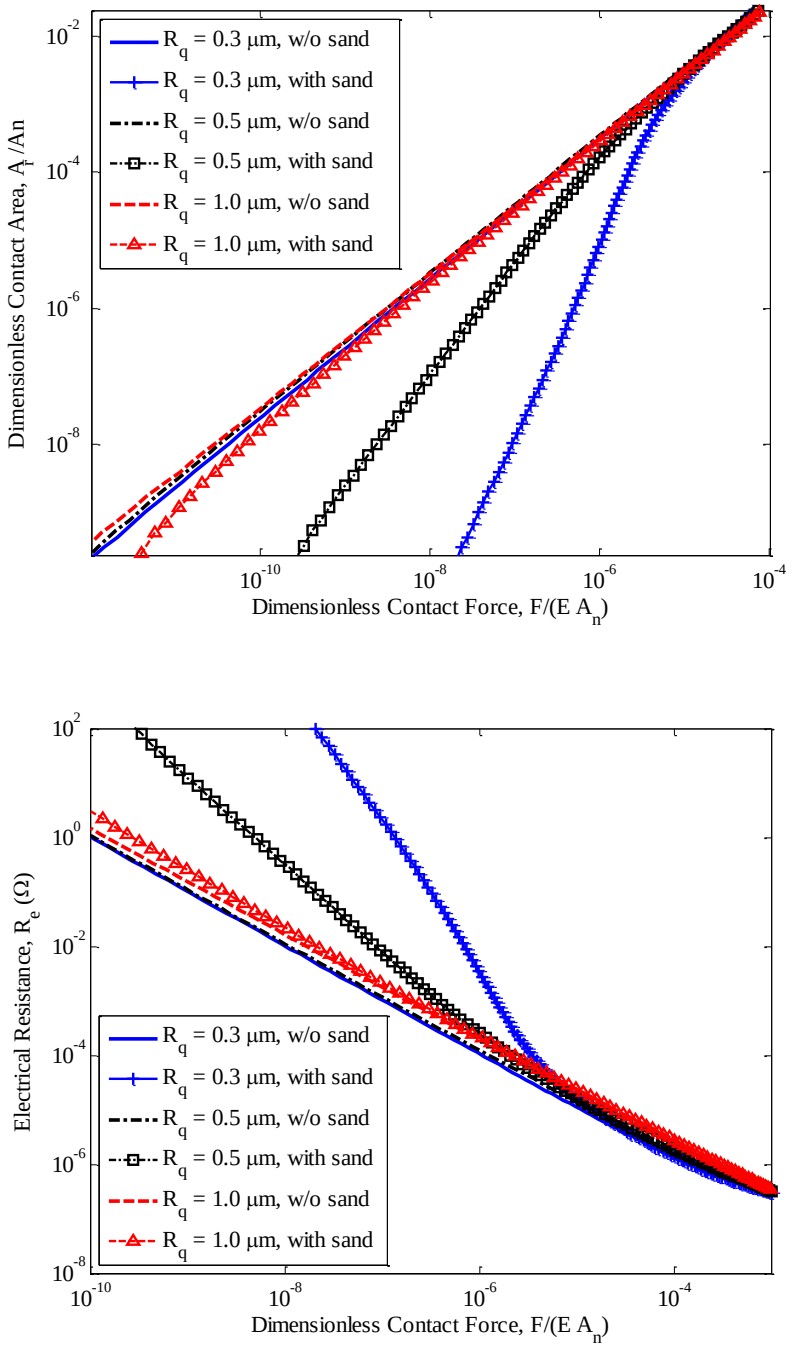

Figure 27: Real area of contact (top) and electrical resistant (bottom) versus contact force for various surface roughness values. Even though lower roughness values (smother surfaces) result in lower contact resistance, they are more susceptible to particle contamination.

4.4. Conclusion

A third body contact model for rough surfaces in contact with a system of third body contact particles is presented. The model is capable of predicting the real area of contact and contact force. The model is then used to predict the electrical contact resistance for cellphone connectors. Appropriate parameters were chosen according to the measurements of real connector surfaces. The results show that the model is capable of capturing the effect of sand contamination of the surfaces. The model can also be used to predict the critical sand content that can result in contact failure due to high contact resistance. The model can also be used to find out the best surface roughness to minimize the contamination issues based on the typical particle content and size. In the future we plan to validate the model with experimental results.

5. The effect of nanoparticles on thin film elasto-hydrodynamic lubrication

Elasto-hydrodynamic lubrication (EHL) has been the topic of extensive studies in the past sixty years. It was originally explored to provide an explanation for the behavior of line and point contact between gears and bearings with a focus on predicting the minimum film thickness [99]. The EHL is interestingly proven to be a very effective lubrication regime especially in the case of thin lubricant films. Various experimental and analytical studies have explored the problems associated with the EHL in different systems [100]. The results suggested that the classical EHL models[101-103] are accurate down to gaps as small as 10 to 20 nm [104, 105]. For very thin films, by using experimental[106], numerical[107] and analytical methods[108], it has been shown that the surface forces promote layering of the lubricant's molecules, which in turn leads to a considerable reduction in the coefficient of friction (COF). This work explores the effect of nanoparticle additives in the thin film EHL regime.

In the context of nano-lubricants, it has been recently reported by different groups of researchers that nanoparticle additives can improve the lubricity of lubricants[37, 38, 41, 109, 110]. However, most of the studies were aimed at the performance of the nanoparticles in the boundary lubrication regime in which substantial contact occurs between the surfaces. Hence, most of the proposed friction reduction mechanisms for nanopaticles such as rolling [11, 111], transfer films [39, 112], formation of tribofilms [110, 113] and reducing the real area of contact [83, 109] require particles/surface interactions. This paper focuses on the performance of nanoparticle additives on thin film elasto-hydrodynamic lubrication in which no significant contact occurs between the lubricated surfaces and the pressure in the lubrication film is high (0.7~1.5 GPa). The hypothesis of the current work is that nano-sized particles can infiltrate into the small gaps between surfaces in the EHL regime and when the size of the gap is comparable to

the particle's size and the film pressure is high, particles may affect the friction properties of the contact pairs. In this study, we have conducted careful experiments using a sphere (pin) on flat (disk) friction tester to demonstrate the effect of nanoparticles on reducing friction in the EHL regime. Moreover, surface analysis and molecular-level simulations have been utilized to investigate the possible interaction between the nanoparticles and the surfaces or lubricant in order to determine the potential enhancing mechanism. The results propose a new friction reducing mechanism induced by the nanoparticles in the EHL lubrication regime.

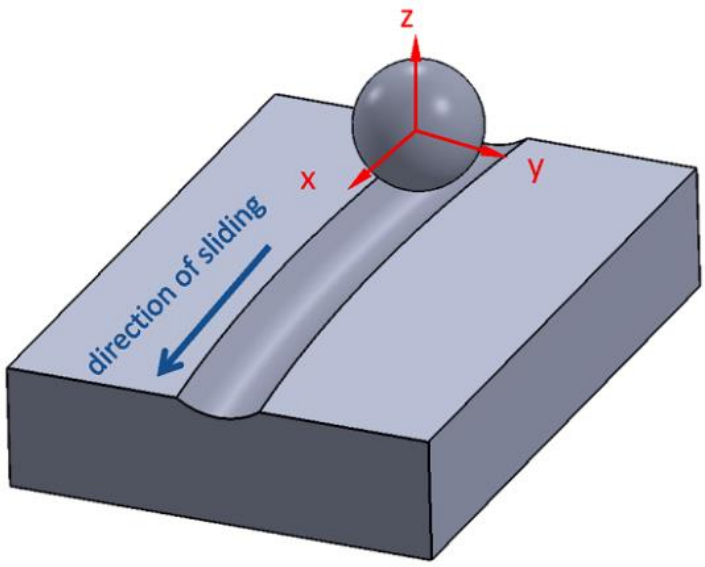

Figure 28. Schematic of the contact pair.

5.1. Nano-lubricant and experiments

The nano-lubricant used in the experiments contains silver nanoparticles with an average size of 7 nm suspended in polyethylene glycol (PEG). The molecular weight of the PEG is 600 g/mol. Polyvinylpyrollidone (PVP) with a molecular weight of 10 Kg/mol is used as the coating agent to stabilize the suspension. The nano-lubricant has 3 mM silver nanoparticles and 1.5 mM PVP suspended in PEG and the control lubricant consists of 1.5 mM of PVP in PEG. The viscosities of the nano-lubricant and the control lubricant are

measured to be 170.8 and 166.4 mPa.s, respectively. Also, the nano-lubricant and the sample are observed to behave as Newtonian fluids in shear rates higher than 10 s^{-1} (data is not given here). The stability of the suspension was studied and the nano-lubricant was observed to be stable for a 6 months period.

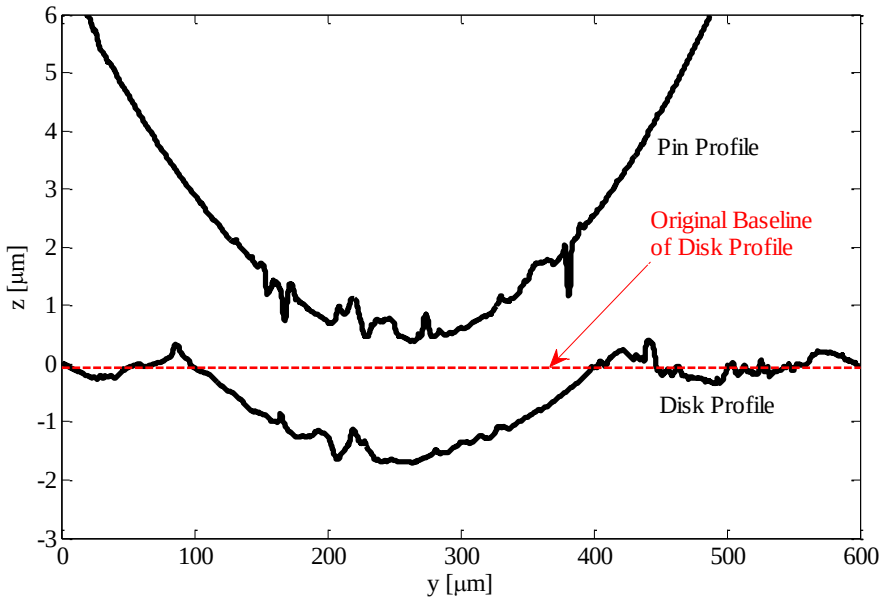

Figure 29. Pin and disk profiles after the friction tests for one of the contact pairs.

Friction tests were performed with a pin-on-disk friction test setup that consists of a spherical pin (10 mm diameter) in contact with a rotating disk (please see appendix I for details). This configuration provides a concentrated point contact between surfaces. The disk part is made of AISI 1080 carbon steel and the pin is made of AISI 52100 chromium steel. The contact is submerged under the lubricant using a reservoir. The sphere and disk are brought into contact by changing the normal force while the lubricant exists between the surfaces. An electrical contact resistant sensor (ECR) is used to detect contact between the solid conductive surfaces.

The test procedure has two steps, first the run-in step during which the surfaces are brought into contact. In this step, the contact pressure (maximum Hertzian contact pressure) is held at 0.97 GPa for 15 min and then increased to 1.40 GPa for another 15

min. During this step the surfaces develop and a shallow groove forms on the disk. Figure 28 shows the schematic of the contact pair and the groove. During the next step of the friction test the force is changed from 2.0 N to 50.0 N in nine increaments over three minute intervals and the friction data is collected. This step tries to collect the data in short intervals so that the change in the geometry of the surfaces is minimal.

Upon completion of the tests, the profiles of the pins and the disks are measured in order to accurately estimate the contact pressures. The profiles of a contact pair are shown in Figure 29. The profiles are used to calculate the actual curvature of the pins and the grooves in the contact region during the data collecting step. The overall effective contact radius in the *y*-direction is $R_{y,e}^{-1} = R_{y,p}^{-1} + R_{y,d}^{-1}$ and in the *x*-direction is $R_{x,e} = R_{y,p}$ where subscripts *x, y, e, p* and *d* stand for *x*-direction, *y*-direction, effective, pin and disk (see Fig.28 for definition of coordinates). $R_{y,p}$, $R_{x,p}$ and $R_{y,d}$ have been measured based on the actual surface profiles. Due to the difference in effective contact radius in the *x*- and *y*-directions the contact region is elliptical in shape. Hence, the contact pressure for elliptical point contact is calculated using the general Hertzian contact solution[114].

The results are plotted in Figure 30 in terms of the COF versus the contact pressure (the maximum Hertzian contact pressure). As the contact pressure increases, the COF first decreases and then increases, which is a typical behavior of lubricated pairs in the EHL regime. The plateaus at the far right of the curves correspond to the initiation of contact between surfaces. The results indicate that the nanoparticle additives enhance friction in the EHL regime which is associated with the contact pressures ≅ 0.8 to 1.6 GPa. This observation confirms that the supplement of nanoparticles improves friction when contact pairs are separated by a film of lubricant. As mentioned earlier, the viscosity of the nano-lubricant is higher than the viscosity of the control lubricant and therefore the enhancement does not originate from the bulk lubricant properties that are effective in the hydrodynamic lubrication regime. In addition, the ECR sensor shows that there is no contact between surfaces, and the pressure is high, showing that the regime is not boundary lubrication either. These observations lead to the conclusion that the

nanoparticles reduce friction in the EHL regime. However the reason and mechanism which allows this is not known.

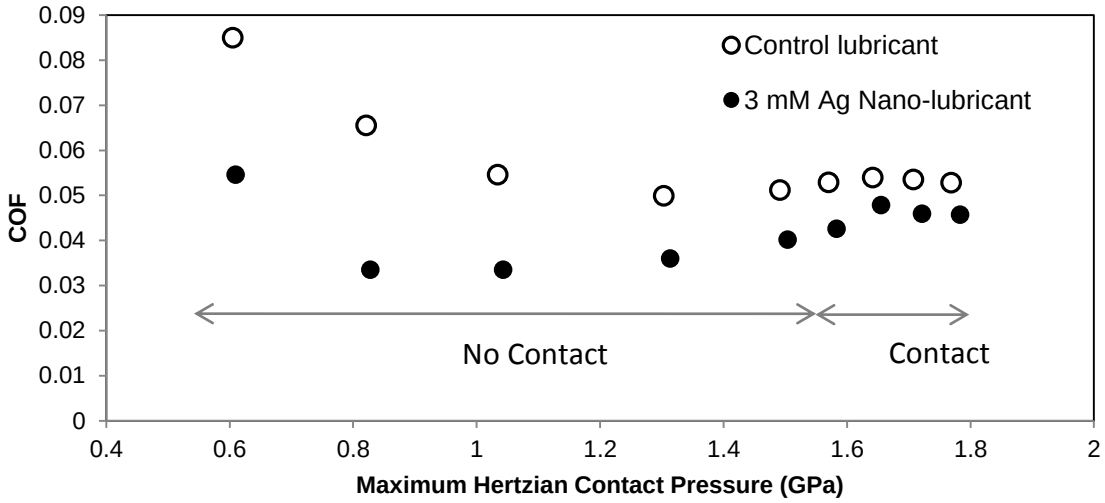

Figure 30. Coefficient of friction versus contact pressure.

The contact system consists of three components, particles, surfaces and the lubricant. Therefore, we need to investigate the interaction between any pair of these components to find the dominant effective mechanism of nanoparticles in the EHL regime. The interaction between the lubricant and the surfaces is the common factor for the nano-lubricant and the control lubricant. Hence, the mechanism should have roots in the interaction between the nanoparticles and the surfaces or the nanoparticles and the lubricant. Possible phenomena that arise from the particle/surface interactions can be either the particles forming nano-structures on the surface or filling up the valleys of the surface, leading to a change in the nano-texture of the surface and therefore affecting the EHL. Particle/lubricant interaction at the thin film EHL may also result in the reduction of the COF. For instance, the nanoparticles can affect the flow pattern or glass transition of the lubricant at high pressures. The rest of this work studies the nanoparticles/surface and the nanoparticles/lubricant interactions in order to find the dominant mechanism responsible for reducing friction.

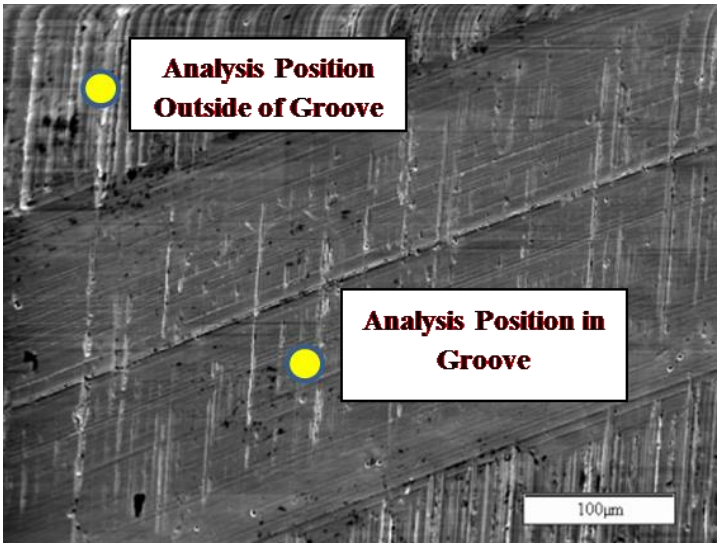

(a)

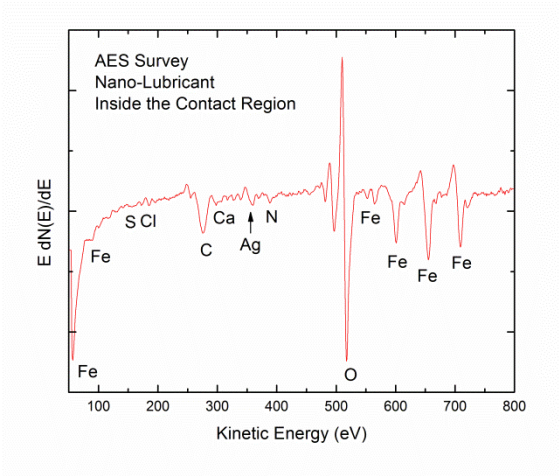

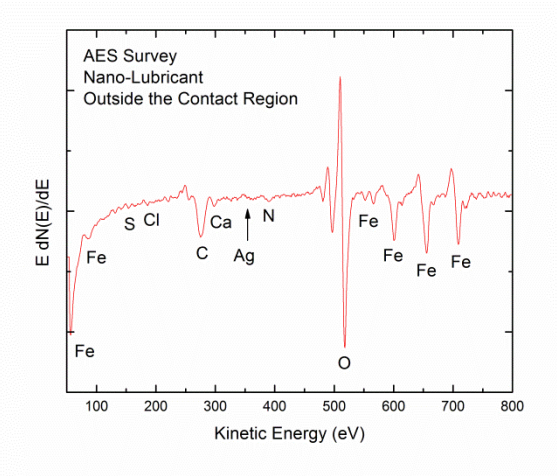

(b) (c)

Figure 31. Picture of contact region obtained with scanning electron microscope, (a) AES spectra inside (b) and outside (c) the contact region.

5.2. Surface analysis

In order to investigate possible particle/surface interactions, various surface analyses were performed on the disk surfaces after the tests. A scanning electron microscope (SEM) image of one of the contact regions is shown in Figure 31 (a). As shown in the figure, Auger electron spectroscopy (AES) spectra were recorded both inside and outside

the contact groove. Results shown in Figure 31 (b) and (c) indicate that there is slightly more Ag inside the wear groove than outside the groove. Surface stoichiometry measurements both outside and inside the contact groove were obtained by X-ray photoelectron spectroscopy (XPS), yielding the average amount of surface Ag to be 0.06 and 0.1 at% for the regions outside and inside the groove, respectively. XPS was used for the stoichiometric measurement rather than AES due to the higher accuracy of XPS in stoichiometric determinations. The analysis on the surfaces tested with the control lubricant showed no evidence of Ag on the surfaces. The next step is to study the configuration of the particles on the surface and detect possible chemical bonding between the nanoparticles and the surfaces. Ar sputter etching was used to drill ~ 12.5 nm into the surface (slightly over the average size of a particle). AES results before and after the drilling shows that the Ag signal completely vanished after drilling (see Figure 32). Moreover, XPS analysis inside the contact region showed that Fe on the surface is largely in an oxide form (Fe_2O_3), with no bonding between Ag and other surface elements. This shows that there is no strong bonding between the Ag nanoparticles and the surface. Figure 33 illustrates the possible scenarios that may happen in regard to the nanoparticles/surface interaction and schematically shows the possible effects of drilling for each scenario. In the first scenario (see Figure 33 (a)), it is assumed that the nanoparticles either (1) deposit in the valleys, (2) coalesce to form nano-structures or (3) bond to the surface. In this scenario, drilling does not remove all of the nanoparticles. In contrast, in the second scenario in which individual nanoparticles are loosely adhered to the surface (see Figure 33 (b)), drilling removes the Ag nanoparticles, which is the phenomenon observed in our tests. Considering that the information depth for both AES/XPS is ~ 5 nm, this analysis along with the surface stoichiometry using XPS suggests that Ag resides strictly on the surface in the form of individual nanoparticles loosely adhered to the surface. We conclude that no influential interaction is taking place between the nanoparticles and the surfaces that can be considered to be the mechanism behind the observed friction reduction.

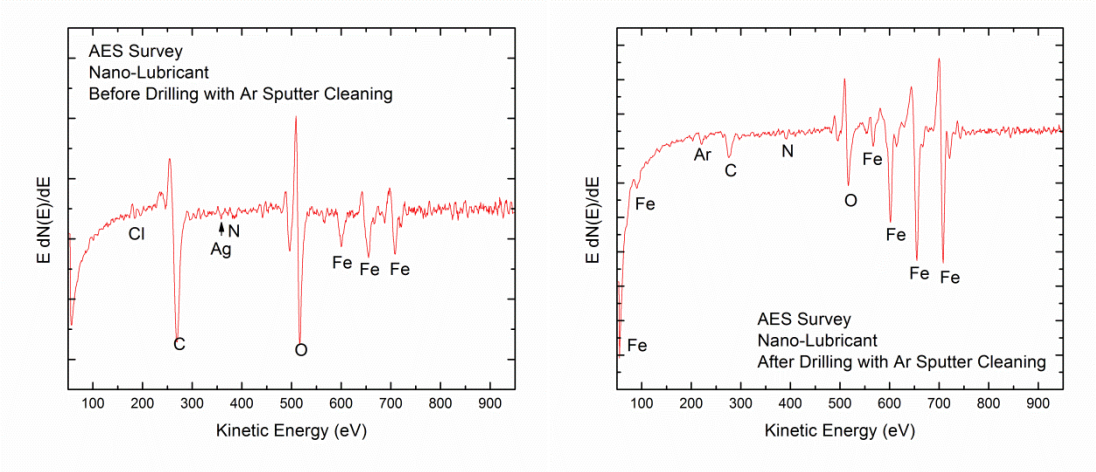

(a) (b)

Figure 32. AES analysis on the surfaces before (a) and after (b) drilling with Ar sputter cleaning.

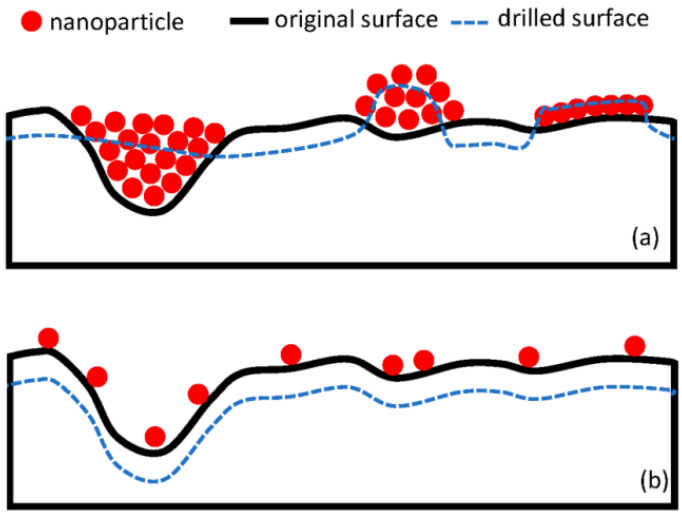

Figure 33. Schematic of possible particle/surface interaction: (a) particles deposit on the surface and inside the valleys (b) scattered loosely adhered particles on the surface.

5.3. Molecular dynamics simulations

Next, molecular dynamics (MD) simulations are utilized to study the underlying mechanisms in relation to the interactions between the nanoparticles, the surfaces and

the lubricant in the thin film EHL (the MD simulations was done by Mr. Hasan Babaei and Dr. Jay Khodadadi of Auburn University Mechanical Engineering Department). In order to simplify our MD simulations, the lubricant is chosen to be n-dodecane. Since the MD simulations are designed to study the mechanistic interactions between the nanoparticles and the lubricant, this choice of lubricant does not affect our overall purpose for performing MD simulation. The minimum film thickness in the friction tests was estimated by theoretical calculations [102, 103] to be 90 nm and the combined roughness in the sliding direction (*x*-direction) was measured to be 70 nm. This means that the gaps between the surfaces are on average around 20 nm. Therefore, the geometries in MD simulations were chosen to have the similar ratio of particle size over gap size.

Simulations were performed on a smaller system containing a nanoparticle with a diameter ~24 or 37 Å suspended within the gap of 54 Å filled with n-dodecane molecules confined between two rigid walls (see Figure 34). The Ag atoms included in the nanoparticle are located on a faced-centered cubic (FCC) lattice with a lattice constant of 4.09 Å [115]. The walls are made of iron atoms located on a body-centered cubic (BCC) lattice with a lattice constant of 2.87 Å [115]. The walls include three layers of atoms with a cross-sectional area of ~60×60 $Å^2$.

A Lennard-Jones (LJ) potential is utilized for interactions among Ag and Fe atoms [115]. The Nath, Escobedo, and de Pablo-revised (NERD) force field [116] is used to describe interactions between dodecane molecules. For the cross-interaction potential between different elements, the Lorentz-Berthelot mixing rule [117] is used for determining the LJ potential parameters. A time step of 1 fs is used in all simulations. All simulations were performed with the large-scale atomic/molecular massively parallel simulator (LAMMPS) molecular dynamics package [118].

The steps of the MD simulations are as follows. Pure fluid (control lubricant) or nano-lubricant (the term that is used for systems containing nanoparticles) systems were initially equilibrated under isobaric-isothermal (NPT) ensembles at *T*=300 K and

atmospheric pressure without the walls. At this stage, the periodic boundary conditions were applied on all directions of simulation boxes. Then, these systems were brought into contact with the two walls and subjected to compression by moving the walls toward each other. In this step, the periodic boundary conditions were applied on the directions parallel to the walls' surfaces, whereas for the normal direction, a fixed non-periodic boundary condition was utilized. A schematic diagram of a nano-lubricant system after compression is exhibited in Figure 34.

The density curves for different gap distances during compression simulations show that by compressing the fluid within the gap, planar layers of the lubricant's molecules are formed. The density curve for gap size of 54 Å without the nanoparticle is shown in Fig. 35(a). This phenomenon is in agreement with the results of other MD works [119-122] on thin films between two walls. However, in our study, upon shearing the walls, the layered structure midway between the walls vanishes, leaving only a few ordered layers in the vicinity of the walls. In this scenario, the pressure and gap distance between the walls change simultaneously. To overcome this problem and to find the dependency of the COF on the pressure independently from the gap distance, simulations were carried out on systems containing different numbers of lubricant molecules (i.e. densities). In other words, the gap distance is kept constant while the pressure changes due to the number of molecules. After the compression step, the systems were equilibrated for 1,000,000 time steps under the isothermal-constant volume (NVT) conditions. Then, the walls were sheared in opposite directions for 4,000,000 to 6,000,000 time steps until the systems reached the steady-state condition. Upon attaining the steady-state condition, the normal and shear stresses on the walls were obtained by dividing the average forces imposed on the walls from the lubricant's molecules by the cross-sectional area of the walls. Figure 35(b) exhibits the calculated COF versus pressure for the pure and nano-lubricant cases. The results show that for all cases, the COF decreases with increasing pressure. In addition, the presence of the nanoparticles leads to a decrease in the COF. The general trend of the friction results from the MD simulations (Figure 35(b)) and the

experiments (Figure 30) corroborate each other on the fact that the presence of the nanoparticle in the contact system results in a decrease in the COF. This also supports the idea that the nanoparticles/lubricant interaction is responsible for improved performance in thin film EHL.

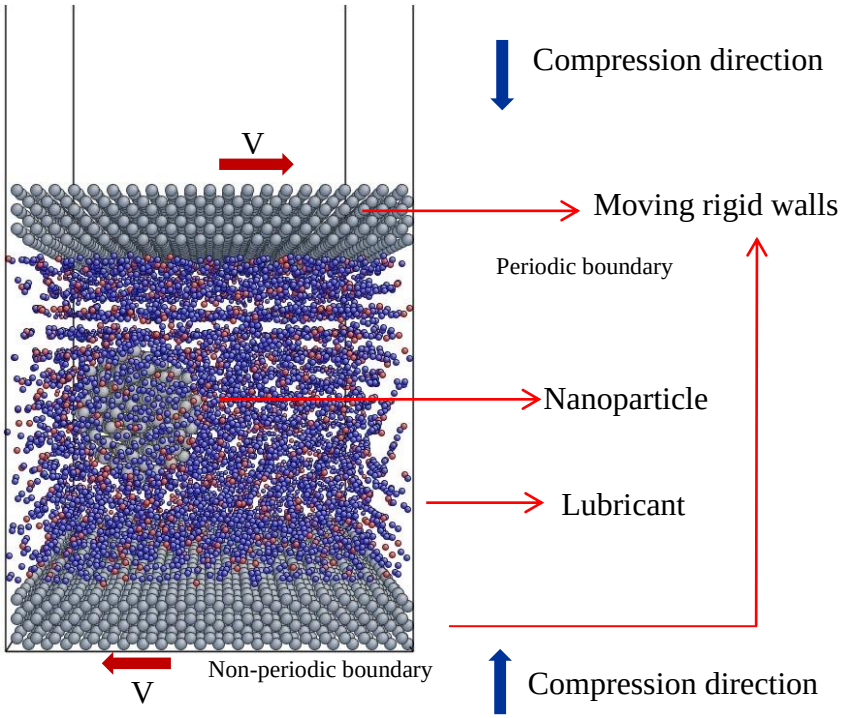

Figure 34. Schematic diagram of the simulation system and boundary conditions.

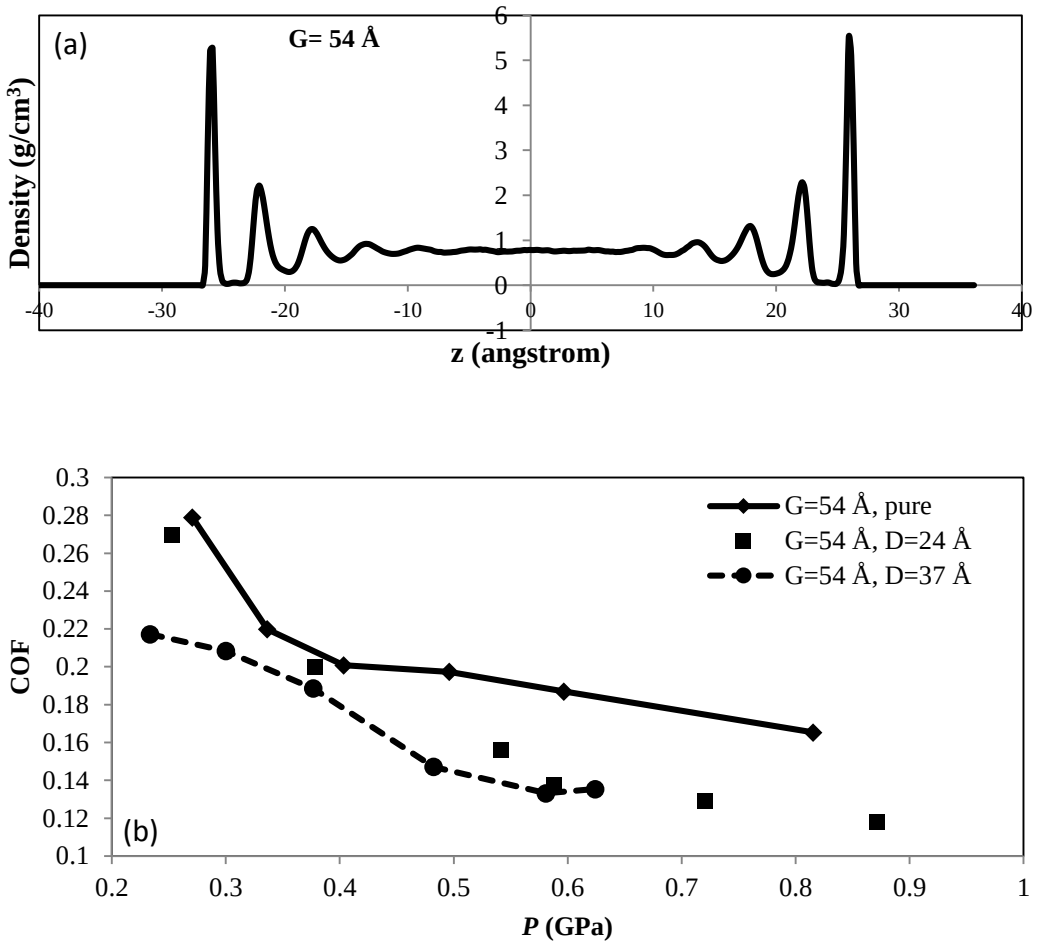

Figure 35. (a) Density curve for pure at *G*=54 Å, showing the formation of planar layers. (b) COF versus pressure at *G*=54 Å for pure system and two nanofluid systems containing nanoparticles with *D*=24 and 37 Å.

By monitoring the motion of lubricant molecules and tracing them when the walls are sheared, we found that the lubricant's molecules move with each nanoparticle (in a translating motion). This is most likely the key mechanism behind the reduction in the COF when a nanoparticle is present. The presence of a nanoparticle forces the lubricant's molecules to move along with the nanoparticle, promoting an obstructed flow (please refer to movies of molecular dynamics simulations available in supporting information section). This is clearly observed in the velocity profile for the nano-lubricant cases given in Figure 36. For obtaining the velocity profiles, the region between the walls is divided into a sufficient number of slabs normal to the *z*-direction. Then, the time-averaged

velocity of all particles within those slabs was calculated. For nano-lubricant cases, there is a flat region in the velocity profiles which indicates that shearing occurs over a few layers of lubricant adjacent to the walls. While for the pure case, the velocity profile includes both a linear region and a jump which shows that shear is distributed through all regions of the gap. The proposed mechanism is further verified by modeling a pure fluid system containing a less number of the lubricant's molecules and a smaller gap. Similar simulation steps were carried out for a gap size of G=18 Å and having a pressure of 0.7 GPa. Despite the aforementioned simulations, in this case, shearing does not destroy the planar structure of the layered molecules and dodecane molecules slip on each other on the sliding layers (see Figure 36). The calculated COF for this case is 0.12, which is closer to the COF for the nano-lubricant systems rather than COF for the pure fluid with G=54 Å and having the same pressure. The similar values of COF suggest that in both cases, the case with a few layers of pure fluid and the nano-lubricant case, the same mechanism occurs. Consequently, this directs us to the conclusion that the mechanism for nanoparticles in the thin film EHL regime is the occurrence of obstructed flow caused by nanoparticles promoting the shearing action over a few layers of the lubricant. One point should be noted about the velocity curves in Fig. 36 and that is the velocity profiles are not symmetrical around zero. This is because firstly the initial arrangement of molecules does not contain symmetry and also the molecules are long and can cross the center line of the simulation box and bend throughout the simulation box leading to an asymmetry case. Moreover, the different strengths of the liquid layering effect due to the walls can destroy symmetry. The only criterion is that the overall momentum needs to be zero in the simulation box which is correct as one looks at the higher velocity next to the top wall due to the higher liquid layering effect.

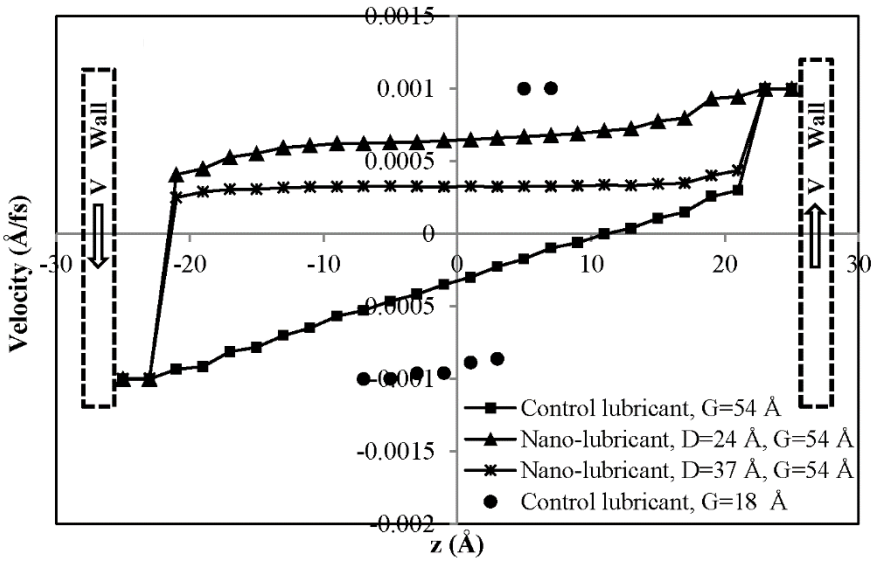

Figure 36. Examples of the velocity profiles for the pure and the nano-lubricant cases with *G*=54 Å and a pure case with *G*=18 Å.

5.4. Conclusion

In summary, in this work, a new friction reduction mechanism was proposed for nano-lubricants in thin film EHL regime. Through careful friction tests it was demonstrated that nanoparticles reduce the COF in the thin film EHL regime. Extensive surface analysis studies shows that there is low amount of Ag nanoparticles on the surface. XPS analyses were unable to detect bonding between the particles and the surfaces. Moreover, surfaces were drilled with Ar sputter cleaning which showed that Ag presence is strictly on the surface and particles are loosely adhered to the surface. Molecular dynamics simulations were performed to elucidate the interactions between the nanoparticles and the lubricant molecules in pressurized thin film EHL. The general trend of the COF curves versus the pressure obtained from simulations (Fig. 35(b)) agrees with the curves obtained from measurements (Fig. 30). Careful observation of molecules flow pattern inside the gap revealed the underlying mechanism to be occurrence of obstructed flow. Nanoparticles are small enough to infiltrate into nano-scale gaps formed between the in-contact surfaces and change the characteristics of the lubrication system locally. Within

the pressurized small gaps, the nanoparticles influence the flow pattern and reduce friction. Conventionally, lubricants with higher viscosity are used to reduce friction in the EHL regime while preventing contact between surfaces. However, the proposed mechanism suggests a new solution to this problem, which is the addition of nano-sized particles to infiltrate into the gaps and enhance local lubricity. Further investigations using in-situ film thickness measuring technics during the friction tests and studying the effect of pressure on bulk viscosity of nano-lubricants are underway for further verification of the proposed mechanism.

6. Tribological performance of silver nanoparticle-enhanced polyethylene glycol lubricants in boundary and mixed lubrication regime

Nanoparticle additives as a lubricant modifier have proven to be effective [37, 38, 41, 109, 123, 124]. Investigations on various type of nanoparticle additives almost unanimously report a decrease in coefficient of friction (COF). However, the effect of particles on wear is reported to be multifarious. Various enhancement mechanisms have been proposed for nanoparticles including, rolling [11, 111], transfer films [39, 112], formation of tribofilms [113] and reducing the real area of contact [83, 109]. This section investigates the tribological effect of silver nanoparticles additives in polyethylene glycol (PEG) as a nano-lubricant and discusses the possible enhancing mechanism. Water-solubility, low volatility, natural lubricity and non-toxicity of PEGs make them a candidate lubricant for a wide range of applications.

Silver nanoparticles are currently the most widely used nanomaterial in commercial products [125]. They are often applied as antibacterial agents in medical products and consumer goods such as wound dressings and disinfectants and fresh box containers. Silver nanoparticles have a very large surface area per mass which increases the release of silver ions which in turn result in cell lysis and results in an antibacterial effect [126]. Silver nanoparticles are also incorporated into plastic, adhesives and fluids to increase the electrical and thermal conductivity [127-129]. Therefore, silver nanoparticles are indeed the most attractive type of nanoparticles from an industrialization standpoint in spite of silver being a high-end value material. Sub-micrometer silver structures have been the topic of compression tests [130]. Experiments showed that submicron silver pillars possess an elevated flow strength (as compared to the bulk property) that is inversely proportional to the pillar's diameter. Nanoindentation studies on silver nanoparticles with an average size of 13 nm reported the hardness to be 3.12 GPa [131]. This flow

strength while being higher that of the bulk, is considered soft as compared to the other type of nanoparticles [7, 10].

The nano-lubricant used in this study is similar to the one introduced in the previous section consisting of silver nanoparticles with an average size of 7 nm suspended in polyethylene glycol (PEG). The nano-lubricant was prepared in three different concentrations of 1.5, 3.0 and 4.5 mM. The results were compared to a control sample containing the same concentration of PVP as the nano-lubricant solutions.

6.1. Viscosity measurements

In order to obtain a complete picture of the Rheological performance of the silver nano-lubricants, viscometery studies were performed. Measurements were carried out using a Brookfield® DV-II +Pro rotational viscometer capable of measuring small volumes at controlled temperatures (please see appendix I for details). Measurements were performed for different concentrations of nano-lubricant (NL) in various temperatures and shear rates. Fig. 37, shows the variation of viscosity versus shear rate at different temperature values. Results show that the nano-lubricant behaves as a Newtonian fluid for shear rates higher than 10 s^{-1} (some minor shear thinning effects were observed at lower shear rates). Therefore, the nano-lubricant behaves as a Newtonian fluid in the shear rate ranges of the experiments in this study and for lubrication applications (which are well above 10 s^{-1}). These viscosity measurements will later be used to generate the Stribeck curve for the control and the nano-lubricant.

Figure 38(a) shows the variation of viscosity versus nanoparticle concentration for a temperature of 30^{o}C. The nano-lubricant's viscosity increases as the nanoparticle content increases in a quasi-linear manner. The addition of nanoparticles accelerates the energy dissipation in the system which translates into an increase in the bulk viscosity. A similar trend was observed in our previous study [109] on CuO particles and by other studies in the field.

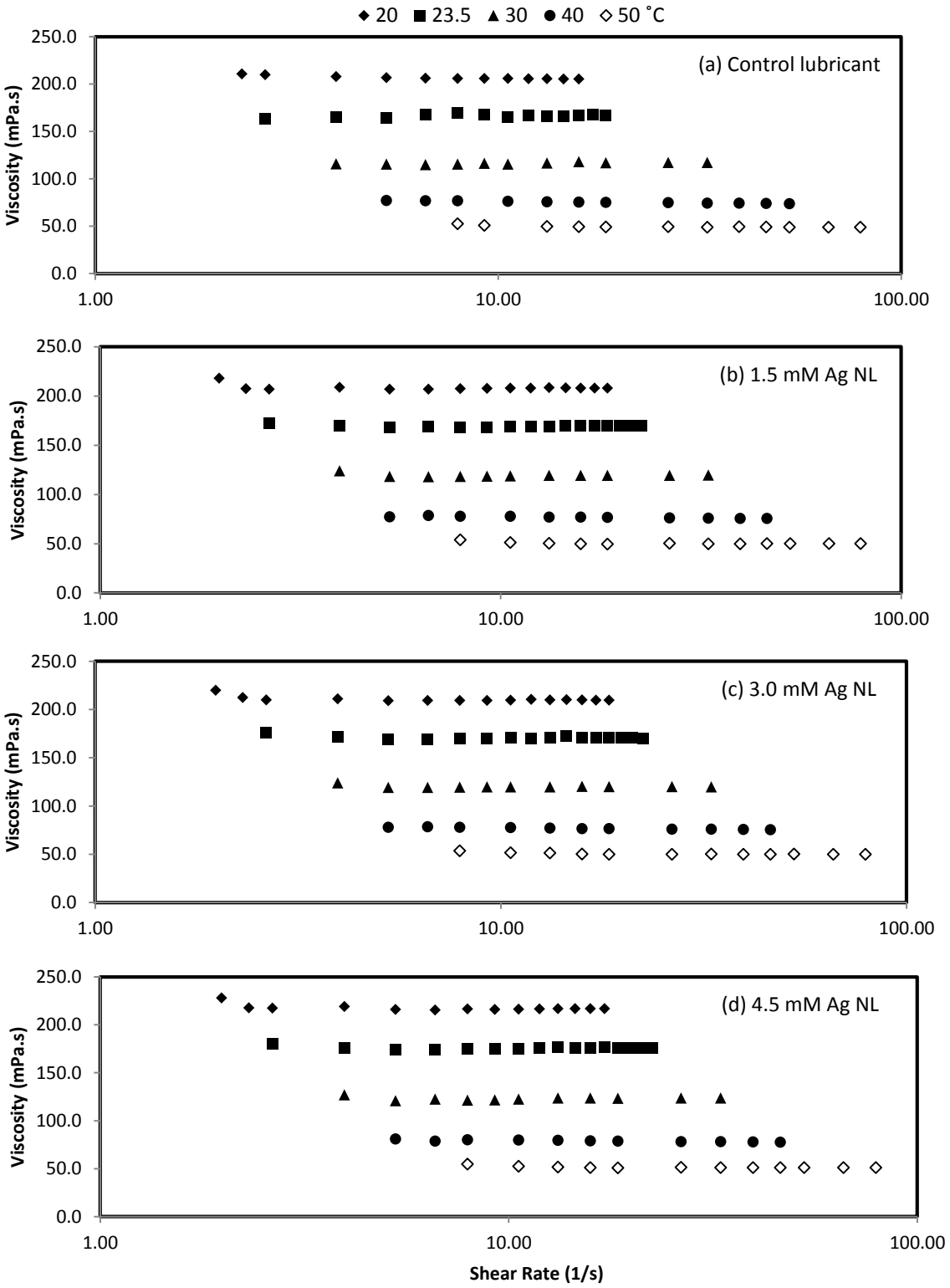

Figure 37: Viscosity versus shear rate for (a) control lubricant, (b) 1.5 mM, (c) 30 mM, (d) 4.5 mM Ag nano-lubricant.

Figure 38(b) shows the dependence of viscosity on temperature for the control lubricant and 4.5 mM Ag nano-lubricant. This graph shows that the viscosity dependency on temperature is greater than its dependency on nanoparticle content. Note that the viscosity value of the other two concentrations of nano-lubricants considered in this work falls in between the two curves.

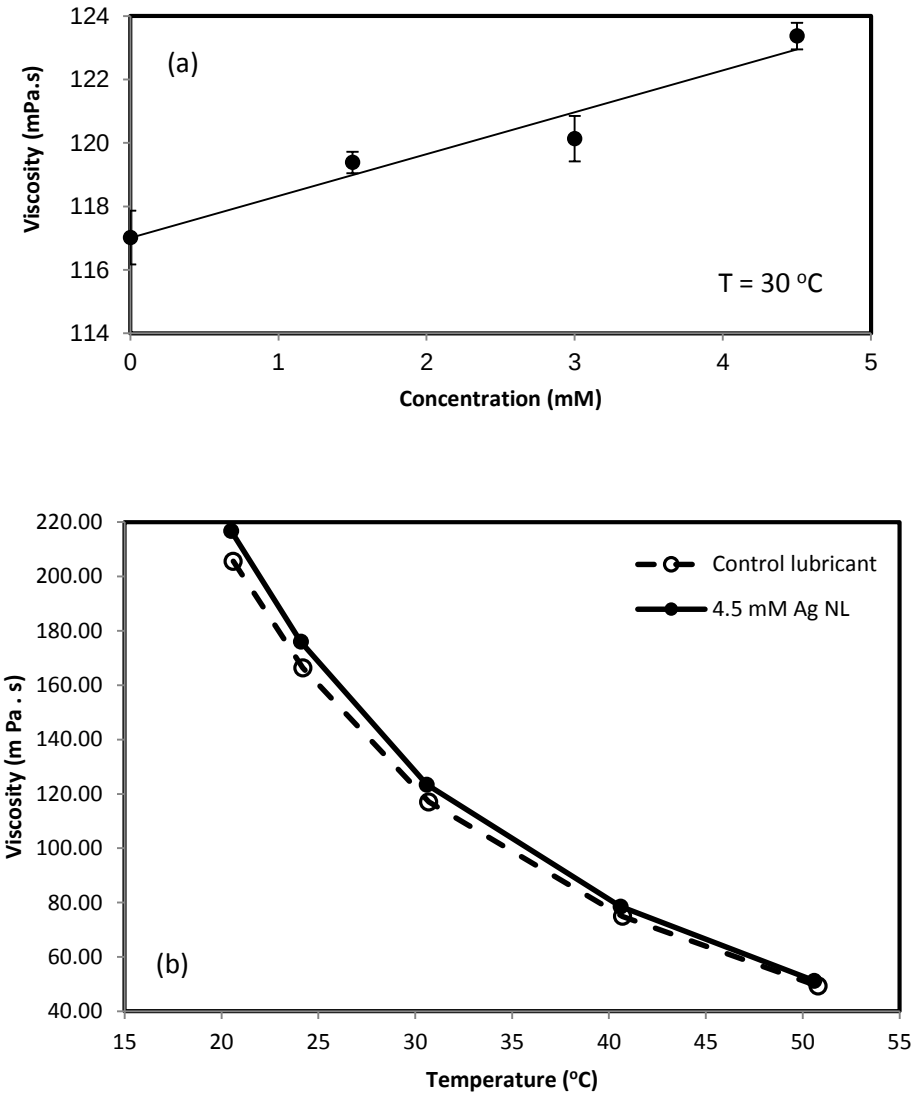

Figure 38: (a) Viscosity versus nanoparticle concentration at T = 30 °C, (b) Change in viscosity versus temperature.

6.2. Friction and wear tests

Friction tests were run using a pin on disk (sphere on flat) tribometer capable of precise controlling of the normal load and the sliding velocity. The pin is mounted on a suspension that helps tuning the normal load as well as sustaining the contact between surfaces during sliding. The disk is submerged under the lubricant and rotating continuously to provide the sliding motion. The pin is a 10 mm sphere made of AISI 52100 chromium steel. The disk is made of AISI 1080 carbon steel with a surface roughness of 0.4 μm. An electrical contact resistor (ECR) is installed in the tribometer to detect direct contact between surfaces. The ECR can be used to distinguish between lubrication regimes. Therefore the machine and the setup are capable of performing finely tuned experiments in different lubrication regimes (please see appendix I for details).

Friction tests were run for a total distance of 2500 m at a sliding speed of 0.5 m/s. The mean Hertzian pressure was set to be 666.7 MPa during the tests. Figure 39 shows the progression of the COF versus sliding distance for different concentrations of nanoparticles. Each curve represents the COF signal of a single test. COF results show that the run in step takes less than 1000 m of sliding distance also that the Ag nanoparticle additives are capable of maintaining a low COF value throughout the experiment. Another observation is that the nanoparticles help with the run-in process as the COF for the nano-lubricants tend to reach a quasi-steady state value earlier. These tests are in the mixed lubrication regime in which there is contact between the surfaces. Consequently, a groove forms on the surface during the tests. Wear measurements were carried out by quantifying the amount of the material that has been removed during the tests [132]. A three dimensional profile of the wear track was obtained using the stylus profilometer which was used to calculate the wear volume. Figure 40 shows the three dimensional profile of one of the wear tracks used in the analysis.

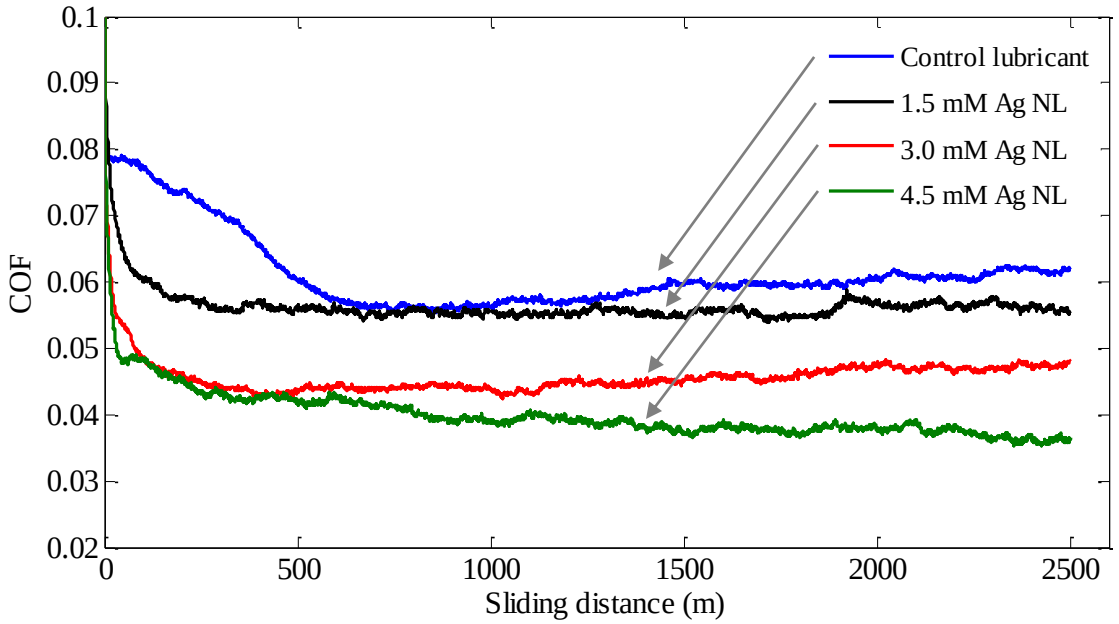

Figure 39: Coefficient of friction versus sliding distance for various concentration of nanoparticles.

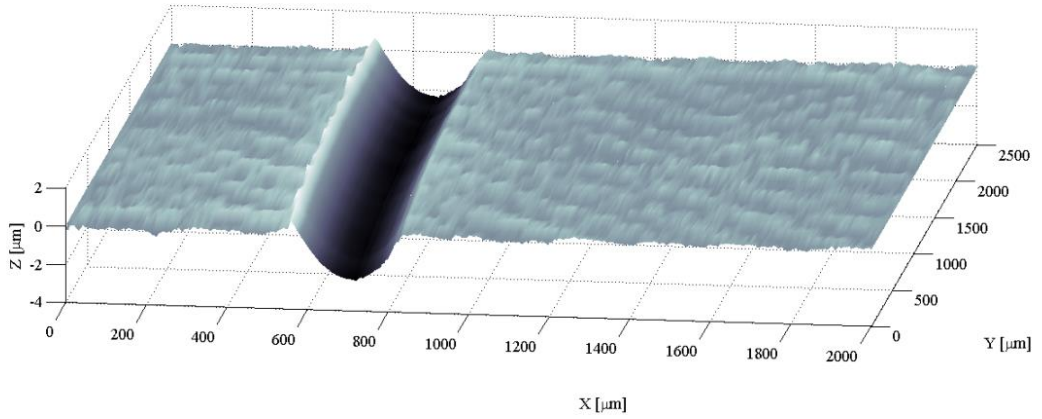

Figure 40: Three dimensional surface profile of a wear track obtained for wear measurements.

Friction experiments were repeated for various nanoparticle concentrations. The average value of COF for sliding distances over the first 1000 m was reported as the COF value of a test. The friction results were paired with the wear measurement as shown in Fig. 41. It was observed that the silver nanoparticle additives are capable of reducing both friction and wear at different nanoparticle concentrations. COF and wear tend to monotonically

decrease as the nanoparticle content increases. A notable point is that the nano-lubricants used in this study include low concentrations of nanoparticles, namely 1.5, 3.0 and 4.5 mM. However, it is observed that both the wear and COF decrease by 35%.

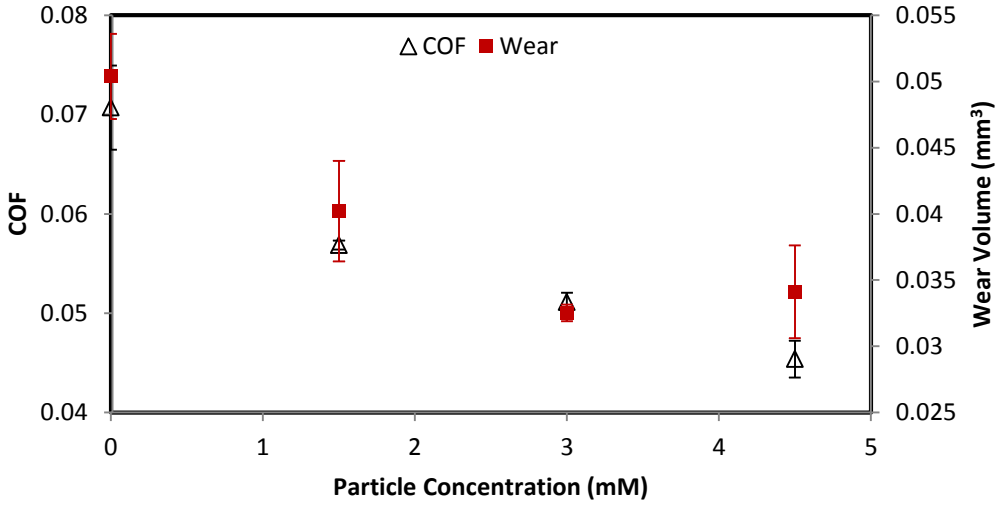

Figure 41: Effect of nanoparticle concentration on friction and wear.

A Stribeck curve analysis was performed in order to investigate the range in which the silver nanoparticle are effective in reducing friction and wear. Stribeck curves characterize the effect of the lubricant in various lubrication regimes i.e. the boundary, mixed, EHL and hydrodynamic lubrication regimes. A Stribeck curve shows the COF values versus viscosity multiplied by speed over load or pressure ($\eta\omega/F$ or $\eta\omega/P$) depending on the availability of a contact pressure value. Such curves are usually generated by changing load or speed and recording the COF. However, it is usually challenging to generate a repeatable Stribeck curve. This is due to the fact that the contact is usually abrasive in the boundary and mixed regimes, hence the geometry of the contact pairs tend to change during the test which will skew the data. In order to overcome this challenge a series of experiments were performed at different normal load and speed values. The test procedures were evaluated based on the repeatability of the results. Finally a test procedure was found using a trial and error scheme that yields repeatable results with

the lowest error values. The Stribeck curves for the control and the 3.0 mM nano-lubricant is shown in Fig. 42. The results demonstrate the effectiveness of silver nanoparticles throughout boundary and mixed lubrication regimes. The nanoparticles decrease the COF the most in the mixed lubrication regime. Deeper into the boundary lubrication regime the particles seem to have a lesser effect on the COF.

An interesting observation is that the performance of the nano-lubricant and the control does not converge at the end of the mixed lubrication regime (right side of the graph). This was in contradiction to our speculation which was that the control lubricant should outperform the nano-lubricant once there is no contact between the surface i.e. EHL or HL. This was speculated due to the fact that the nano-lubricant has a higher viscosity and should yield in a greater COF value once the genesis of the friction is from the shearing of the lubricant film. However the graphs in Fig. 42 did not support that idea as the curves do not seem to converge at the end of the mixed lubrication regime. This phenomenon was investigated in depth [123] and the results were discussed in the previous chapter.

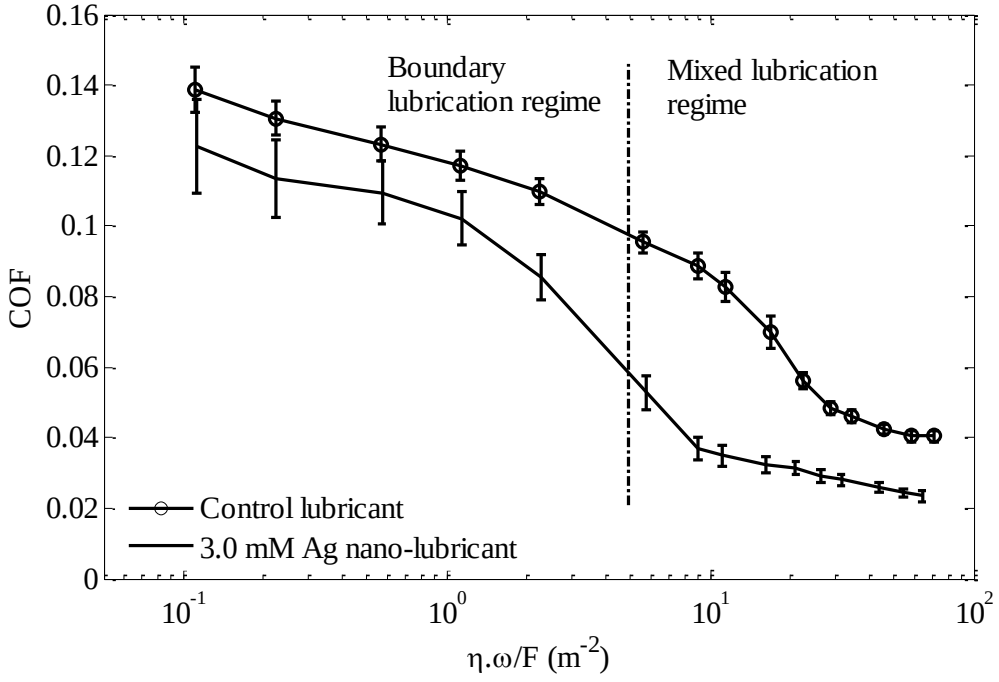

Figure 42: The Stribeck curve obtained for the nano-lubricant and the control showing the performance of the lubricants in boundary and mixed lubrication regimes.

6.3. Surface analysis

X-ray photoelectron spectroscopy (XPS) analysis were performed on the surfaces in order to investigate the effect of the Ag nanoparticles on the surface. XPS is strictly a surface method having a probing depth of about 6 nm. XPS is capable of detecting small amounts of elements on the surface. In addition, XPS can detect the bonds between the elements by measuring the shift in energy peaks. Therefore, XPS is an excellent tool to be used for our tribological purposes. The surfaces were rinsed with distilled water prior to surface analysis. The analyses were performed inside and outside of the wear grooves. It was observed that the wear surface is largely Fe oxide, as observed by the Fe2p peak shape and binding energy (Figs. 43 and 44). The Fe2p peak has the general shape and energy as Fe_2O_3 which is the stoichiometric native oxide of Fe. Analysis also revealed that there is slightly more Ag in the wear groove than outside the groove. XPS outside the groove shows that the amount of surface Ag is very small (~ 0.5 wt%). Moreover, no bond between the Ag and any other surface element was found. Given these points, it was concluded the Ag particles don't chemically interact with the surface or physically deposit on the surfaces in large numbers.

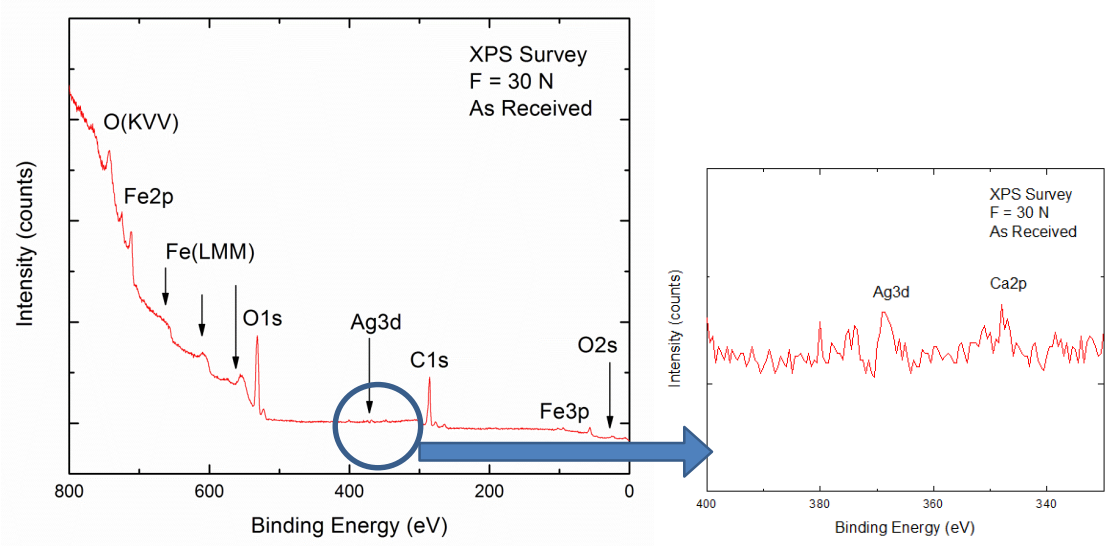

Figure 43: XPS analysis spectrum obtained inside the groove of a sample tested with the nano-lubricant.

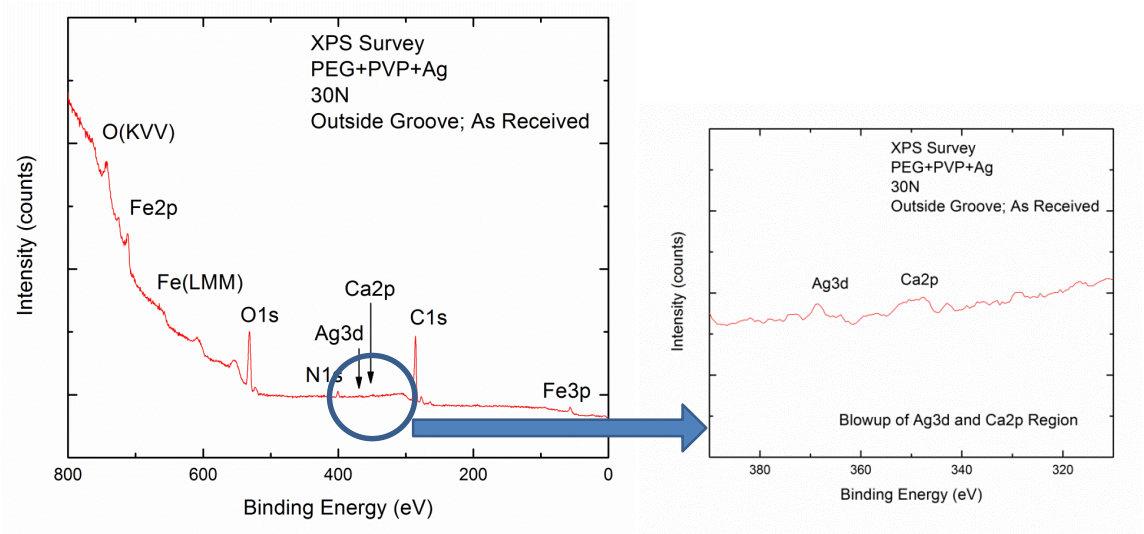

Figure 44: XPS analysis spectrum obtained outside the groove of a sample tested with the nano-lubricant.

6.4. Discussion and conclusion

In this work a new type of polyethylene glycol (PEG) based nano-lubricant was introduced. The reaction of the nano-lubricant to shearing starin was investigated using viscometry experiments. The viscosity of the nano-lubricant was measured at different temperatures, shear rates and particle concentrations. Friction experiments were carried out using a pin on disk tribometer. Wear analysis were performed using a stylus profilometer. Results showed that the Ag particle (even in small concentration, 4.5 mM) are very effective in reducing both the COF and wear. Moreover, Stribeck curve analysis revealed that the particles are effective throughout the mixed and boundary lubrication regime. However, silver particles are most effective in the mixed lubrication regime, yielding up to 35% reduction in the COF and wear. Surface analysis was performed that suggested the particles don't interact with or alter the surface significantly.

The results are in agreement with the previous studies on CuO particles. However, in this study softer Ag nanoparticles don't scratch the surface to generate abrasive wear. On the contrary, the Ag particles can reduce wear as was predicted using the reduction in the

real area of contact mechanism. Unlike the CuO particles Ag particles seems to have a more pronounced effect on the mixed lubrication regime's performance. CuO particles were observed to be more influential deeper in the boundary lubrication regime. This is because Ag particles are softer and tend to yield easier than the CuO particles. Our observation offers a method for tailoring the nanoparticle additives for a specific application. For example, if the system of interest is performing in the boundary lubrication regime, harder particles are likely to be more effective, while softer particles such as Ag particles are better suited for applications in the mixed lubrication regime.

7. The performance of nanoparticles in fully formulated oils

Nanoparticles when suspended in a lubricant can infiltrate small gaps between a rough surface contact and alter the contact's tribological performance. The ability of nano-size particles to pass through conventional filters, penetrate into contacts that larger particles cannot, along with the enhanced scale dependent properties of the nano-sized particles have made them a promising new type of lubricant additive. Different nanoparticles have proven to reduce the coefficient of friction up to 25% and 50% in recent studies[39, 109]. However, there are contradictions in the reported effects of nanoparticles on wear. Moreover, the dominant enhancing mechanisms of nanoparticles are uncertain or unknown with few exceptions (such as for MoS_2 particles). All of the proposed active mechanisms for nanoparticles such as rolling [111], transfer films [39], formation of tribofilms [113], polishing [133], and reducing the real area of contact [83, 109] would justify the friction reduction induced by the nanoparticles. However, a physical understanding that explains the synergic effect of these mechanisms and the effect of nanoparticles on wear is yet to be formalized. This is the missing link in our understanding on the nano-lubricants and hinders the industrialization of nano-lubricants in major applications. Also by studying the effect of nanoparticles on wear one can differentiate between and evaluate the proposed mechanisms for nanoparticles. Therefore, the current work will study the effect of different nanoparticle additives in fully formulated oils on friction and wear.

Some of the results in the literature are inconclusive and contradicting, some classic examples are studies reporting the use of diamond nanoparticles to reduce wear [111, 134] while they are used for gemstone polishing because they produce "the highest material removal rates" [135, 136]. Another example is that some particles are reported to increase or decrease wear and friction in different studies. When it comes to

investigating nano-lubricants, there are several pitfalls and complications that entangle the conclusion of the studies. (1) Abrasive particles can polish the surfaces and change the surface roughness (nanopolishing) and (2) nanoparticles will influence viscosity which in turn could change the tribology of contact or regime of lubrication. (3) Nano-lubricants studied in nano or micro-tribometers neglect the macro effects of the system such as the elastic deformation of surfaces and hydrodynamic pressure. (4) There exists a lack of information about the contact mechanics of nanoparticles; for example, if particles are not loaded enough to yield, the formation of transfer films by particles can't be the active mechanism. That is why the current work uses strategically designed and thorough experimental analyses to assess the full effect of nanoparticles on wear and friction in fully formulated oils. A secondary focus will be on elucidating the role of nanoparticle additives in lubrication.

7.1. Experimental approach

Friction and wear in a nano-lubricated interface is the result of nanoparticle to surface and surface to surface interactions. The current work aims to investigate both of these interactions independently to better understand the role of the nanoparticles in a fully formulated oil. Three sets of experiments were designed to investigate the system in depth.

(1) Nanoparticles in dry form: in these experiments CuO particles in powder form were used to conduct dry friction experiments. The CuO nanoparticles can be obtained in and out of solution without any chemical interventions. Therefore, CuO particles are an ideal candidate to perform dry friction tests to understand the explicit role of nanoparticles in contact.

(2) Base lubricant's effect: in these experiments CuO particles are suspended in (i) dodecane, (ii) polyalphaolefin (PAO) base oil and (iii) fully formulated SAE 5W20 engine oil. The friction experiments on nano-lubricants with the same type and concentration of the nanoparticles can reveal the role of surface to surface interactions in the system.

(3) Nanoparticle's effect: In order to study the effect of nanoparticle's character on these systems three types of nanoparticles were used: silver (Ag), copper oxide (CuO) and diamond nanoparticles (all are stable in the suspensions). Our previous studies showed that Ag nanoparticles decrease the wear while CuO particles can result in a decrease or increase in wear based on the test conditions and diamond nanoparticles are abrasive. Therefore, this choice of nanoparticles covers the full spectrum of nanoparticle hardness.

The CuO nanoparticles are similar to the particles described and used in the studies of section 2, i.e. CuO nanoparticles coated with sodium oleate. However, for this study the particles were obtained in a chloroform solution. The nanoparticles in the chloroform solution were applied on the surface and dried using a heating lamp. This would leave dry CuO particles in powder form on the surface for dry tests. Moreover, the same solution can be used to make the nano-lubricants. This was done by applying the CuO-chloroform solution to the base lubricant and evaporating the chloroform using heat and vacuum while stirring the solution. All the CuO nano-lubricants were prepared at a concentration of 5.0 %wt of CuO particles to highlight the particles' effect in the experiments. It should be noted that this is a very high concentration of nanoparticles which is far from the optimum concentration of nanoparticle additives. However, for the purpose of investigating the effect of particle to surface interaction it is a logical choice.

The CuO nano-lubricant in fully formulated SAW 5W20 is also prepared as mentioned above. Hence consisting of 5.0 %wt of CuO nanoparticles coated with sodium oleate in 5W20. The diamond nano-lubricant consists of 20 nm particle suspended in 5W20 along with polyolester (POE) oil as the dispersing agent. The Ag nano-lubricant consists of 10 nm particles in 5W20 along with oleoyl sarcosine as the dispersing agent (please see appendix I for details).

7.2. Results

The experiments were carried out using the pin on disk and disk on disk methods described in previous sections. Figure 45 shows the COF versus time for the CuO

nanoparticles dry test versus the control test. It should be noted that the tests were done by a pin on disk setup with 1 Hz frequency so the time axis is also the cycle axis in these tests. Figure 45(a) shows the results for a normal load of 20 N. In this test the dry CuO nanoparticles reduce the COF significantly in the first 150 cycles. However the COF then increases to the value of the control after 150 cycles. The test was then repeated for a lower normal load of 2.0 N. The COF results on Fig 45 (b) show that the nanoparticles reduce the COF in this load as well. However, in this test the dry nanoparticles stop performing after 400 cycles. After this the COF values increases up to the value of the control again. The hypothesis was that the nanoparticles are pushed out of contact during the test and that is why there is an increase in the COF signal.

In order to put this hypothesis to the test, a new experiment on dry CuO nanoparticles were conducted using a disk on disk setup. The disk on disk setup allows for lower contact pressures. Additionally, the initial concentration of the nanoparticles on surface can be controlled due to the large contact area in this setup. Two disks were prepared for the tests with two different concentration of nanoparticles deposited on them (see Figs. 46 (a),(b) and (c)). Figure 46(d) shows the results in terms of COF versus time. The particles are able to reduce friction in both cases. The disk with the higher concentration of nanoparticles stop performing at about 1200 sec whereas the disk with the lower concentration of the nanoparticles stops performing at about 600 sec. Figure 46 (e) shows the same graphs as Fig 46(e) only the graph for the lower nanoparticle sample is shifted to the right. It is interesting to see the two graphs overlap one another and the only difference is the starting point. In case of the higher concentration of the particles, it takes longer for the particles to get pushed out of contact. It seems like there is a critical concentration below which the nanoparticles can't sustain a reduced COF. The initial concentration of the particles on the surface determines how long it takes for the critical concentration to be reached in the test. This provides more proof that the behavior observed in this study so far is governed by the concentration of the nanoparticles on the surface.

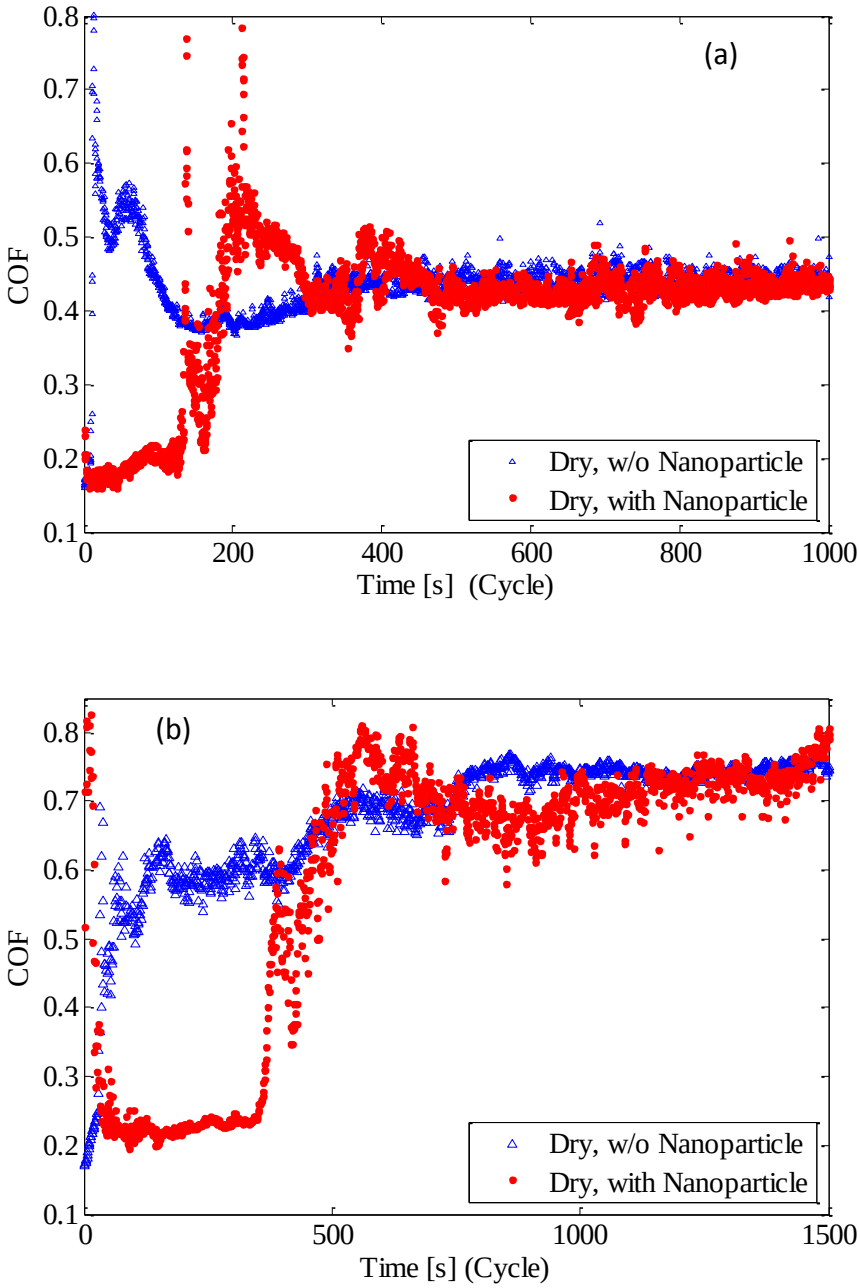

Figure 45: Pin on disk dry tests performed on CuO particles with the normal load of (a) F=20 N and (b) F=2.0 N

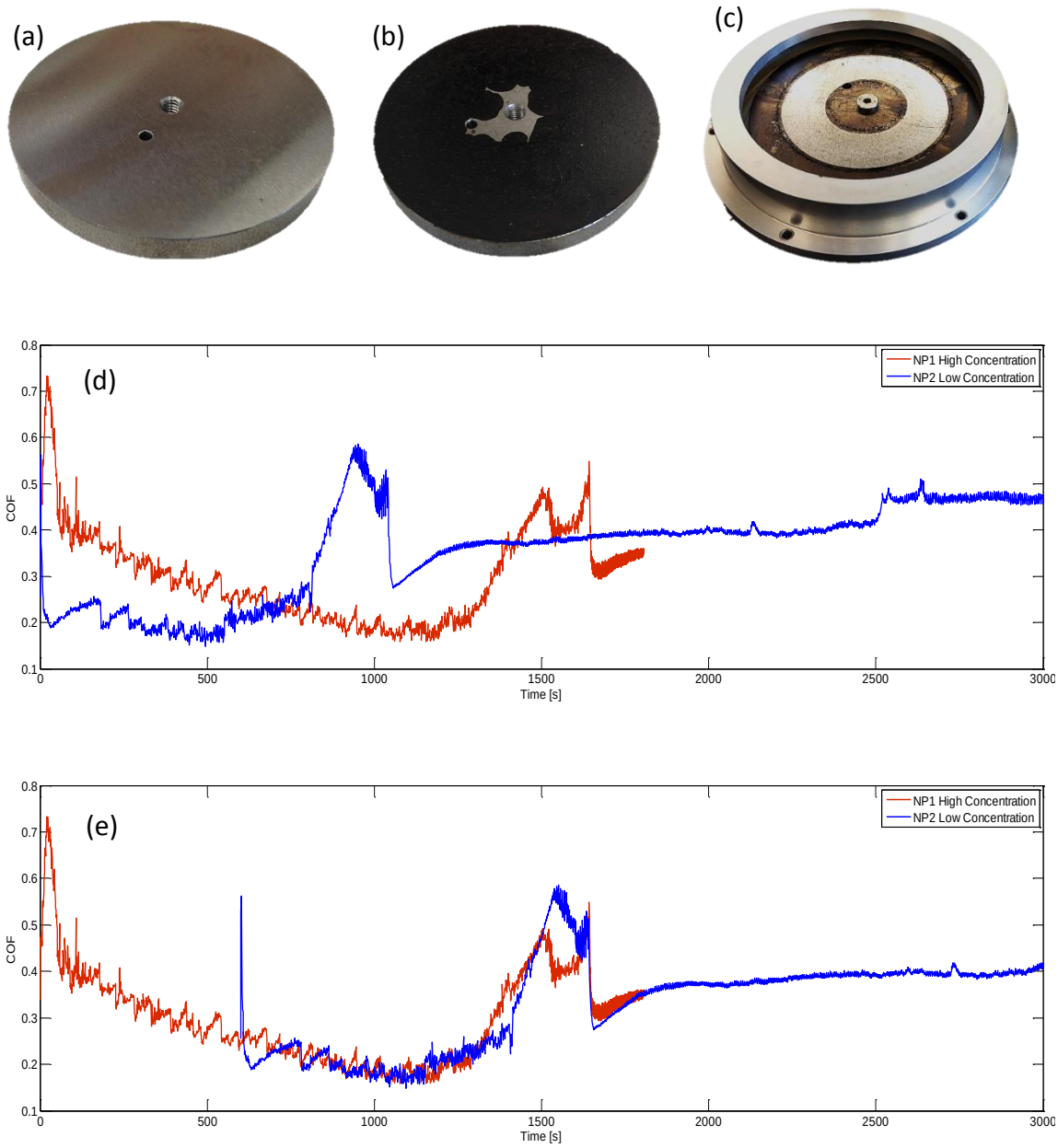

Figure 46: (a) The control disk without any nanoparticles, (b) The disk with the high concentration of dry nanoparticles, (c) The disk with the low concentration of nanoparticles stopped at 600 sec. (d) Disk on disk dry tests performed on CuO particles with two different concentration of particles on the surface. (e) The low concentration curve was shifted to right to demonstrate the repeatability of the tests.

In order to prove that the performance of the particles on the surface is solely governed by their concentration another dry test was run. In this experiment the nanoparticles were deposited on the surface in the powder form and the test was run at normal load of

F=2.0 N. As was expected the dry CuO particles stopped reducing COF at about 400 cycles, Fig 47. However, this time the test was stopped and dry CuO nanoparticles were applied to the surface to account for the particles pushed out of contact zone. The test was resumed afterwards and as the results show on Fig. 47 the particles decreased the COF for another 400 cycles. Afterwards, the COF began increasing again. This time the test was stopped and some of the nanoparticles in the pile-up around the edges of the contact were pushed back to contact zone. The test was resumed and it was observed that the small amount of the particles could decrease the COF again. This test proved that the reduction of the nanoparticles concentration is most responsible for the increase in friction. However, there is another major observation to be made here that is, there is a critical concentration of the nanoparticles below which the nanoparticles can't decrease friction. In other words, as the nanoparticle content is being reduces as the test progresses (Figs. 45 and 47) the COF seems to be fairly constant until it reaches a certain point. Beyond this point the nanoparticles can't decrease the COF anymore and the COF begins increasing rapidly until it reaches the control's value. In order to measure this critical concentration a test was stopped right before the particles stop performing. An XPS analysis was performed inside the contact zone to measure the stoichiometry of the elements on the surface. The measurement showed that there is 1.6 at% of Cu on the surface right before the particles stop performing. The XPS analysis on the control sample did not show any trace of Cu element. Additionally surfaces were drilled by 12.5 nm using Ar sputter cleaning. Analysis on the drilled surface didn't show any trace of Cu which means Cu is strictly present on the surface only.

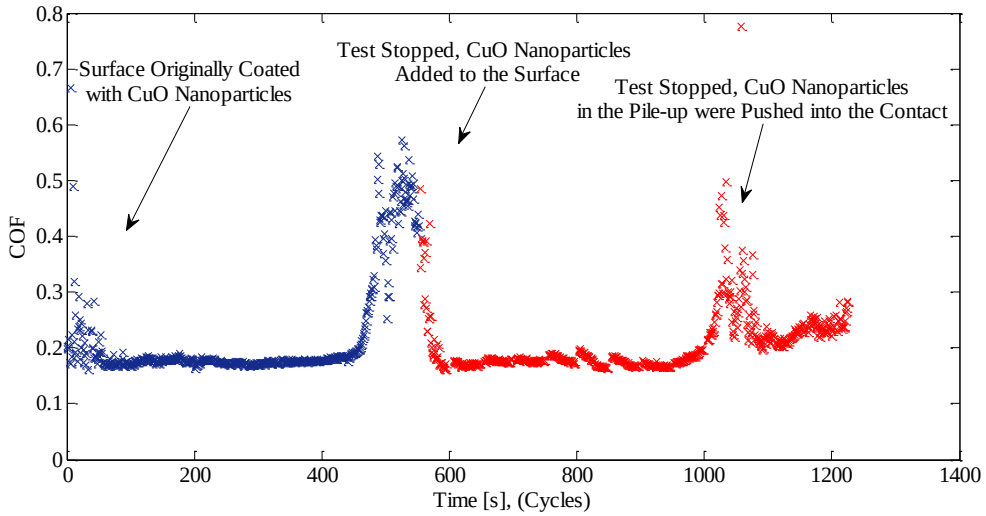

Figure 47: COF in a pin on disk dry test performed on CuO particles. The test was stopped when the nanoparticles stopped performing to add particles to the contact and resume the experiment.

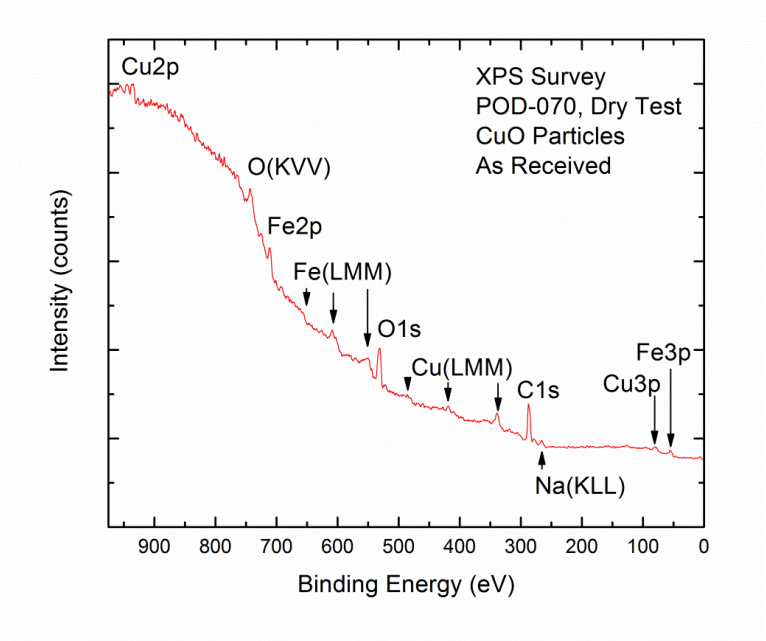

Figure 48: XPS surface analysis inside the groove of a sample tested with the dry nanoparticles right before the particles stop performing to measure the critical nanoparticle concentration.

More dry experiments using the CuO particles were run to investigate the effect of the particles on wear. Results presented in Fig. 49 show that the nanoparticles in dry form significantly reduced the wear as well as the friction.

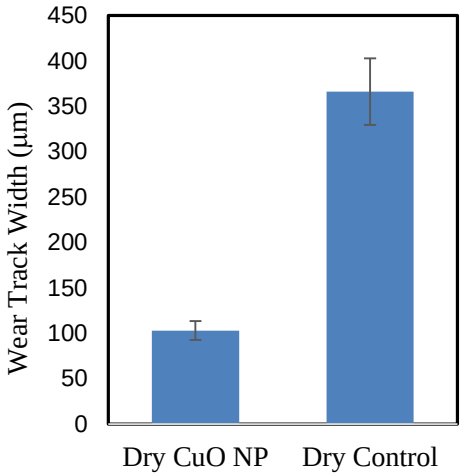

Figure 49: Wear measurement for a samples tested with the dry nanoparticles versus a dry control test.

The next round of experiments were done using the CuO particles in various base lubricants. The tests were started with CuO suspended in dodecane ($C_{12}H_{26}$). Dodecane was chosen as it represents an inferior lubricant relative to commercial oils. A 5.0 %wt solution of the CuO nanoparticles in dodecane was prepared. Friction tests were performed using the pin on disk setup at normal loads of 2.0 and 20 N. Figure 50 shows the COF versus time for normal load of 2.0 N. The results show that the CuO particles are able to decrease the COF significantly throughout the experiment.

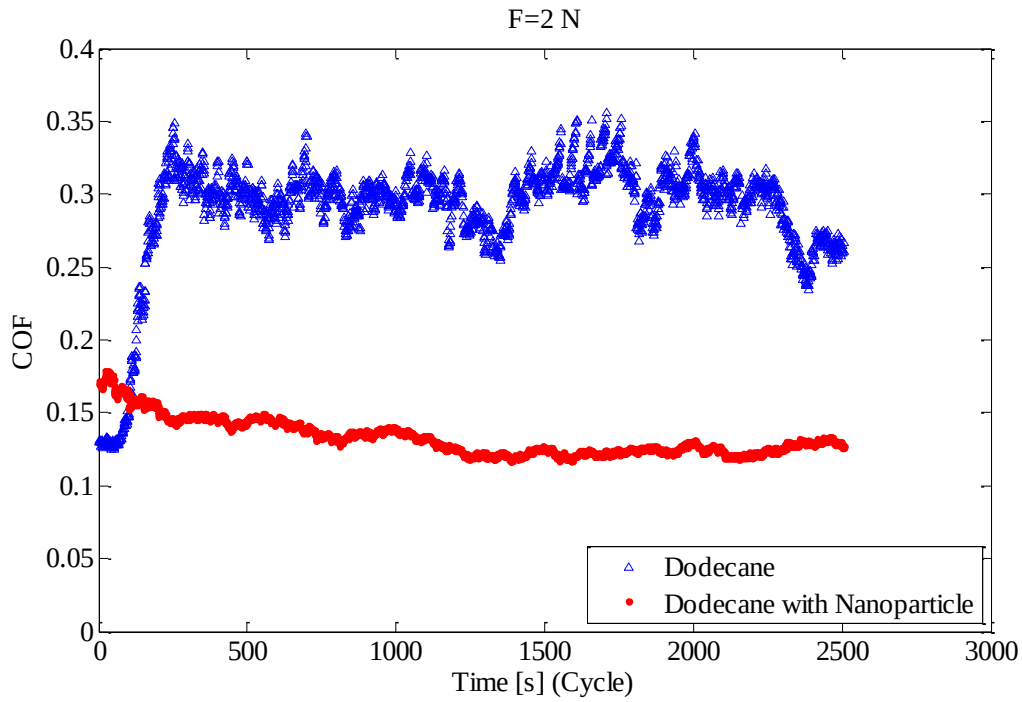

Figure 50: COF versus test progress for CuO dodecane nano-lubricant and the control at normal load value of F=2.0 N.

The tests were repeated and the wear measurements were carried out using the three dimensional profiles, Fig. 51. The results are presented in Fig. 52 and show that the CuO particles when suspended in dodecane can reduce both friction and wear significantly. It should be noted that in Fig. 51, for the nano-lubricant at a normal load of F=2.0 N, no measurable wear was induced during the test. The wear results are in sync with the friction results and the nanoparticles are effectively reducing friction for different normal loads.

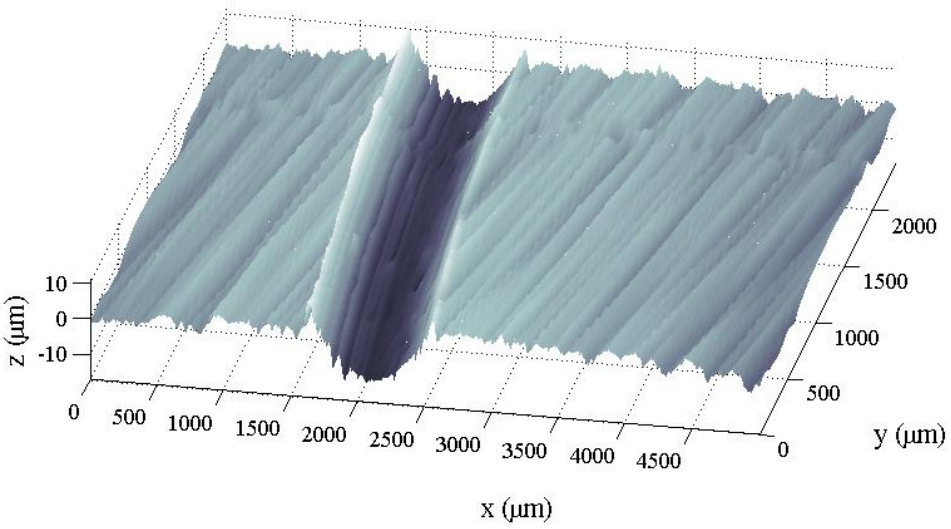

Figure 51: Three dimensional profile of the wear track for a sample tested with the control dodecane solution at normal load of F=20 N.

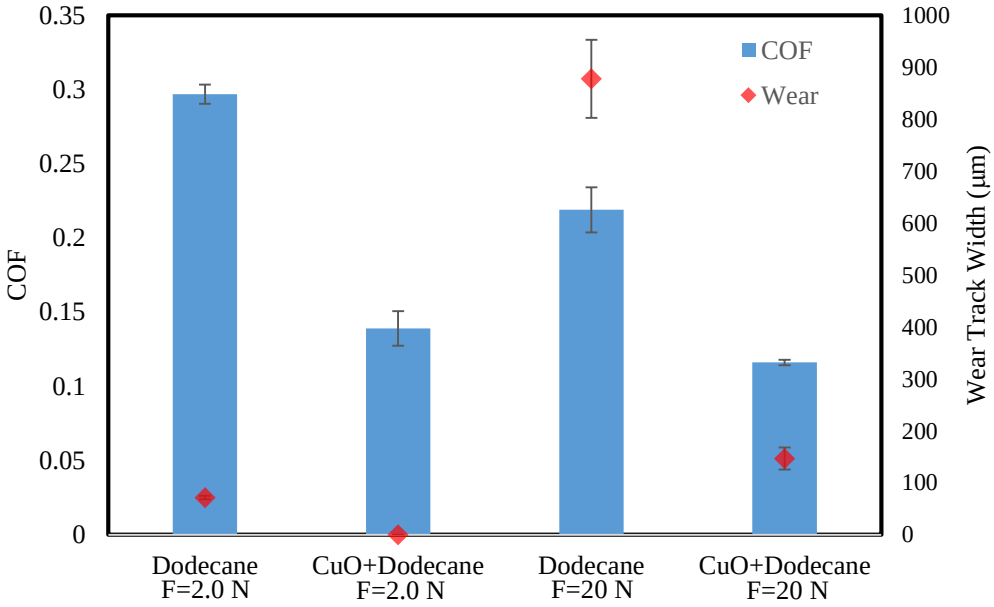

Figure 52: Friction and Wear analysis for CuO nanoparticles suspended in dodacane at various normal loads.

The next round of the tests were perform on a nano-lubricant containing CuO particles in PAO. PAO is a common synthetic base oil and is used in our experiments as a superior base oil. Fig. 53 shows the COF versus time (cycle) for a pin on disk test at normal load of

F=20N. In this case it is observed that the control PAO sample marginally out performs the nano-lubricant. However, when the test was repeated at a higher normal load of F=50 N, the nano-lubricant yields a lower COF value, Fig 54. The tests were repeated and a wear analysis was performed using three dimensional profiles of the wear tracks (Fig.55).

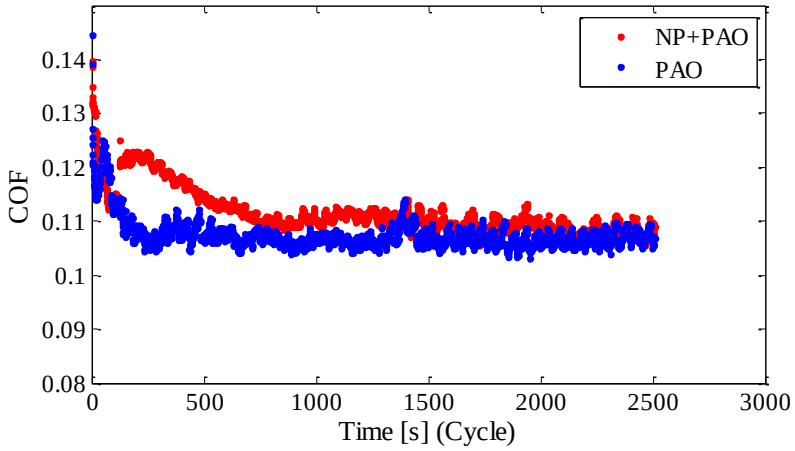

Figure 53: COF versus test progress for CuO PAO nano-lubricant and the control at normal load value of F=20 N.

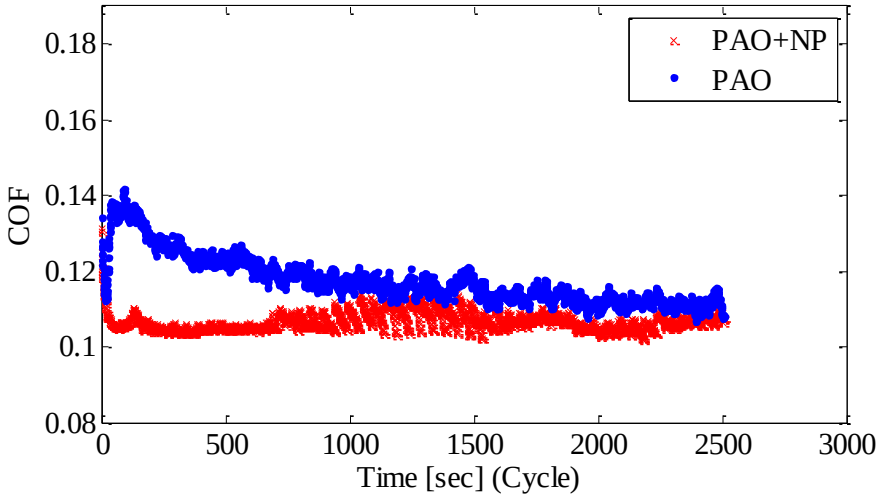

Figure 54: COF versus test progress for CuO PAO nano-lubricant and the control at normal load value of F=50 N.

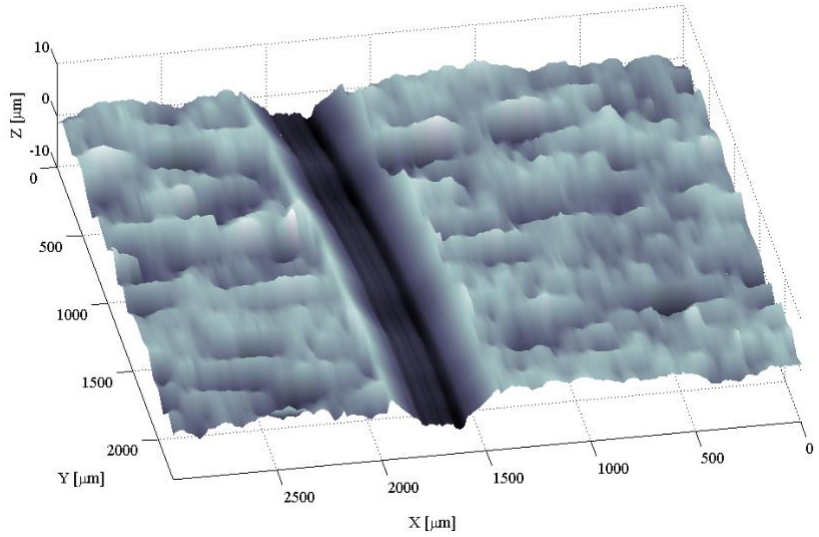

Figure 55: Three dimensional profile of the wear track for a sample tested with the control PAO solution at normal load of F=50 N.

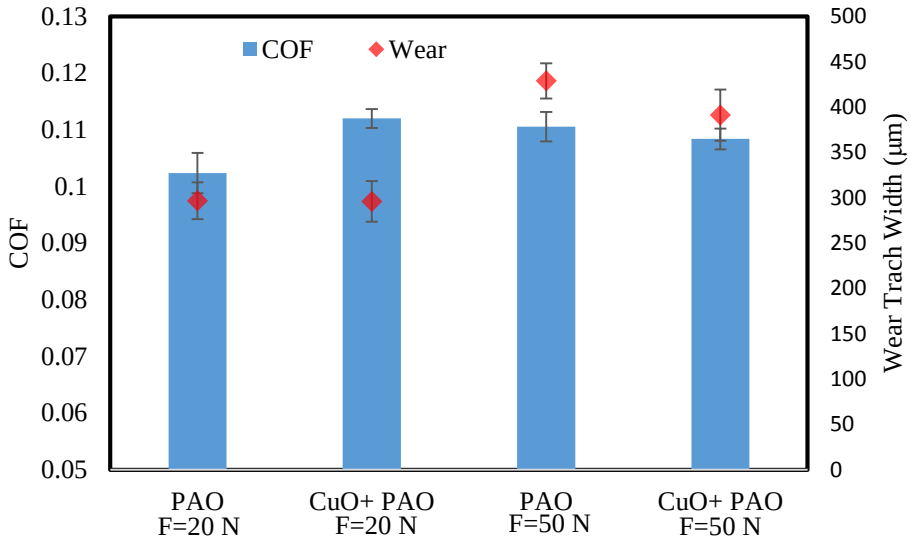

Figure 56: Friction and Wear analysis for CuO nanoparticles suspended in PAO at various normal loads.

The friction and wear results presented in Fig. 56, show that the performance of the CuO particle in PAO depends on the normal force. The particles are increasing friction at a lower normal load of F=20 N while they decrease friction at F=50 N. The effect of particle

on wear is also mixed. The CuO particle additives don't affect wear at F=20 N while decreasing wear at F=50 N. A possible explanation is that at higher loads there is higher possibility of particles engaging in contact hence promoting the reduction in contact area mechanism. This is probably why particles have a more positive effect at higher loads.

Next, a set of experiments were conducted that focused on the effect of CuO nanoparticle additives on fully formulated SAE 5W20. Commercial oils such as 5W20 usually contain 10% to 20% additives by volume. Lubrication additives influence different properties of the base oil such as viscosity modifiers, anti-oxidants, extreme pressure additives, friction modifiers, antiwear additives, corrosion inhibitors, pour point modifiers, anti-misting additives, anti-foam additives, etc. Some of these, such as extreme pressure additives and antiwear additives are designed to form a protective layer on the surface called a tribofilm (often called boundary films). A tribofilm can physically or chemically bond to the surface and has a sacrificial role in lubrication. These nano size tribofilms help minimize direct metal on metal contact, which would result in severe wear and friction.

CuO particles were added to 5W20 engine oil by a concentration of 5.0 %wt and the pin on disk setup was used to perform the experiments. The friction tests were performed at normal loads of 20, 50 and 150 N. Wear measurements were performed using three dimensional surface profilometry. The friction and wear results are presented in Fig. 57. CuO particles are observed to consistently increase the COF when added to the formulated oil (this is due to the high concentration of the particles that was used in this test.). However the effect of nanoparticles on wear is mixed and varies with the normal load. At the lower loads of 20 and 50 N the nanoparticles were capable of reducing the wear. However, when the load was increased to 150 N, nanoparticles had a negative effect on wear. At higher loads, the film forming additives of the 5W20 are more active. In addition, nanoparticles are more inclined to abrade the contact surfaces at higher loads. Therefore, there is possibility of nanoparticles interaction with the tribo-films (absorbed films) which needs to be investigated.

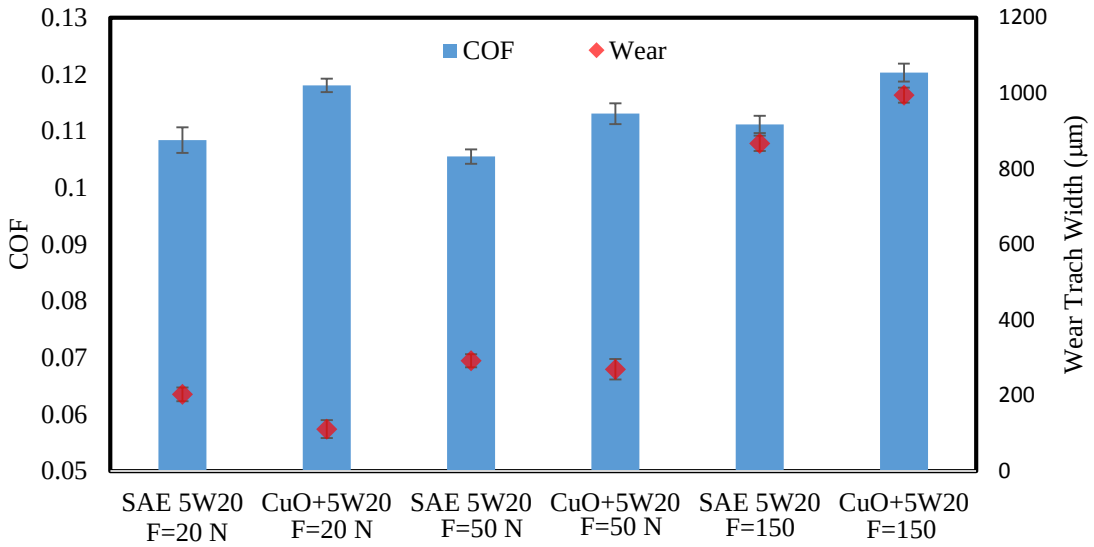

Figure 57: Friction and Wear analysis for CuO nanoparticles suspended in the fully formulated SAE 5W20 engine oil at various normal loads.

A surface that was tested with a solution of CuO particle in 5W20 and a control surface were analyzed using the XPS. Two analyses were performed on each surface, one on the surface as received after the tests and another analysis was performed after the surfaces were drilled 12 nm with the Ar sputter cleaning. On the control sample traces of Fe, O, C, F and Si were detected (see Fig 58). The majority the surface is made of C which is from the lubricant residues on the surface. The analysis after Ag sputter cleaning showed that the drilling process removed all of the F and Si on the surface and only Fe, O and Carbon was detected. Therefore it is evident that F and Si are within the absorbed layers (tribofilms) of the 5W20 on the surface. Similar analysis was performed on a sample tested with the CuO nano-lubricant. Traces of Fe, O, C, F, Si and Cu were detected on the surface. However, the amount of F and Si on the surface is lower than that of the control sample. Similar to the control, the traces of F, Si and Cu vanished after the Ar sputter cleaning. This result shows that the presence of the particles in high concentrations can

interfere with the formation of tribofilms. The wear analysis that showed particles increase wear also supports this idea.

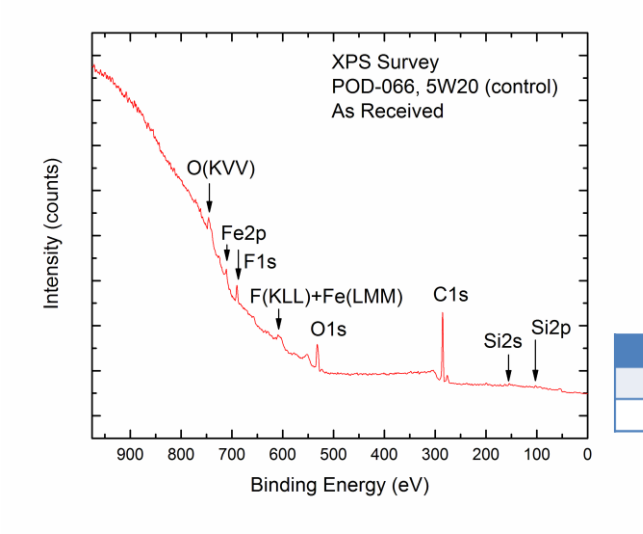

XPS Surface Elemental Composition (at%)				
Fe	O	C	F	Si
1.0	12.3	80.4	3.3	3.1

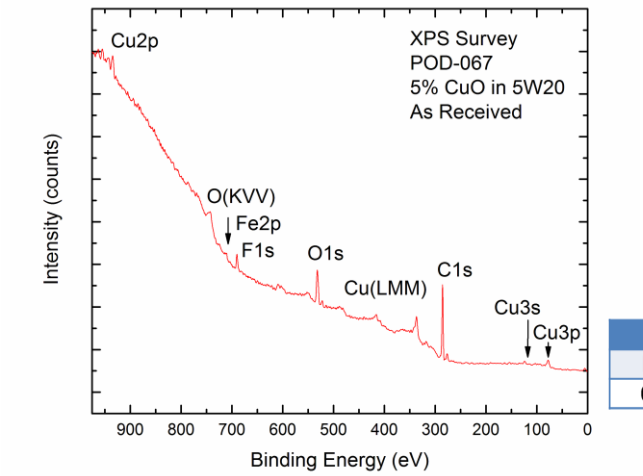

XPS Surface Elemental Composition (at%)					
Fe	O	C	F	Si	Cu
0.5	15.7	78.7	2.4	1.4	1.2

Figure 58: XPS surface analysis performed on samples tested with (top) control and (b) the CuO nano-lubricant in the 5W20 oil at normal load of F=150 N.

The next set of experiments were conducted using the diamond nanoparticles suspended in fully formulated SAE 5W20 engine oil. The first objective of this study was to investigate the effect of particle concentration on the performance of the nano-lubricant. The experiments were run on eight samples containing various concentrations of diamond particles. The concentrations used in the study were 0.0, 0.005, 0.01, 0.015, 0.03, 0.05,

0.08, 0.12 %wt. The experiments were conducted using a pin on disk setup at a normal load of 100 N. Each test was run for three hours and repeated three times. The wear analysis was performed using surface profilometry. Fig. 59 shows the variation of the COF versus diamond nanoparticle concentration. The results showed that there is a minimum COF value that corresponds to a concentration of 0.01 %wt of the diamond particles. At higher concentrations the COF rises again and reaches a plateau at about 0.08%wt. It is also interesting to note that this optimal concentration occurs over a relatively narrow range.

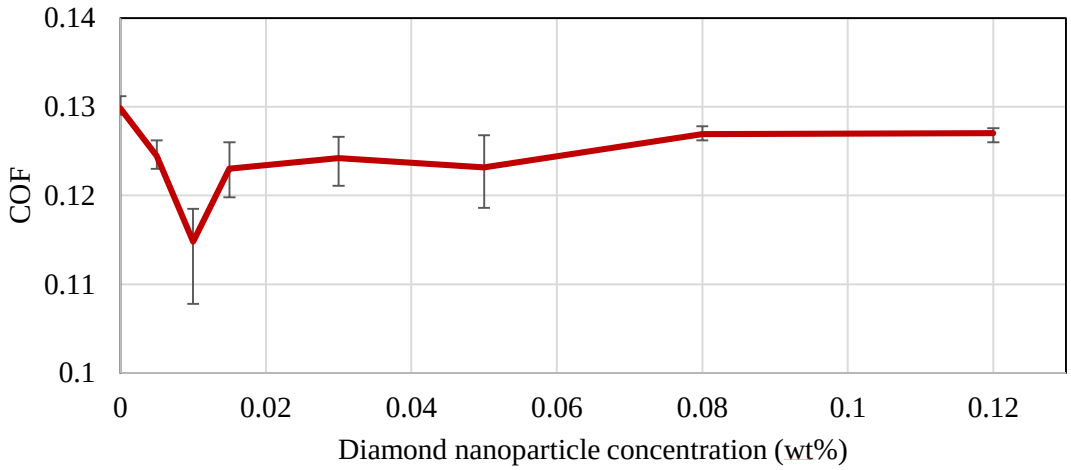

Figure 59: Friction analysis for various concentrations of diamond nanoparticles suspended in the fully formulated SAE 5W20 engine oil.

The effect of diamond particles on wear is shown on Fig. 60. It is observed that the particles can reduce the wear marginally at low concentrations (<0.05 %wt). However, at the higher concentrations diamond particles increase wear in the system. This is similar to the effect observed with the CuO particles and due to the abrasive effect of particles on the absorbed films (tribofilms).

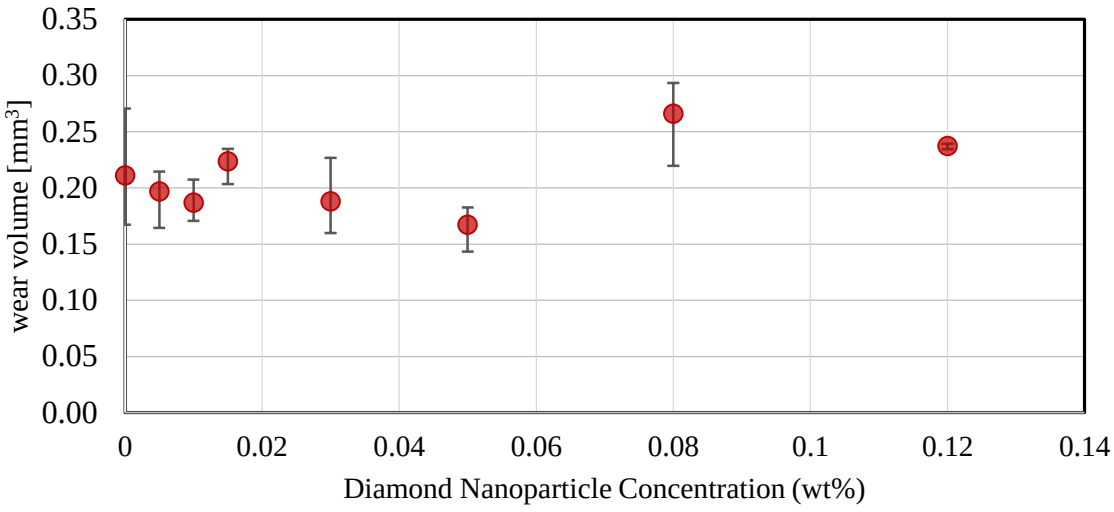

Figure 60: Wear analysis for various concentrations of diamond nanoparticles suspended in the fully formulated SAE 5W20 engine oil.

As evident from Fig. 60 higher concentration of diamond particles have a minor but observable abrasive influence on the contact pairs. Some claim that such an abrasive effect could result in minor but positive change in the surface morphology [137]. For example, nanoparticles can re-polish the old contact pair surfaces such as old gears and reduce roughness. This could also help with the break-in period of machinery. Particles may also abrade away the soot and residue buildups on the surfaces, especially in automotive engines to enhance the overall performance. Therefore the next set of analysis was focused on the quantifying the polishing effect of diamond particles on the surfaces. First it should be noted that the polishing effect, even though has genesis in abrasive contact, is different than wear. Wear is simply a measure of the amount of material that is moved or removed during the course of contact. On the contrary, polishing is the effect of the contact process on the texture of the remaining surface. Therefore, proper methodology is required to quantify the polishing effect induced by the particles while avoiding the confusion with wear.

An optical surface profilometer was used to accurately measure the wear groove geometry. The measurements were performed inside the wear grooves in an area of 450 μm by 450 μm. The resolution was set to be 0.1 μm in the direction of sliding and 1.0 μm

in the perpendicular direction. Fig. 61 shows one of the profiles obtained using the optical profilometer. Several calculation methods and parameters were considered to measure the polishing effect during the contact. The more accurate method was to subtract a cylindrical fit from the profile to find the overlay roughness inside the wear groove. Fig. 62 shows the cylindrical fit to the profile shown in Fig 61 and the resultant overlay roughness. Using the overlay roughness the polishing effect was quantified as a root mean square roughness, $R_q = \left(\frac{1}{N} \sum \sum \left(Z(i,j) - \bar{Z} \right)^2 \right)^{1/2}$. The results showed that diamond nanoparticle have a polishing effect on the contact surfaces and reduce the overlay roughness inside the wear groove, Fig. 63.

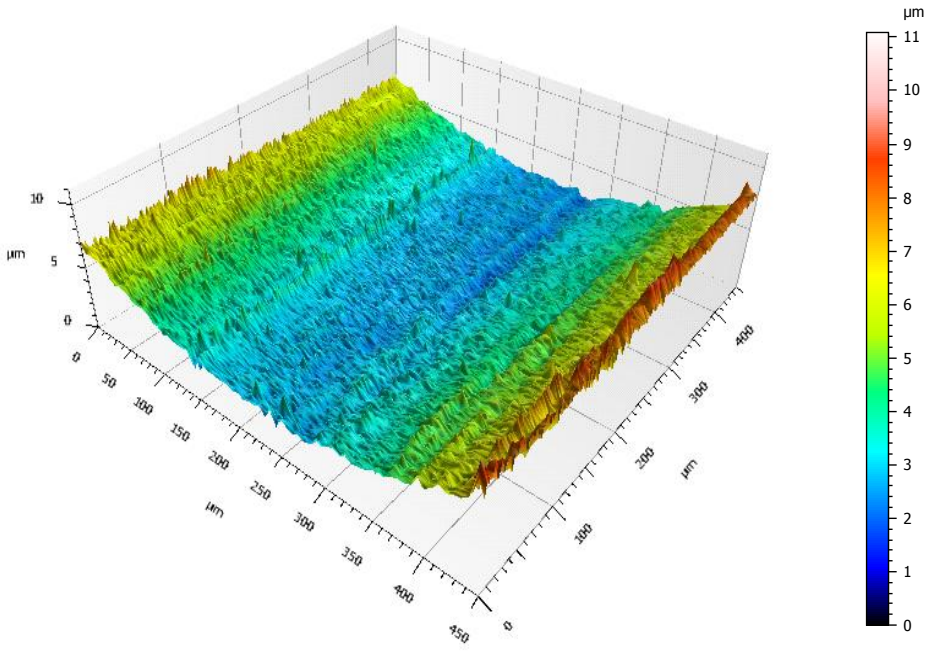

Figure 61: Three dimensional surface profile of inside a wear track obtained using an optical profilometer.

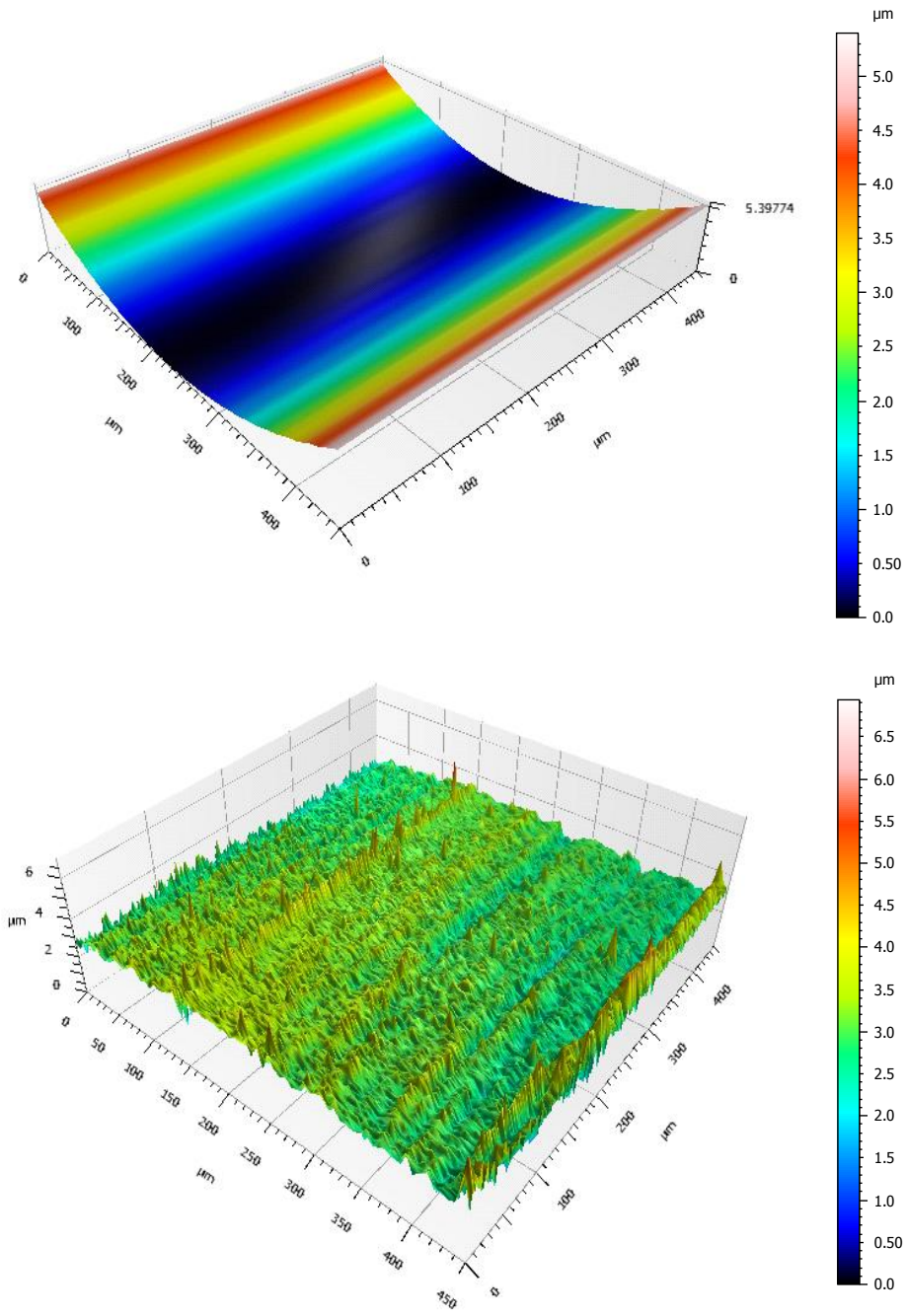

Figure 62: A three dimensional profile of the wear track decomposed into a cylindrical fit (top) and the overlay roughness (bottom).

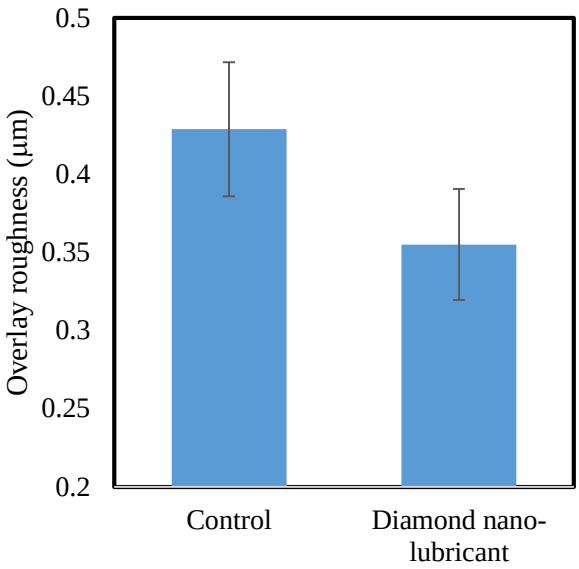

Figure 63: Overlay roughness for the control and the diamond nano-lubricant showing the effect of polishing of the diamond particles.

The last set of experiments presented in this section is on the effect of Ag nanoparticles on the fully formulated SAE 5W20 oil. A solution of 0.65 %wt Ag in 5W20 was prepared for the experiments. The experiments were conducted using a reciprocating pin on disk test scheme at a normal load of 150N. The wear measurements were also performed using three dimensional surface profilometry. The results showed a significant decrease in both friction and wear as shown in Fig. 64. Addition of the Ag particles at a low concentration of 0.65 %wt yield about a 10% reduction in COF and about a 7% reduction in wear. This result is similar to our previous experiments on the Ag nano-lubricant in PEG. Ag particles don't hinder the formation of tribofilms because of the compatibility of the metallic Ag particles with the film forming additives.

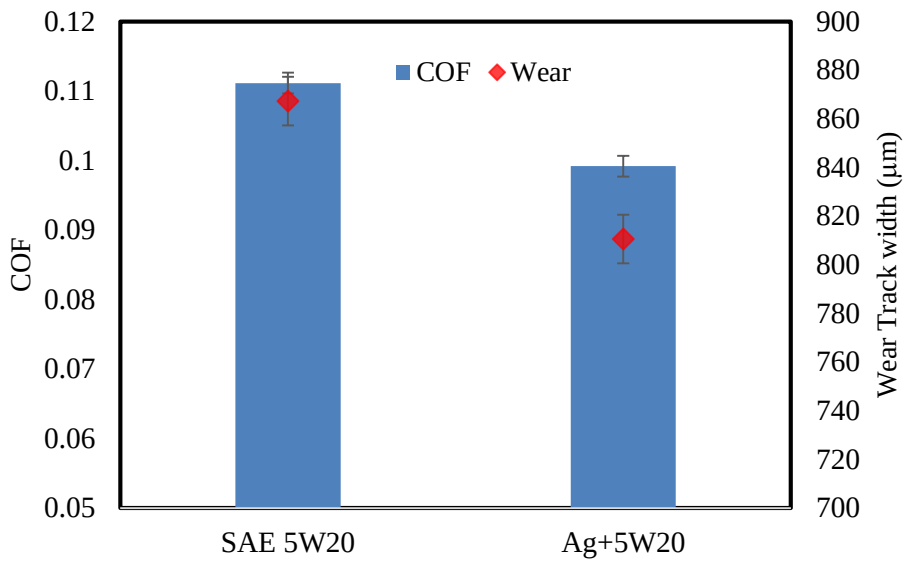

Figure 64: Friction and Wear analysis for Ag nanoparticles suspended in the fully formulated SAE 5W20 engine oil.

7.3. Discussion

The dry friction tests using the CuO particles offered some key observations. The most important was that there is a critical concentration of nanoparticles below which the particles can't sustain a reduced COF. The dry friction test offers a methodology to measure the critical value and it was found to be 1.6 at% for CuO particles. From a practical stand point this means that the particle concentration in the nano-lubricant should be such that this critical amount is fed into the contact zone. Also, the reduced COF value was observed to not be directly related to the nanoparticle content in contact as long as the concentration is above the critical value. This observation is in agreement with the proposed reduction in the real area of contact mechanism. If this mechanism is responsible for the reduced COF, high concentrations of nanoparticles result in an overlap between the void areas around the particles. Thus explaining why the reduced COF value is independent from the nanoparticle content at higher concentrations. While at low concentrations the average force on the nanoparticles is increased and they can't sustain

a gap between the surfaces. This means that they can't create void areas and thus can't decrease the COF by reducing the real area of contact.

The tests on dry CuO and CuO solution in dodecane, PAO and 5W20 showed some interesting trends. The particles are more effective at reducing friction and wear when suspended in an inferior lubricant or in a dry form. The particle's effect on PAO base oil is dependent on the normal force (contact pressure) and is desired at higher loads. The particle's effect on fully formulated SAE 5W20 is also dependent on the normal force (contact pressure). All things considered it is as if the CuO particles exhibit competing effects on a contact's tribology. The effect of CuO particles exists in two forms, (i) abrasive interaction with the surfaces and (ii) reduction in the area of contact. The schematic of different effects of particles is shown in Fig. 65. Particles create voids that reduce the real area of contact. In addition, their interaction with the surface also affect the contact's tribology. In case of CuO particles, it is an abrasive interaction with the surface. Both of these interactions affect the overall friction and wear in the system. The overall friction in the system has two components, the friction force as the result of surface to surface interaction and the friction force as the result of particle to surface interaction, Eq. (25).

$$F_{overall} = F_{surface} + F_{particle} \tag{25}$$

The $F_{surface}$ can be rewritten as $A_s \times \tau_s$ that is the area of contact between the surfaces times the average shear stress between the surface. Substituting this into Eq. (25) yields the overall friction as shown in Eq. (26).

$$F_{overall} = A_s \tau_s + F_{particle} \tag{26}$$

The CuO particles affect both of the friction components. They directly induce a friction force by scratching the surface, $F_{particle}$, They also affect the friction force between the surfaces by reducing the area of contact, A_s. These two effects are competing and one can dominate the system depending on the normal force, the lubricant type (τ_s) and the particle content. In the case of dry tests or inferior lubricants, τ_s is so large that the first

term dominates the equation and the friction induced by the particles is negligible. That is why the only effect that can be seen is the positive effect of the particles on the area of contact. Hence, the results are in agreement with the reduction in the area of contact mechanism. However when a superior lubricant is used, such as the PAO, both of the terms contribute to the overall friction. Hence, this results in mixed effects based on the conditions. Similar arguments stand for the effect of nanoparticles on wear.

Expanding this discussion to the other types of nanoparticle additives one can say nanoparticle additives have a dual effect on the tribology of contact. They have a direct effect, that is the interaction of particle with the surfaces. This effect could be plowing, deposition of transfer films or rolling, see Fig 65. This interaction is dependent on the character of the individual particles. The particles also have an indirect effect, that is nanoparticles reducing the real area of contact between surfaces. This in turn can tune the effect of the lubricant on the system. This is more of a general effect induced by particles on the contact. The overall effect of the nanoparticle additives on friction and wear is determined by adding the two effects together. This explains some of the common contradictions in the nanoparticle research such as; why hard particles can decrease wear. That is because the reduction in wear is the result of the particles indirect effect on the area of contact. Another contradiction is why some particles can reduce or increase the COF depending on the base oil. That is because particles when suspended in an inferior lubricant can better influence the contact tribology through the indirect effect. Whereas, in case of a superior lubricant the particle's direct effect may over shadow that.

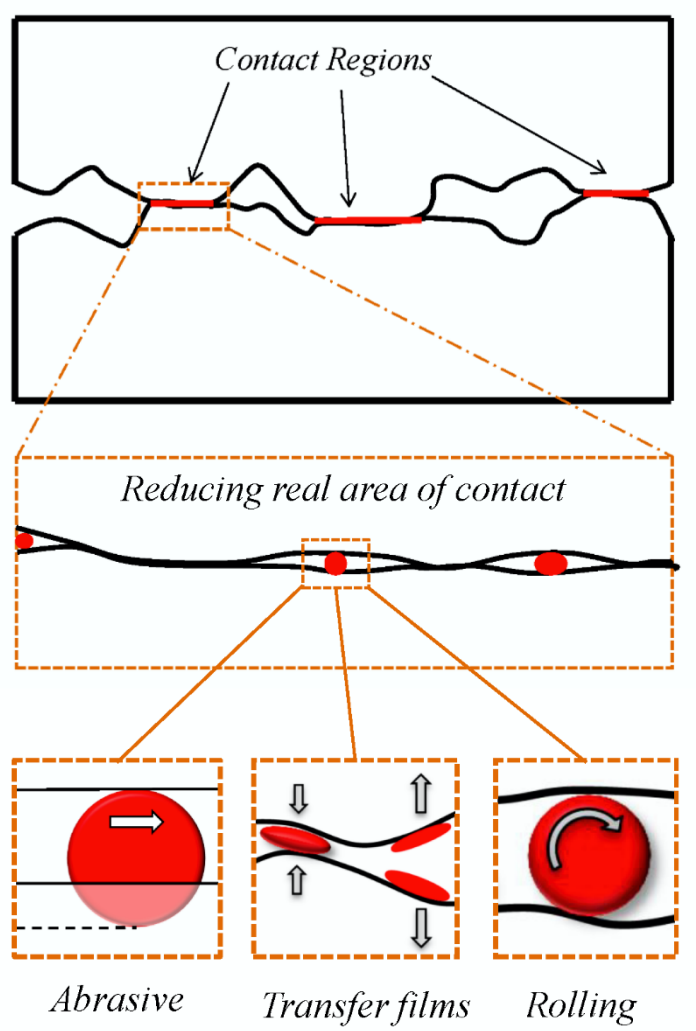

Figure 65: Schematic showing various roles of nanoparticles in a contacts' tribology.

The last discussion in this section is on the effect of the particles on fully formulated oils. The investigations on CuO particles in fully formulated 5W20 showed that the particles have a negative effect on the absorbed films (tribofilms) at higher loads. There are three possible ways to prevent this negative synergic effect of nanoparticles and film forming additives. (i) Using film forming particles: a solution is to use nanoparticles capable of forming easy-to-shear films on the surface such as MoS_2 and WS_2. (ii) Low concentrations of harder particles: harder diamond nanoparticles in low concentrations could improve lubrication while not affecting the absorbed film formation. (iii) Metallic particles: most

of the film forming additives are designed to interact with the metallic surface. Therefore, they can effectively interact with the metallic particles and tune their abrasive effect. The first option, film forming nanoparticles, has been the topic of repeated studies [11, 39, 110, 138] and therefore the current work investigated and demonstrated the viability of the latter two options.

7.4. Conclusion

In this work strategically designed experiments were used to investigate the role of nanoparticles in a contact's tribology and the effect of nanoparticles on fully formulated oils. The experiments were run using the dry CuO particles powder form and CuO particles suspended in dodecane and PAO. Experiments were also run on fully formulated SAE 5W20 oil containing CuO, Ag and diamond nanoparticles.

The dry experiments showed that the nanoparticles even absent of the lubricants can reduce both friction and wear. The behavior of the dry nanoparticles was in agreement with the reduction in the contact area mechanism. The dry experiments also presented a practical way of measuring the critical concentration of particles below which particles can't maintain a reduced COF. The studies on the effect of CuO particles in dodecane and PAO suggested that the particles have a dual effect on the contact's tribology. CuO particles can affect the tribology through direct interaction with the surfaces or by reducing the area of contact. This is why the nanoparticle effectiveness depends on the type of the lubricant and the normal load.

The effect of nanoparticles on the formation of absorbed films (tribofilms) was investigated. The results showed that the CuO particles in high concentrations have a negative effect on formation of the absorbed films. Two solution were suggested to avoid the negative effect of particles on the absorbed film. One is to use low concentrations (0.01 %wt) of hard diamond nanoparticles and the other is to use Ag metallic nanoparticles. The studies on diamond nanoparticles showed that the COF can be reduced while the wear is unaffected. Surface analysis using an optical surface

profilometer showed that the diamond particle can have a positive polishing effect on the surface. This means that these particles can reduce the overlay roughness inside the contact zones. The investigations on Ag nanoparticle additives showed that this type of particle is very effective in reducing both friction and wear. A reduction of 10% and 7% was yielded by addition of 0.65 %wt of the Ag particle to SAE5W20.

8. Conclusion

This dissertation was dedicated to study the effect of nanoparticle additives for lubrication purposes. The goal of the research was on the performance of these additives in different lubrication regimes with a focus on the enhancing mechanisms. The significant contribution of this dissertation was illuminating the performance enhancing mechanisms of nanoparticle additives in the lubricants.

The first study was performed on CuO nanoparticle additives in mineral base oils in the absence of any other additive. The particles consisted of 9 nm CuO particles coated with sodium oleate. The friction and viscosity experiments were conducted on nano-lubricants containing 0.0, 0.5, 1.0, 2.0 %wt nanoparticles. Post-test analysis was performed using a stylus profilometer and SEM/EDX. The three dimensional profile of the wear grooves were used to calculate the wear induced during the friction tests. Results showed that the wear in the system has a maximum value at approximately a 1.0 %wt concentration of particles. SED/EDX analysis was performed to measure the stoichiometry of the elements on the surface and evaluate the formation of the tribofilms. The surface analysis suggested that there is no uniform film of nanoparticles on the surface. The nanoparticles seem to be scattered randomly on the surface. Based on the results, it was suggested that the particles reduce the real area of contact which in turn decreases the COF.

The next step was to evaluate the validity of the proposed mechanism, the reduction of the area of contact, through analytical modeling. A model was developed that breaks the system into two scales of contact; (i) contact between the surface asperities and (ii) contact between the surfaces and the nanoparticles. A multiscale sub-contact model was used to model contact between the surfaces. A sub-contact model was developed to model nanoparticles in contact between two flat surfaces. An algorithm was develop to

solve the force balance equation between the sub-contact models. The results of the model were in agreement with the observations and experiments. The model also offered a great deal of insight on the contact mechanics of the system.

A major contribution of the current work is development of a contact model for nanoparticles in contact between the rough surfaces. Therefore, we decided to expand the model to a general third body contact scenario in which a group of particle (not necessary nano sized) are in contact between two rough surfaces. An electrical contact application was chosen to allow for experimental validation of the model. The model was developed using the statistical approach to contact mechanics. This contact model is capable of modeling third body systems and reporting the contact parameters such as the real area of contact, contact force and a contact's electrical resistance. The results agree well with the general trends of the available data.

The next set of experiments were on a solution of Ag nanoparticles in PEG. This nano-lubricant was used to investigate the effect of the nanoparticles on different lubrication regimes. Studies were performed on the thin film elasto-hydrodynamic lubrication (EHL) regime, the mixed lubrication regime and the boundary lubrication regime. It was demonstrated for the first time that the nanoparticles affect the EHL regime and lower the COF. In search of a mechanism to explain the experiments the tests were repeated and a thorough surface analysis were performed. The surface analysis did not show any sign of substantial interaction between the particles and the surface. Therefore, the investigations were expanded to the mutual effect of nanoparticles and the lubricant film. Molecular dynamics simulations were also used to model the thin film EHL system. The investigations pointed towards a mechanistic phenomenon in the thin film. The results MD results suggested that the nanoparticle induce a plug flow that reduces the COF. This is done by forcing the median layers in the thin film to move with a uniform speed and localizing shear to the layers adjacent to the walls.

Next the performance of the Ag nano-lubricant was evaluated in the mixed and boundary lubrication regimes. Viscometry measurements showed that the nano-lubricant acts as Newtonian fluid in the typical operating ranges of lubricated contacts. The friction experiments were conducted that showed the silver nanoparticles reduce both friction and wear significantly. A Stribeck curve analysis was also performed that showed that the nanoparticles are effective throughout the mixed and boundary lubrication regimes. However, the most reduction in the COF was recorded in the mixed lubrication regime. The results and surface analysis pointed towards the reduction of the real area of contact as the dominant mechanism.

The next set of experiment were spear headed towards the role of nanoparticle in fully formulated oils. However, to paint a complete picture and better understand the system experiments were started on CuO particles in a dry form. The results showed that the dry particles in powder form can effectively reduce both the COF and wear. Also, it was demonstrated that there is a critical concentration of particles in contact below which particles can't sustain a reduced COF. Next studies were performed on CuO particles in dodecane, PAO and fully formulated SAE 5W20 engine oil. The results suggested that the CuO particles are more effective in reducing the COF and wear when suspended in an inferior lubricant. Whereas, the performance of CuO particle in PAO and 5W20 depends on the applied normal load. Surface analysis revealed that the CuO particle can have a negative effect on the formation of absorbed films in 5W20. Considering all the results, it was suggested that the nanoparticles have a dual effect on the contact's tribology. They have a direct effect when they interact with the surfaces. The particles also have an indirect effect by reducing the real area of contact between surfaces. The overall effect of the particles is determined by considering the two effects simultaneously. The last set of experiments were focused on the performance of diamond and Ag nanoparticles in 5W20. Results showed that the diamond nanoparticles in low concentrations can reduce the COF while avoiding an increase in wear. It was also demonstrated that the contact tribology can benefit from the polishing effect of the diamond nanoparticles. The results

showed that the Ag nanoparticle additives can significantly reduce both friction and wear. Metallic Ag particle interact positively with the other additives in the fully formulated oils. In addition they possess the right size and characteristics to take advantage of both the direct and indirect effects of the nanoparticles on a contact's tribology. They are a very effective type of nanoparticle additives for fully formulated oils.

9. References

1. Greer, J.R. and W.D. Nix, *Size dependence of mechanical properties of gold at the sub-micron scale.* Applied Physics A: Materials Science & Processing, 2005. **80**(8): p. 1625-1629.
2. Deneen Nowak, J., et al., *Fracturing a nanoparticle.* Philisophical Magazine, 2007. **87**(1): p. 29-37.
3. Mook, W.M., et al., *Compressive stress effects on nanoparticle modulus and fracture.* Physical Review B, 2007. **75**(21): p. 1-10.
4. Shan, Z.W., et al., *Ultrahigh stress and strain in hierarchically structured hollow nanoparticles.* Nature Material, 2008. **7**(12): p. 947-952.
5. Shan, Z.W., et al., *Mechanical annealing and source-limited deformation in submicrometre-diameter Ni crystals.* Nature Material, 2008. **7**(2): p. 115-119.
6. Deng, C. and F. Sansoz, *Fundamental differences in the plasticity of periodically twinned nanowires in Au, Ag, Al, Cu, Pb and Ni.* Acta Materialia, 2009. **57**(20): p. 6090-6101.
7. Gerberich, W.W., et al., *Scale effects for strength, ductility, and toughness in "brittle" materials.* Journal of Materials Research, 2009. **24**(3): p. 898-906.
8. Lockwood, A.J. and B.J. Inkson, *In situ TEM nanoindentation and deformation of Si-nanoparticle clusters.* Journal of Physics D: Applied Physics, 2009. **42**(3): p. 1-5.
9. Kedzierski, M.A., et al., *Viscosity Measurements on Colloidal Dispersions (Nanofluids) for Heat Transfer Applications.* Applied Rheology Journal, 2010. **20**(4): p. 1-7.
10. Mook, W.M., et al., *Compression of freestanding gold nanostructures: from stochastic yield to predictable flow.* Nanotechnology, 2010. **21**(5): p. 1-9.
11. Lahouij, I., et al., *In Situ TEM Observation of the Behavior of an Individual Fullerene-Like MoS2 Nanoparticle in a Dynamic Contact.* Tribology Letters, 2011. **42**(2): p. 133-140.
12. Ohmae, N., J.M. Martin, and S. Mori, *Micro and Nanotribology.* 2005: ASME: p.129-150.
13. Xu, T., Z. Jiazheng, and X. Kang, *The ball-bearing effect of diamond nanoparticles as an oil additive.* Journal of Physics D: Applied Physics, 1996. **29**(11): p. 2932-2937.
14. Zhou, J., et al., *Tribological behavior and lubricating mechanism of Cu nanoparticles in oil.* Tribology Letters, 2000. **8**(4): p. 213-218.
15. Rapoport, L., et al., *Tribological properties of WS2 nanoparticles under mixed lubrication.* Wear, 2003. **255**(7-12): p. 785-793.
16. Sajith, V., et al., *An Investigation of the Effect of Addition of Nanoparticles on the Properties of Lubricating Oil.* ASME Conference Proceedings, 2007. **2**: p. 329-335.
17. Gu, C.X., et al., *Tribological effects of oxide based nanoparticles in lubricating oils.* Journal of marine science application, 2009. **8**(1): p. 71-76.
18. Lee, C.G., et al., *A study on the tribological characteristics of graphite nano lubricants.* International Journal of Precision Engineering and Manufacturing, 2009. **10**(1): p. 85-90.
19. Zhang, M., et al., *Performance and anti-wear mechanism of CaCO3 nanoparticles as a green additive in poly-alpha-olefin.* Tribology International, 2009. **42**(7): p. 1029-1039.
20. Zhang, M., et al., *Performance and anti-wear mechanism of Cu nanoparticles as lubricating oil additives.* Industrial Lubrication and Tribology, 2009. **61**(6): p. 311 - 318.
21. Gu, C.X., et al., *Tribological Effects of Nano-Copper with Different Diameters in Lubricants.* Advanced Materials Research, 2010. **123 - 125**: p. 1059-1062.
22. Hernández Battez, A., et al., *CuO, ZrO2 and ZnO nanoparticles as antiwear additive in oil lubricants.* Wear, 2008. **265**(3-4): p. 422-428.

23. Lee, K., et al., *Performance evaluation of nano-lubricants of fullerene nanoparticles in refrigeration mineral oil.* Current Applied Physics, 2009. **9**(2, Supplement 1): p. e128-e131.
24. Hernández Battez, A., et al., *Friction reduction properties of a CuO nanolubricant used as lubricant for a NiCrBSi coating.* Wear, 2010. **268**(1-2): p. 325-328.
25. Wu, Y.Y., W.C. Tsui, and T.C. Liu, *Experimental Analysis of Tribological Properties of Lubricating Oils with Nanoparticle Additives.* Wear, 2007. **262**: p. 819-825.
26. Hwang, Y., et al., *Thermal Conductivity and Lubrication Characteristics of Nanofluids.* Current Applied Physics, 2006. **6**(1): p. e67-e71.
27. Szlufarska, I., M. Chandross, and R. Carpick, W. , *Recent advances in single-asperity nanotribology.* Journal of Physics D: Applied Physics, 2008. **41**(12): p. 123001.
28. Bhushan, B., J.N. Israelachvili, and U. Landman, *Nanotribology: friction, wear and lubrication at the atomic scale.* Nature, 1995. **374**(6523): p. 607-616.
29. Harrison, J.A., et al., *Effect of atomic-scale surface roughness on friction: A molecular dynamics study of diamond surfaces.* Wear, 1993. **168**(1-2): p. 127-133.
30. Zhang, L. and H. Tanaka, *Atomic scale deformation in silicon monocrystals induced by two-body and three-body contact sliding.* Tribology International, 1998. **31**(8): p. 425-433.
31. Chantrenne, P., et al., *Molecular dynamics simulations of friction.* Heat and Technology, 2000. **18**(SUPPL 1): p. 49-56.
32. Landman, U., W.D. Luedtke, and E.M. Ringer, *Atomistic mechanisms of adhesive contact formation and interfacial processes.* Wear, 1992. **153**(1): p. 3-30.
33. Nowak, J.D., et al., *Small size strength dependence on dislocation nucleation.* Scripta Materialia, 2010. **62**(11): p. 819-822.
34. Zhang, N., et al., *Deformation mechanisms in silicon nanoparticles.* Journal of Applied Physics, 2011. **109**(6): p. 063534.
35. Deneen, J., et al., *In situ deformation of silicon nanospheres.* Journal of materials science, 2006. **41**(14): p. 4477-4483.
36. Wu, Y.Y., W.C. Tsui, and T.C. Liu, *Experimental analysis of tribological properties of lubricating oils with nanoparticle additives.* Wear, 2007. **262**(7-8): p. 819-825.
37. Tarasov, S., et al., *Study of friction reduction by nanocopper additives to motor oil.* Wear, 2002. **252**(1–2): p. 63-69.
38. Zhao, Y., Z. Zhang, and H. Dang, *A novel solution route for preparing indium nanoparticles.* The Journal of Physical Chemistry B, 2003. **107**(31): p. 7574-7576.
39. Greenberg, R., et al., *The effect of WS 2 nanoparticles on friction reduction in various lubrication regimes.* Tribology Letters, 2004. **17**(2): p. 179-186.
40. Zhao, Y., Z. Zhang, and H. Dang, *Synthesis of In–Sn alloy nanoparticles by a solution dispersion method.* Journal of Materials Chemistry, 2004. **14**(3): p. 299-302.
41. Martin, J.M. and N. Ohmae, *Nanolubricants*. Tribology Series 2008, England: John Wiley & Sons Ltd.
42. Ghaednia, H., R.L. Jackson, and J.M. Khodadadi, *Experimental Analysis of Stable CuO Nanoparticle Enhanced Lubricants.* Journal of Experimental Nanoscience, 2013: p. 1-18.
43. Fan, L. and J.M. Khodadadi, *An experimental investigation of enhanced thermal conductivity and expedited unidirectional freezing of cyclohexane-based nanoparticle suspensions utilized as nano-enhanced phase change materials.* International Journal Thermal Sciences, 2012. **62**: p. 120-126.
44. Liu, G., et al., *Investigation of the Mending Effect and Mechanism of Copper Nanoparticles on a Tribologically Stressed Surface.* Tribology Letters, 2004. **17**(4): p. 961-966.

45. Poon, C.Y. and B. Bhushan, *Nano-asperity contact analysis and surface optimization for magnetic head slider/disk contact.* Wear, 1996. **202**(1): p. 83-98.
46. Adams, G.G., Müftü, S., Azhar, N. M., *A Scale-Dependant Model for Multi-Asperity Contact and Friction.* ASME Journal Tribology, 2003. **125**: p. 700-708.
47. Adams, G.G. and S. Muftu, *Improvements to a scale-dependent model for contact and friction.* Journal of Physics D: Applied Physics, 2005. **38**(9): p. 1402-1409.
48. Almeida, L., et al., *Laterally actuated multicontact MEMS relay fabricated using MetalMUMPS process: experimental characterization and multiscale contact modeling.* Journal Micro/Nanolithography MEMS MOEMS, 2007. **6**(2): p. 023009.
49. Bhushan, B., Nosonovsky, M., *Scale effects in friction using strain gradient plasticity and dislocation-assisted sliding (microslip).* Acta Materialia, 2003. **51**: p. 4331-4345.
50. Jackson, R.L., *The Effect of Scale Dependant Hardness on Elasto-plastic Asperity Contact between Rough Surfaces.* STLE Tribology Transaction, 2006. **49**(2): p. 135-150.
51. Jackson, R.L., S.H. Bhavnani, and T.P. Ferguson, *A Multi-scale Model of Thermal Contact Resistance between Rough Surfaces.* ASME Journal Heat Transfer, 2008. **130**: p. 081301.
52. Polonsky, I.A., Keer, L. M., *Scale Effects of Elastic-Plastic Behavior of Microscopic Asperity Contacts.* ASME Journal Tribology, 1996. **118**: p. 335-340.
53. Dareing, D.W. and M. Khonsari, *Liquid Transported Powder Lubricant Study*, 1995, DTIC Document.
54. HUA, D.Y. and M.M. Khonsari, *Elastohydrodynamic lubrication by powder slurries.* Journal of Tribology, 1996. **118**(1): p. 67-73.
55. Khonsari, M.M., *On the modeling of multi-body interaction problems in tribology.* Wear, 1997. **207**(1–2): p. 55-62.
56. Trezona, R.I., D.N. Allsopp, and I.M. Hutchings, *Transitions between two-body and three-body abrasive wear: influence of test conditions in the microscale abrasive wear test.* Wear, 1999. **225–229, Part 1**: p. 205-214.
57. Adachi, K. and I.M. Hutchings, *Wear-mode mapping for the micro-scale abrasion test.* Wear, 2003. **255**(1–6): p. 23-29.
58. Clary, D.R. and G. Mills, *Preparation and Thermal Properties of CuO Particles.* The Journal of Physical Chemistry C, 2011. **115**(5): p. 1767-1775.
59. Jackson, R.L., Green, I. , *Study of the Tribological Behavior of a Thrust Washer Bearing.* Tribology Transaction, 2001. **44**(3): p. 504-508.
60. Venerus, D., et al., *Viscosity measurements on colloidal dispersions (nanofluids) for heat transfer applications.* Applied Rheology, 2010. **20**: p. 1-7.
61. Einstein, A., *Eine neue bestimmung der molekuldimensionen.* Ann. Phys., 1906. **19**: p. 289.
62. Williams, J.A., *Engineering Tribology,* 2000, New York: Oxford.
63. Jackson, R.L. and I. Green, *The behavior of thrust washer bearings considering mixed lubrication and asperity contact.* Tribology Transactions, 2006. **49**: p. 233-247.
64. Chang, W.R., Etsion, I., Bogy, D., B., *Static Friction Coefficient Model for Metallic Rough Surfaces.* ASME J. Tribol., 1988. **110**(1): p. 57-63.
65. Cohen, D., Y. Kligerman, and I. Etsion, *A Model for Contact and Static Friction of Nominally Flat Rough Surfaces Under Full Stick Contact Condition.* ASME Journal Tribology, 2008. **130**(3): p. 031401.
66. Etsion, I., et al., *Experimental investigation of the elastic-plastic contact area and static friction of a sphere on flat.* ASME Journal of Tribology, 2005. **127**(1): p. 47-50.
67. Kogut, L. and I. Etsion, *A static friction model for elastic-plastic contacting rough surfaces.* ASME Journal of Tribology, 2004. **126**(1): p. 1-34.

68. Dickey, R.D.I., R.L. Jackson, and G.T. Flowers, *Measurements of the Static Friction Coefficient Between Tin Surfaces and Comparison to a Theoretical Model.* Journal of Tribology, 2011. **133**(3): p. 031408-7.
69. Polycarpou, A.A. and I. Etsion, *Comparison of the Static Friction Subboundary Lubrication Model with Experimental Measurements on Thin-Film Disks.* Tribology Transactions, 1998. **41**(2): p. 217-224.
70. Lee, C.-H., M. Eriten, and A.A. Polycarpou, *Application of Elastic-Plastic Static Friction Models to Rough Surfaces With Asymmetric Asperity Distribution.* Journal of Tribology, 2010. **132**(3): p. 031602-11.
71. Lee, C.-H. and A.A. Polycarpou, *Static Friction Experiments and Verification of an Improved Elastic-Plastic Model Including Roughness Effects.* Journal of Tribology, 2007. **129**(4): p. 754-760.
72. Stempfle, P., et al., *Evaluation of the real contact area in three-body dry friction by micro-thermal analysis.* Tribology International, 2010. **43**(10): p. 1794-1805.
73. Greenwood, J. and J. Williamson, *Contact of nominally flat surfaces.* Proceedings of the Royal Society of London. Series A. Mathematical and Physical Sciences, 1966. **295**(1442): p. 300-319.
74. Jackson, R.L., *An Analytical Solution to an Archard-Type Fractal Rough Surface Contact Model.* Tribology Transactions, 2010. **53**(4): p. 543-553.
75. Jackson, R.L., et al., *A Closed-Form Multiscale Thermal Contact Resistance Model.* Components, Packaging and Manufacturing Technology, IEEE Transactions on, 2012. **2**(7): p. 1158-1171.
76. Jackson, R.L., et al. *A Simplified Model of Multiscale Electrical Contact Resistance and Comparison to Existing Closed Form Models*. in *Electrical Contacts, 2009 Proceedings of the 55th IEEE Holm Conference on*. 2009.
77. Wadwalkar, S., R. Jackson, and L. Kogut, *A study of the elastic—plastic deformation of heavily deformed spherical contacts.* Proceedings of the Institution of Mechanical Engineers, Part J: Journal of Engineering Tribology, 2010. **224**(10): p. 1091-1102.
78. Ohmura, T., K. Tsuzaki, and S. Matsuoka, *Nanohardness measurement of high-purity Fe–C martensite.* Scripta Materialia, 2001. **45**(8): p. 889-894.
79. Williams, J., *Engineering Tribology.* 2005: Cambridge University Press.
80. Lahouij, I., et al., *Real Time TEM Imaging of Compression and Shear of Single Fullerene-Like MoS 2 Nanoparticle.* Tribology Letters, 2011: p. 1-11.
81. Mishra, M. and I. Szlufarska, *Analytical Model for Plowing Friction at Nanoscale.* Tribology Letters, 2012: p. 1-10.
82. Greer, J.R., W.C. Oliver, and W.D. Nix, *Size dependence of mechanical properties of gold at the micron scale in the absence of strain gradients.* Acta Materialia, 2005. **53**(6): p. 1821-1830.
83. Ghaednia, H. and R.L. Jackson, *The Effect of NanoParticles on the Real Area of Contact, Friction and Wear.* Journal of Tribology 2013. **135**(4): p. 041603.
84. Zakipour, S. and C. Leygraf, *Evaluation of laboratory tests to simulate indoor corrosion of electrical contact materials.* Journal of the Electrochemical Society, 1986. **133**(1): p. 21-30.
85. Gao, J., et al. *The Influence of Particulate Contaminants on Vibration-Induced Fretting Degradation in Electrical Connectors*. in *Electrical Contacts (HOLM), 2010 Proceedings of the 56th IEEE Holm Conference on*. 2010. IEEE.

86. Ghaednia, H., A. Rostami, and R.L. Jackson. *The Influence of Thermal Expansion and Plastic Deformation on a Thermo-Electro Mechanical Spherical Asperity Contact*. in *Electrical Contacts (Holm), 2012 IEEE 58th Holm Conference on*. 2012. IEEE.
87. Zhang, J.G. *Effect of dust contamination on electrical contact failure*. in *Electrical contacts-2007, the 53rd ieee holm conference on*. 2007. IEEE.
88. Williamson, J., J. Greenwood, and J. Harris, *The influence of dust particles on the contact of solids.* Proceedings of the Royal Society of London. Series A. Mathematical and Physical Sciences, 1956. **237**(1211): p. 560-573.
89. Mano, K., *"Contact failure by Dust Contamination Reliability of Contact Components"*. 3rd ed. 1981, Japan: General Electronics Publisher.
90. Reagor, B.T. and C. Russell, *A survey of problems in telecommunication equipment resulting from chemical contamination.* Components, Hybrids, and Manufacturing Technology, IEEE Transactions on, 1986. **9**(2): p. 209-214.
91. Liang, Y., J. Zhang, and J. Liu. *Identification of inorganic compounds of dust and their effects on electrical contact failure*. in *Electrical Contacts, 1997., Proceedings of the Forty-Third IEEE Holm Conference on*. 1997. IEEE.
92. Zhang, J.-g., et al. *Analysis of compounds in airborne dust collected in Beijing*. in *Electrical Contacts, 1998. Proceedings of the Forty-Fourth IEEE Holm Conference on*. 1998. IEEE.
93. Greenwood, J., *Constriction resistance and the real area of contact.* British Journal of Applied Physics, 1966. **17**(12): p. 1621-30.
94. Daphalapurkar, N., et al., *Determination of mechanical properties of sand grains by nanoindentation.* Experimental Mechanics, 2011. **51**(5): p. 719-728.
95. Komvopoulos, K. and N. Ye, *Three-dimensional contact analysis of elastic-plastic layered media with fractal surface topographies.* Journal of Tribology, 2001. **123**(3): p. 632-640.
96. Jackson, R.L. and I. Green, *A finite element study of elasto-plastic hemispherical contact against a rigid flat.* Journal of Tribology, 2005. **127**(2): p. 343-354.
97. Feng, C., et al. *Inspection of the contaminants at failed connector contacts*. in *Electrical Contacts, 2005. Proceedings of the Fifty-First IEEE Holm Conference on*. 2005. IEEE.
98. He, Z. and L. Hu. *Micro motion at the failed contact interfaces*. in *Electrical Contacts, 2005. Proceedings of the Fifty-First IEEE Holm Conference on*. 2005. IEEE.
99. Greenwood, J., *Film thicknesses in circular elastohydrodynamic contacts.* Proceedings of the Institution of Mechanical Engineers, Part C: Journal of Mechanical Engineering Science, 1988. **202**(1): p. 11-17.
100. Dowson, D., *Elastohydrodynamic and micro-elastohydrodynamic lubrication.* Wear, 1995. **190**(2): p. 125-138.
101. Dowson, D. and G. Higginson, *A numerical solution to the elasto-hydrodynamic problem.* Journal of Mechanical Engineering Science, 1959. **1**(1): p. 6-15.
102. Hamrock, B. and D. Dowson, *Isothermal Elastohydrodynamic Lubrication of Point Contacts: Part II—Ellipticity Parameter Results.* Journal of Lubrication Technology, 1976. **98**: p. 375-385.
103. Hamrock, B.J. and D. Dowson, *Isothermal Elastohydrodynamic Lubrication of Point Contacts: Part 1—Theoretical Formulation.* Journal of Lubrication Technology, 1976. **98**: p. 223-235.
104. Johnston, G., R. Wayte, and H. Spikes, *The measurement and study of very thin lubricant films in concentrated contacts.* Tribology Transactions, 1991. **34**(2): p. 187-194.
105. Cooper, D. and A. Moore, *Application of the ultra-thin elastohydrodynamic oil film thickness technique to the study of automotive engine oils.* Wear, 1994. **175**(1): p. 93-105.

106. Zhang, C., *Research on thin film lubrication: state of the art.* Tribology International, 2005. **38**(4): p. 443-448.
107. Gao, J., W. Luedtke, and U. Landman, *Nano-elastohydrodynamics: structure, dynamics, and flow in nonuniform lubricated junctions.* Science, 1995. **270**(5236): p. 605-608.
108. Abd-AlSamieh, M. and H. Rahnejat, *Nano-lubricant film formation due to combined elastohydrodynamic and surface force action under isothermal conditions.* Proceedings of the Institution of Mechanical Engineers, Part C: Journal of Mechanical Engineering Science, 2001. **215**(9): p. 1019-1029.
109. Ghaednia, H., R.L. Jackson, and J.M. Khodadadi, *Experimental analysis of stable CuO nanoparticle enhanced lubricants.* Journal of Experimental Nanoscience, 2013: p. 1-18.
110. Kalin, M., J. Kogovšek, and M. Remškar, *Mechanisms and improvements in the friction and wear behavior using MoS_2 nanotubes as potential oil additives.* Wear, 2012. **280**: p. 36-45.
111. Tao, X., Z. Jiazheng, and X. Kang, *The ball-bearing effect of diamond nanoparticles as an oil additive.* Journal of Physics D: Applied Physics, 1996. **29**(11): p. 2932.
112. Tannous, J., et al., *Understanding the tribochemical mechanisms of IF-MoS 2 nanoparticles under boundary lubrication.* Tribology Letters, 2011. **41**(1): p. 55-64.
113. Li, B., et al., *Tribochemistry and antiwear mechanism of organic–inorganic nanoparticles as lubricant additives.* Tribology Letters, 2006. **22**(1): p. 79-84.
114. Johnson, K.L., *Contact mechanics.* 1987: Cambridge university press.
115. Zhen, S. and G. Davies, *Calculation of the Lennard-Jones n–m potential energy parameters for metals.* physica status solidi (a), 1983. **78**(2): p. 595-605.
116. Nath, S.K., F.A. Escobedo, and J.J. de Pablo, *On the simulation of vapor–liquid equilibria for alkanes.* The Journal of Chemical Physics, 1998. **108**: p. 9905.
117. Allen, M.P. and D.J. Tildesley, *Computer simulation of liquids.* 1989: Oxford university press.
118. Plimpton, S., *Fast parallel algorithms for short-range molecular dynamics.* Journal of Computational Physics, 1995. **117**(1): p. 1-19.
119. Gao, J., W. Luedtke, and U. Landman, *Layering transitions and dynamics of confined liquid films.* Physical review letters, 1997. **79**(4): p. 705-708.
120. Gao, J., W.D. Luedtke, and U. Landman, *Origins of Solvation Forces in Confined Films.* *Journal* Physical Chemistry B*,* 1997. **5647**: p. 4013-4023.
121. Dijkstra, M., *Confined thin films of linear and branched alkanes.* Journal of Chemical Physics, 1997. **107**(8): p. 3277-3288.
122. Zhang, L., et al., *Nonequilibrium molecular dynamics simulations of confined fluids in contact with the bulk.* The Journal of Chemical Physics, 2001. **114**: p. 6869.
123. Ghaednia, H., et al., *The effect of nanoparticles on thin film elasto-hydrodynamic lubrication.* Applied Physics Letters, 2013. **103**(26): p. 263111.
124. Ghaednia, H., et al., *The Effect of Nanoparticle Additives in the Elastohydrodynamic Lubrication Regime.* Tribology & Lubrication Technology, 2013. **69**(12): p. 18-22.
125. *An Inventory of Nanotechnology-based Consumer Products Currently on the Market*. Available from: http://www.nanotechproject.org/inventories/consumer/analysis_draft/.
126. Xiu, Z.-m., et al., *Negligible Particle-Specific Antibacterial Activity of Silver Nanoparticles.* Nano Letters, 2012. **12**(8): p. 4271-4275.
127. Jiang, H., et al., *Surface Functionalized Silver Nanoparticles for Ultrahigh Conductive Polymer Composites.* Chemistry of Materials, 2006. **18**(13): p. 2969-2973.

128. Moon, K.-S., et al., *Thermal behavior of silver nanoparticles for low-temperature interconnect applications.* Journal of Electronic Materials, 2005. **34**(2): p. 168-175.
129. Lee, H.-H., K.-S. Chou, and K.-C. Huang, *Inkjet printing of nanosized silver colloids.* Nanotechnology, 2005. **16**(10): p. 2436.
130. Buzzi, S., et al., *Deformation behavior of silver submicrometer-pillars prepared by nanoimprinting.* Philosophical Magazine, 2009. **89**(10): p. 869-884.
131. Saha, D.R., et al. *Nanoindentation studies on silver nanoparticles*. in *AIP Conference Proceedings*. 2013.
132. Neuffer, H., H. Ghaednia, and R. Jackson, *Wear Volume Analysis Using a Nano-Lubricant for Ball-on-Disk Testing.* Tribology & Lubrication Technology, 2014. **2**: p. 1-3.
133. Zeng, T. and T. Sun, *Size effect of nanoparticles in chemical mechanical polishing-a transient model.* Semiconductor Manufacturing, IEEE Transactions on, 2005. **18**(4): p. 655-663.
134. Peng, D.X., et al., *Tribological properties of diamond and SiO2 nanoparticles added in paraffin.* Tribology International, 2009. **42**(6): p. 911-917.
135. ACS-Material. Available from: http://www.acsmaterial.com/product.asp?CID=22&ID=39.
136. Filatov, Y.D., et al., *Surface roughness in diamond abrasive finishing.* Journal of Superhard Materials, 2009. **31**(3): p. 191-195.
137. Mosleh, M. and K.A. Shirvani, *In-situ nanopolishing by nanolubricants for enhanced elastohydrodynamic lubrication.* Wear, 2013. **301**(1–2): p. 137-143.
138. Tannous, J., et al., *Synthesis and Tribological Performance of Novel $Mo_x W_{1-x} S_2$ ($0 \leq x \leq 1$) Inorganic Fullerenes.* Tribology Letters, 2010. **37**(1): p. 83-92.
139. Ghaednia, H. and A. Ohadi, *Effect of Thermal Growth on Vibration Behavior of Flexible Rotor System Mounted on MR Squeeze Film Damper.* ASME Conference Proceedings, 2010. **2010**(49156): p. 567-576.
140. Ghaednia, H. and A. Ohadi, *Vibration Behavior of Flexible Rotor System Mounted on MR Squeeze Film Damper With Thermal Growth Effect.* Journal of Vibration and Acoustics, 2012. **134**: p. 011015.
141. Jackson, R.L. and I. Green, *A Finite Element Study of Elasto-Plastic Hemispherical Contact.* ASME Journal Tribology, 2005. **127**(2): p. 343-354.

Appendices

Appendix I.

This appendix presents detailed descriptions and pictures of the samples and experimental apparatuses used in the experiments.

The CuO nanoparticles coated with sodium oleate were used in sections 2 and 7. The CuO nano-lubricant used in section 2 consisted of the particles in mineral base oil and dodecane as the dispersant. Fig. A1 shows the control sample and the nano-lubricant used in the experimental studies of section 2. Later the procedure of suspending the CuO nanoparticle in the base oils was refined. The refined process used the CuO particles in chloroform solution as described in section 7 to prepare the nano-lubricant. This process didn't require dodecane to stabilize the suspension. Therefore the CuO nano-lubricant in PAO and 5W20 used in section 6 didn't include any dodacene.

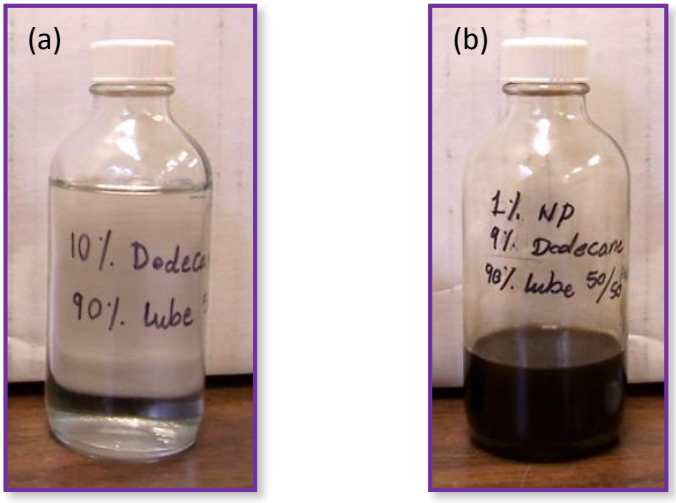

Figure A1: (a) Mineral oil control sample consisting of 10 %wt dodecane in mineral base oil. (b) 1.0%wt of CuO nanoparticles suspended in Mineral base oil along with dodecane as the dispersant.

Fig. A2 shows the control sample and the Ag nano-lubricant in PEG 600. The control sample was transparent and consisted of 1.5 mM PVP in PEG 600. The nano-lubricant consisted of 1.5, 3.0 or 4.5 mM of Ag particles in PEG 600 along with 1.5 mM of PVP as the coating agent.

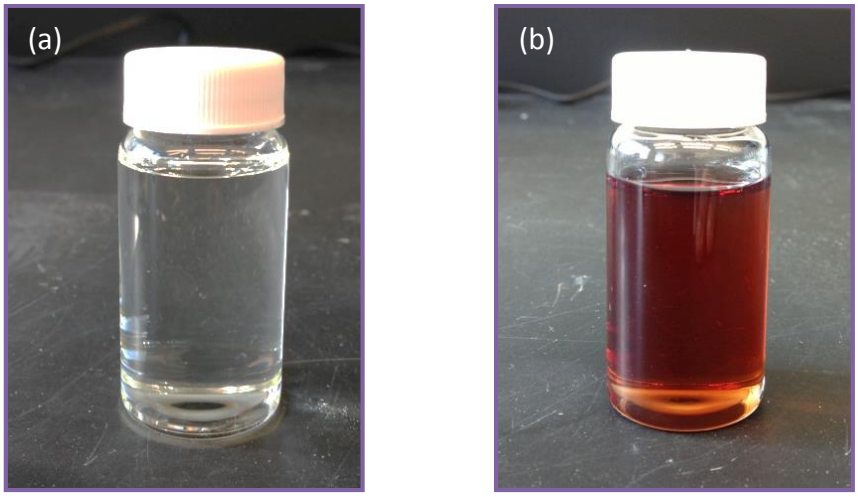

Figure A2: (a) PEG control sample consisting of 1.5 mM PVP in PEG 600. (b) 30mM of Ag nanoparticles suspended in PEG 600 along with PVP as the dispersant (coating agent).

Fig. A3 shows the picture of different nano-lubricants prepared with the fully formulated SAE 5W20 engine oil. The SAE 5W20 is a commercial engine oil and is a common lubricant for internal combustion engines, see Fig A3 (a). The CuO nano-lubricant in fully formulated SAW 5W20 was prepared using the CuO particles in chloroform solution. Hence consisting of 5.0%wt of CuO nanoparticles coated with sodium oleate in 5W20, see Fig A3 (b). The diamond nano-lubricant consists of 20nm particle suspended in 5W20 along with polyolester (POE) oil as the dispersing agent, see Fig A3 (c). The Ag nano-lubricant consists of 10 nm particles in 5W20 along with oleoyl sarcosine as the dispersing agent, see Fig A3 (d).

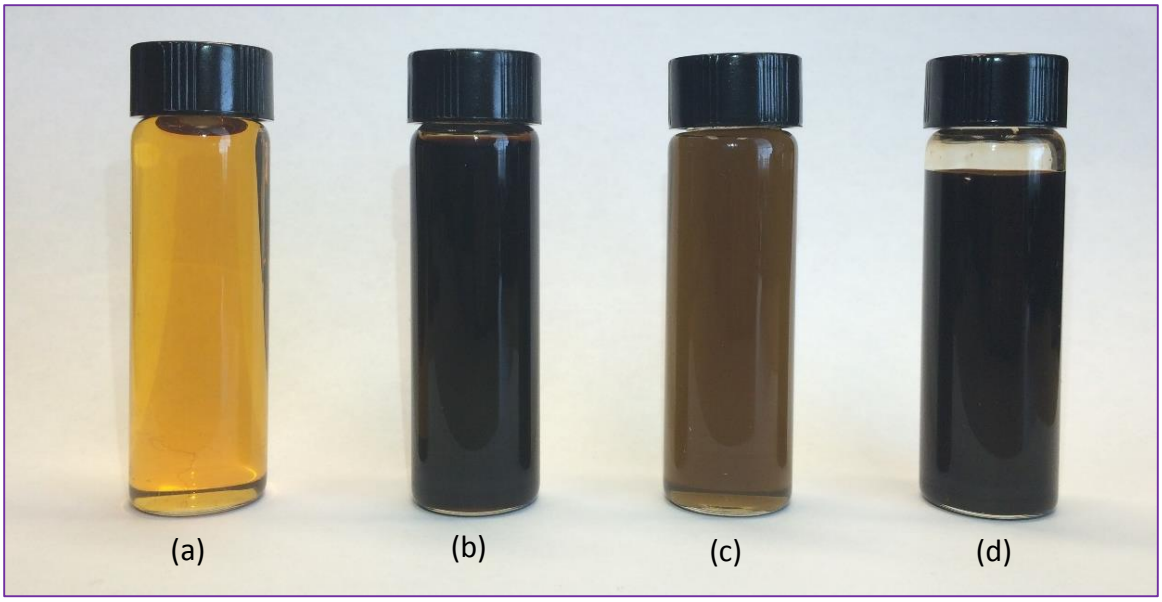

Figure A3: (a) Fully formulated SAE 5W20 engine oil, (b) 5.0 %wt CuO nanoparticles in 5W20, (c) 0.01 %wt diamond nanoparticles in 5W20, (d) 0.65 %wt Ag nanoparticles in 5W20.

Figure A4 shows the pin on disk test setup used to run the friction tests. The pin was mounted using a pin holder and supported by a suspension system. The flexibility of the suspension was crucial to maintain the contact during the sliding motion. The disk was mounted inside a reservoir and was submerged under the sample lubricant. The disk and the reservoir were mounted on a rotating stage that provided the sliding motion. The force sensor reported the lateral and normal loads used to calculate COF. The system had a feedback control system to maintain a constant normal load during the sliding. . An electrical contact resistant sensor (ECR) was used to detect contact between the solid conductive surfaces. The schematic of the pin on disk test setup is also shown on Fig A4. The pin is a sphere (10 mm diameter) in contact with a flat surface. The non-conformal contact geometry allowed for performing experiments in different lubrication regimes. The disk part was made of AISI 1080 carbon steel and the pin was made of AISI 52100 chromium steel, see Fig A5.

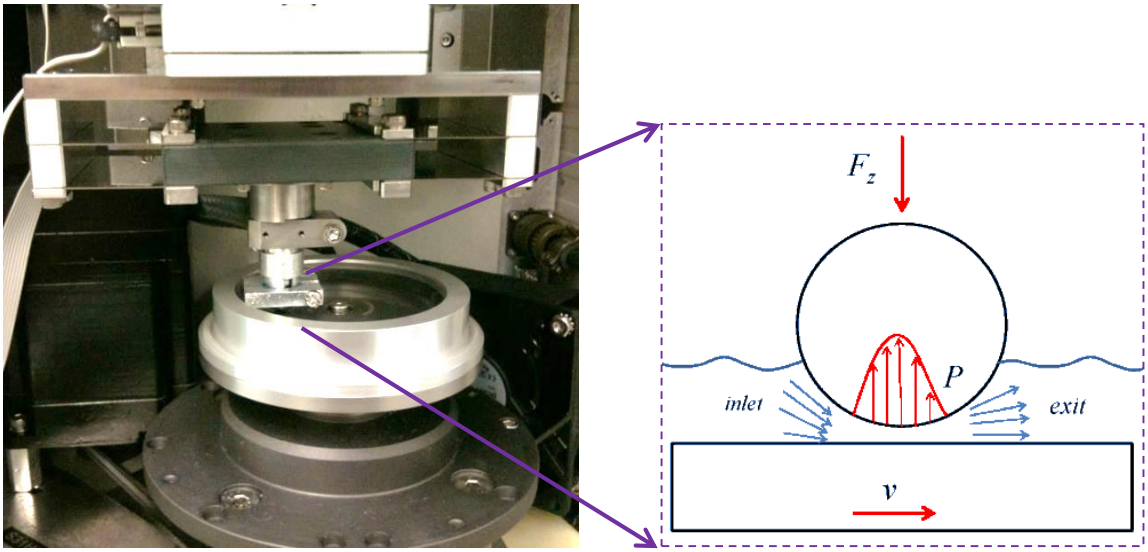

Figure A4: The pin on disk test setup used in the experiments and the schematic of the contact pair.

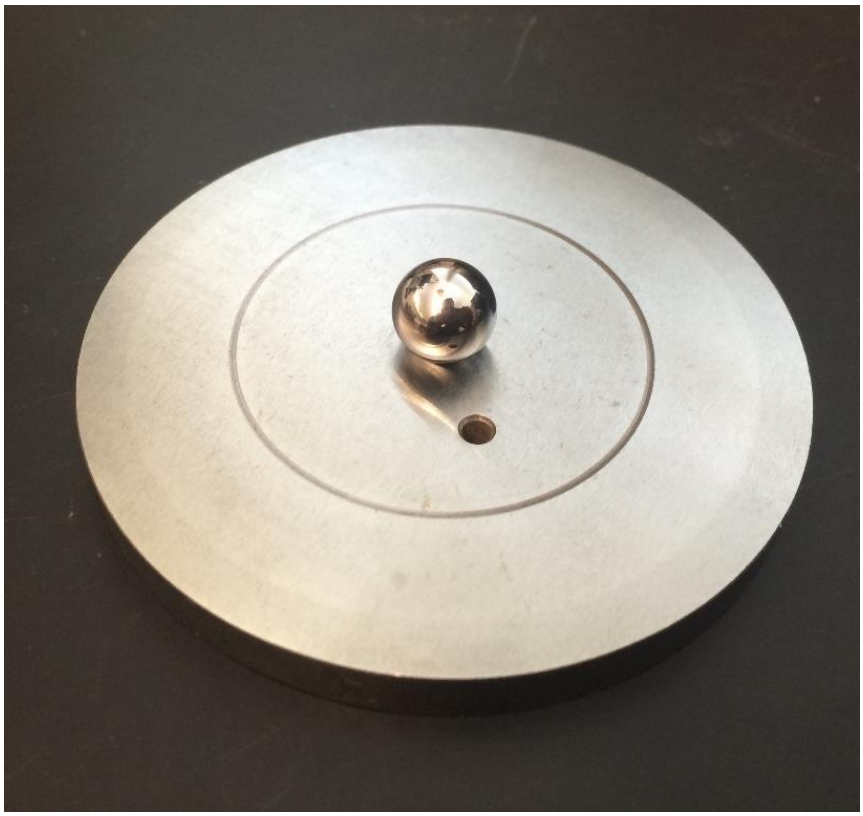

Figure A5: Pin and disk samples used in a pin on disk test.

Fig. A6 shows the disk on disk test setup used to run the friction tests. This setup was similar to the pin on disk setup except for a torque sensor that was used to calculate the COF. The upper disk was smaller than the lower disk and provided a ring shaped contact region with inner and outer diameter of 25.4 and 50.8 mm. The schematic of the contact geometries is shown on Fig. A6. This friction setup had conformal contact surfaces and was used to perform experiments at a lower contact pressure. The upper and lower disk parts were made of AISI 1080 carbon steel, see Fig A7.

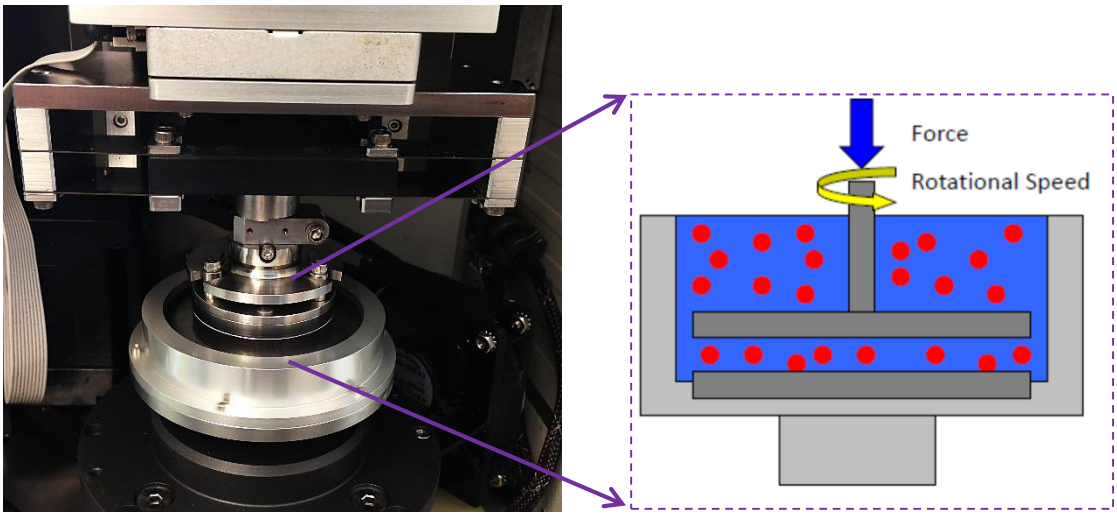

Figure A6: The disk on disk test setup used in the experiments and the schematic of the contact pair.

Figure A8 shows the experimental setup used for the viscometry analysis. It is vital to understand the rheological behavior of the lubricants. Because it could substantially influence the lubrication and the mechanical behavior of the system. An example is the effect of magnetorheological fluids (non-Newtonian fluids) on the performance of the bearings and rotors [139, 140]. The viscometer used in our experiments had a cylindrical spindle submerged in a cylindrical reservoir that held the sample. The reservoir was surrounded by a water jacket which was connected to a water bath to control the temperature. The spindle was suspended from a torque sensor and a motor. The motor rotated the spindle inside the fluid sample and the torque sensor was used to measure

the drag force from the fluid sample. The torque signal is then translated into viscosity value using the machine's software. The motor was able to fine control the rotational velocity of the spindle hence making it possible to run tests in different shear rates.

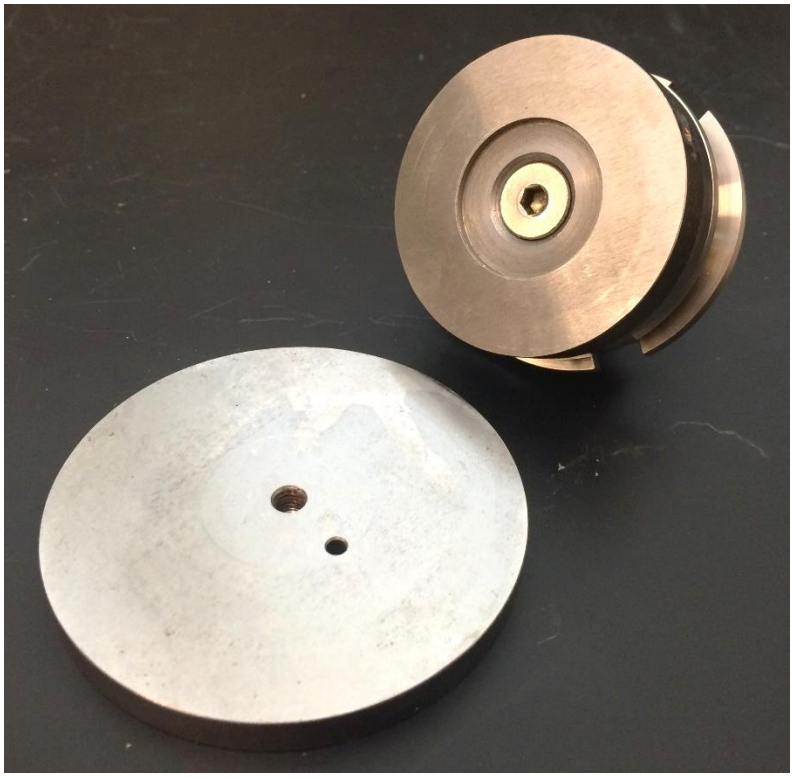

Figure A 7: The disk samples used in a disk on disk test.

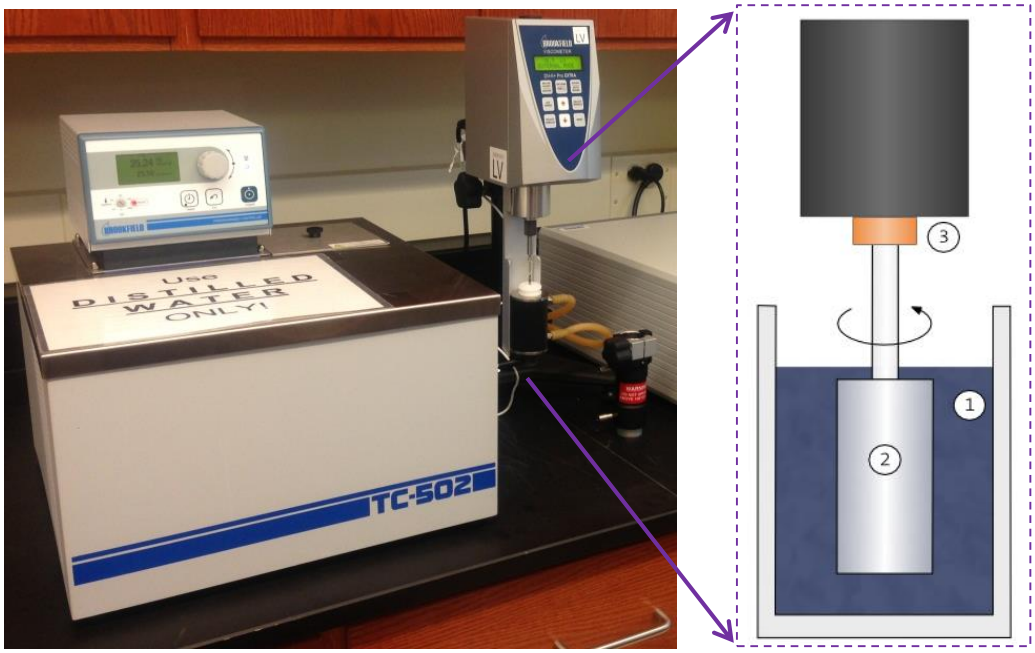

Figure A8: The viscometer and the water bath setup used to run the rheology and viscosity measurements. The schematic of the cylindrical spindle and the fluid reservoir is shown on the right.

Figure A9 (a) shows the stylus profilometer used throughout this dissertation to obtain two or three dimensional profiles of the surfaces. Figure A9 (b) and (c) show the stylus profilometer performing analysis on a pin and a disk sample. The stylus had a 2.5 μm tip that drags over the surface and measured the height of the surface profile. The vertical resolution of the machine is 1 nm. Fig. A9 (d) shows a close up picture of the stylus moving over a wear groove.

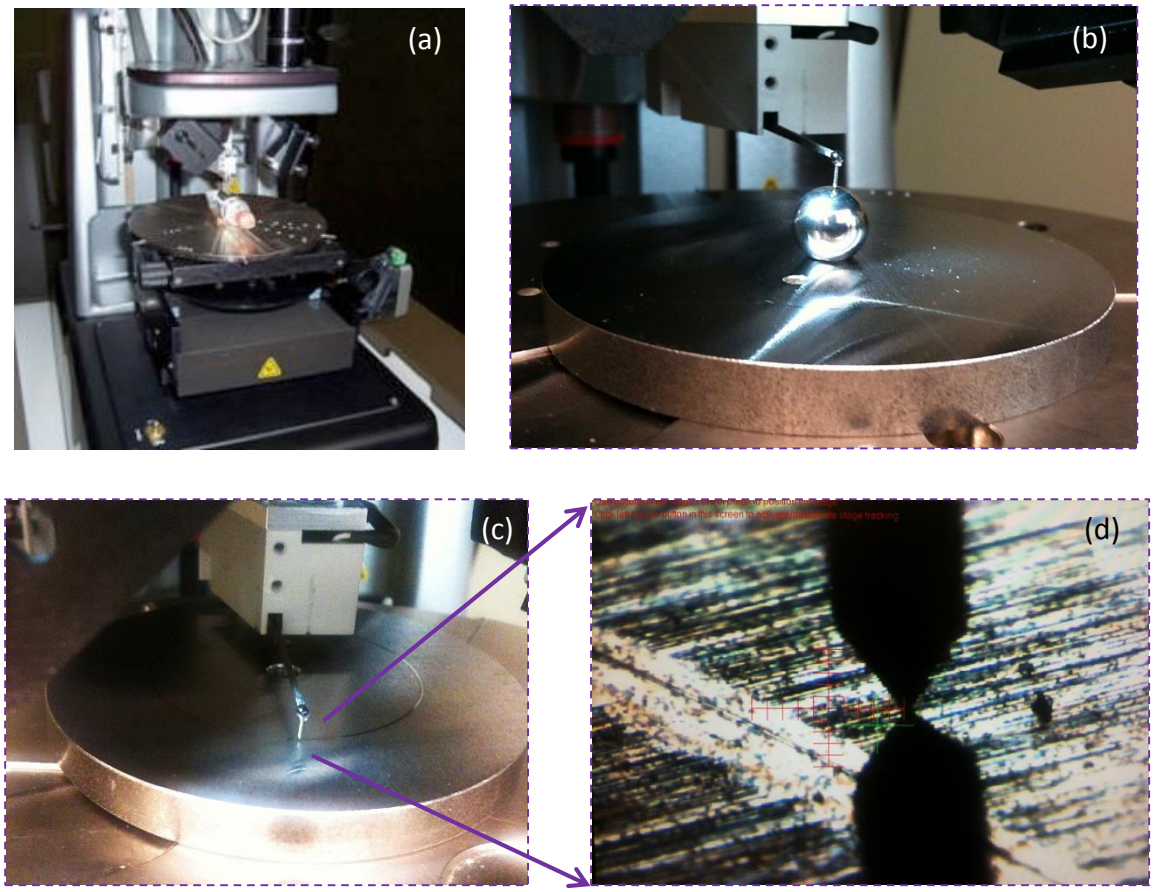

Figure A9: (a) the stylus profilometer used to run the surface metrology. (b) Performing surface profilometry on a pin sample. (c) Performing surface profilometry on a disk sample. (d) A close up picture of the stylus moving over a wear groove.

Appendix II.

The model for heavily loaded spheres was developed by Wadwalkar et al [77]. The model assumes elastic perfectly plastic deformation and accounts for the preservation of volume. In order to take the scale dependent nanoparticles strength [2, 3, 33, 35] into consideration the model was fitted to the data so that the ultimate strength reported by the model matches the failure strength of nanoparticles. Also, the solution was frozen at the ultimate strength to account for fracture of particles. According to the modified model the average failure strain of particles was reported to be 42%. This is compared to the average particle strain reported by Mook et al [3] to be 45% which shows a good agreement between the models. The final equations used to find the contact radius of a particle is presented in Eq. (A1).

$$\left(\frac{a}{R}\right)=\left(\frac{a}{R}\right)_1+A_1\left(\frac{\omega}{\omega_c}\right)^2-A_2\left(\frac{\omega}{\omega_c}\right),\ A_1=0.0826\left(\frac{S_y}{E'}\right)^{3.148},\ A_2=0.3805\left(\frac{S_y}{E'}\right)^{1.545}$$
$$\left(\frac{a}{R}\right)_1=\sqrt{\frac{\omega}{R}}\left(\frac{\omega}{1.9\omega_c}\right)^{B/2},B=0.14\exp\left(23\frac{S_y}{E'}\right) \quad \text{(A1)}$$

Where a, R, ω, S_y and E' are radius of contact, particles radius, indentation, yield strength and the contact modulus, see Fig.15. The area of contact for a single nano particle is $A_{NP}=\pi a^2$, assuming axisymmetric contact. The parameter ω_c is the critical indentation defined as [141]

$$\omega_c=\left(\frac{\pi c S_y}{2E'}\right)^2 R,\ \ c=1.295\exp\left(0.736\nu\right) \quad \text{(A2)}$$

The equations for the particle force is presented in the Eq. (A3) where P is the average pressure during fully plastic contact and F_c is the critical force as defined in Eq. (A4).

$$\frac{F_{NP}}{F_c} = \left\{ \exp\left[-\frac{1}{4}\left(\frac{\omega}{\omega_c} \right)^{5/12} \right] \right\} \left(\frac{\omega}{\omega_c} \right)^{3/2} + \frac{P}{F_c} \pi R^2 \left(\frac{a}{R} \right)^2 \left\{ 1 - \exp\left[-\frac{1}{25}\left(\frac{\omega}{\omega_c} \right)^{5/9} \right] \right\} \quad \text{(A3)}$$

$$\frac{P}{S_y} = 2.84 - 0.92\left[1 - \cos\left(\pi \frac{a}{R_2} \right) \right], \quad R_2 = \sqrt{\frac{R^3}{0.76(R-\omega)} - \frac{a^2}{2}}$$

$$F_c = \frac{4}{3}\left(\frac{R}{E'} \right)^2 \left(\frac{c}{2} \pi S_y \right)^3 \quad \text{(A4)}$$

Appendix III.

Numerical parameters and other resources used in the numerical studies are presented in this appendix. Table A1 contains the numerical values of the parameters used in the studies.

Table A1: Numerical values of the parameters used in the studies

Lubricants density	ρ_{lub}*=0.773 g/cc*
Nanoparticle density	ρ_{NP}*=2.329 g/cc*
Surface Poisson ratio	ν_s*=0.33*
nanoparticle Poisson ratio	ν_{NP}*=0.22*
Surface elastic modulus	E_s*=200 GPa*
Nanoparticle elastic modulus	E_{NP}*=160 GPa*
Surface yield strength	S_y*=1.03 GPa*

Particles are assumed to have a normal Gaussian size distribution, Fig. 19(b), which is characterized by particle average size (D_{avg}) and variance (σ_g). Equation (A5) presents the formulation used in this work.

$$\phi(D) = \frac{1}{\sigma_g \sqrt{2\pi}} \exp\left[-0.5 \left(\frac{D - D_{avg}}{\sigma_g} \right)^2 \right] \tag{A5}$$

Value for τ_s was measured based on the lubricated disk of disk experiments for typical group II base oil according to reference [42] to be τ_s*=37 MPa*. The shear stress between the nanoparticle and surface was estimated according to the surface hardness according to reference[78] to be τ_p*=1.67 GPa* which corresponds to nano-hardness of *H=10 GPa*. However, based on the simulation results the particle area of contact to surface area of contact ratio was found to be on average about A_p/A_s*=3e-7.* Therefore, based on the Eq. 14, the coefficient of friction is practically independent of τ_p.

Actual surface profiles and the fast Fourier transform were used to find B_{max} and λ_{max} and model rough surfaces in contact. As an example, the profile and fast Fourier analysis of one of the surfaces used in this paper (referred to as Rq=0.05 μm) is shown on Fig A10. The maximum value *B* and the corresponding λ_{max} is also shown on Fig. A10(b).

(a)

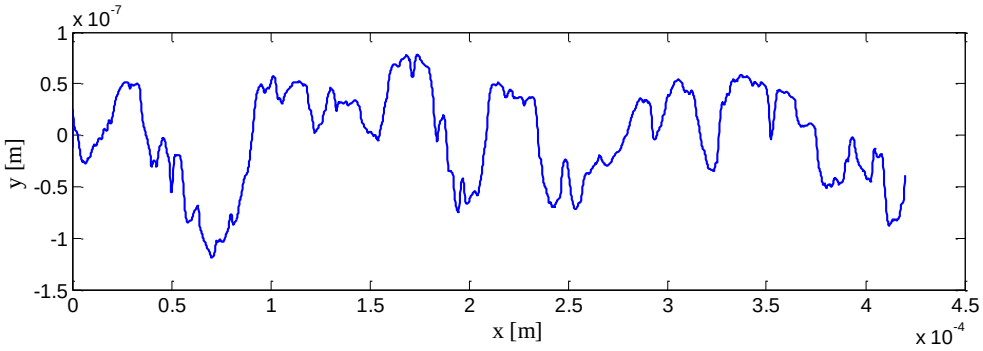

(b)

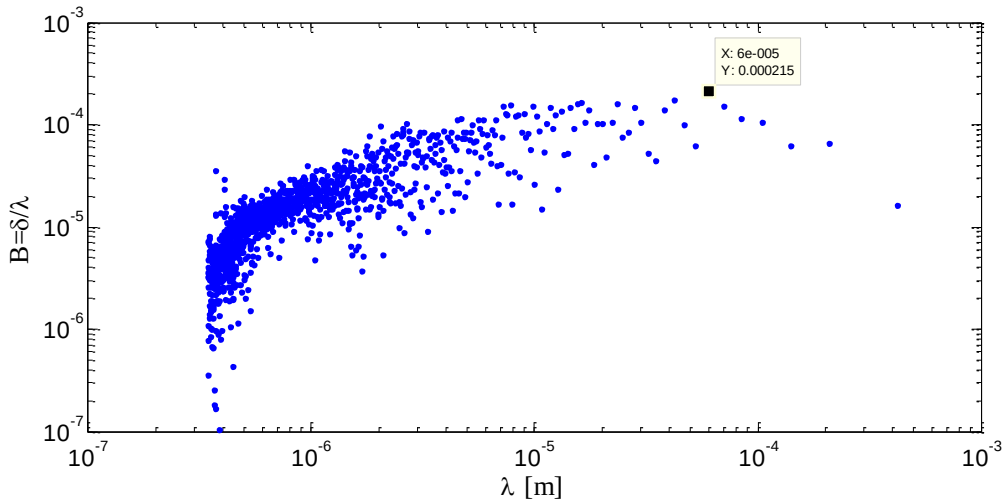

Figure A10: Surface profile (a) and fast Fourier transform analysis (b) of one of the surfaces used in this paper.